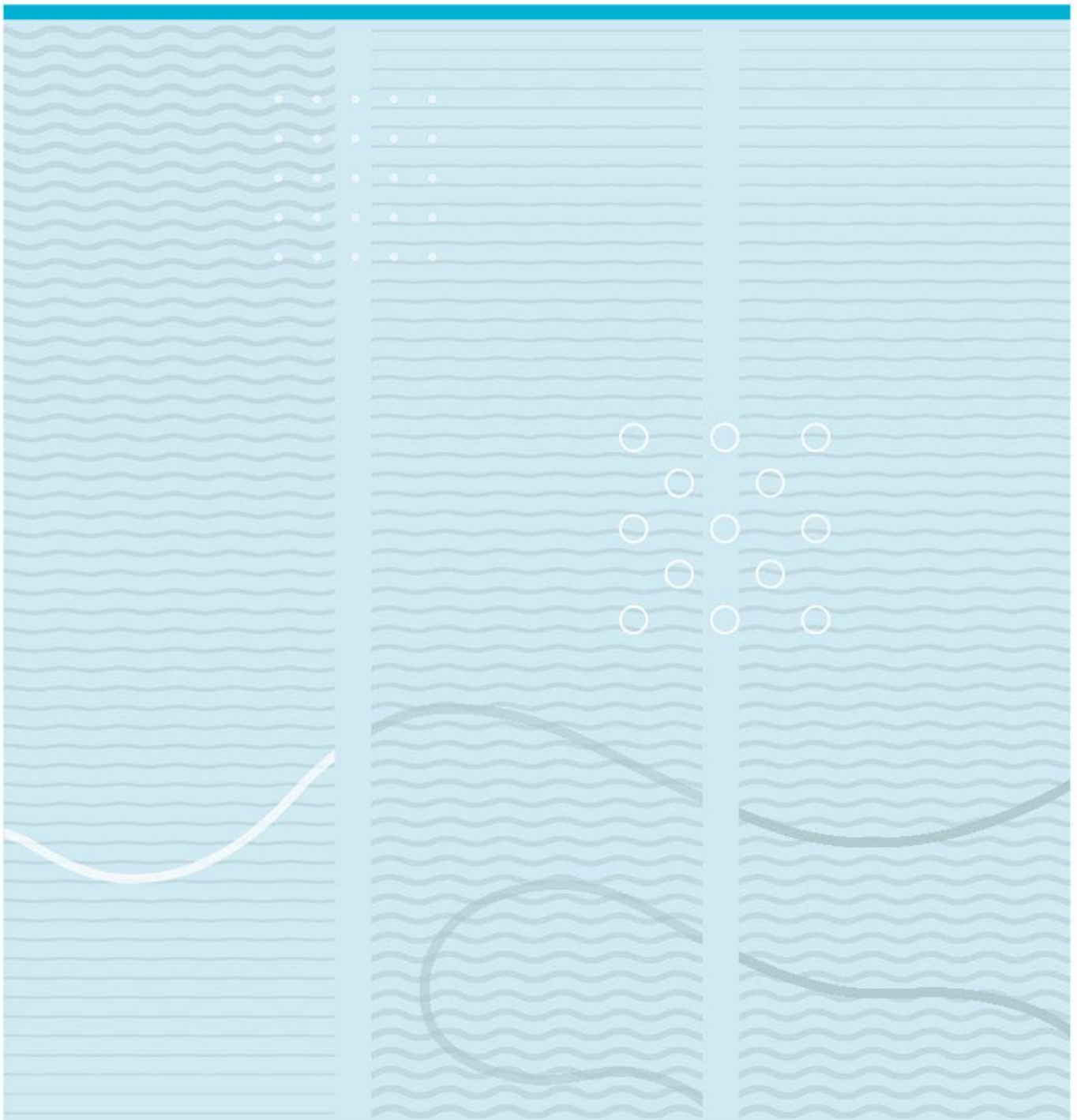


Josh Hoi Yi Siu

Fabrication and Characterization of a Low-Frequency Array for a Hybrid PZT-CMUT Transducer



University of South-Eastern Norway
Faculty of Technology, Natural Sciences and Maritime Sciences
Department of Microsystems.
Raveien 215
NO-3184 Borre, Norway

<http://www.usn.no>

© 2021 <Josh Hoi Yi Siu>

Abstract

Piezocomposite comprises of a periodic structure of active piezoelectric material and passive polymer phase. Piezocomposite material is widely used in medical ultrasound transducer due to the advantages of piezocomposite over pure piezoelectric material such as the high electromechanical coupling, reduction in lateral crosstalk and the low acoustic impedance for matching with human tissue. This work studies the design, modelling and fabrication of a 2 MHz 2-2 piezocomposite plate and array as the low frequency part of a DHUT structure at USN ultrasound laboratory. The piezocomposites were designed and modelled in a 1D Mason equivalent circuit model and a 2D finite element model. The fabricated piezocomposite were characterized by the electrical impedance and phase angle and compared to the modelled result. The fabrication procedure for piezocomposite was also developed for the USN ultrasound laboratory and discussed in detail.

Acknowledgement

First and foremost, I would like to express my gratitude to my supervisor, Professor Lars Hoff and Associate Professor Tung Manh for providing with invaluable guidance, discussions and comments at every stage throughout my research. Their tremendous understanding of acoustics and ultrasound transducer has provided me a solid foundation in the subject matter.

I am also grateful for the support and technical training from my co-supervisor Ph.D. Candidate Per Kristian Bolstad. Since the beginning to the completion of this thesis, his laboratory knowledge has taught me a great deal about practical laboratory know-how. Without his continuous support and encouragement, my work would not be possible.

I am also very appreciative to Thai Anh Tuan, Muhammad Tayyib, and Birgitte Kasin Hnsvall, laboratory employees, for their training and consistent assistance. My gratitude also extends to the other students and teachers I met throughout my time as a master's student at USN, who made my time there meaningful.

Finally, I would love to send my thanks to my family and friends who has been supporting me in this scientific journey.

List of Symbols

ν	Poisson's ratio	—
$\phi_p(\omega)$	Transmission ratio	—
ε^S	Relative permittivity at constant strain	—
A	Area	m^2
c_l	Longitudinal wave velocity	m/s
c_s	Shear wave velocity	m/s
$c_{i,j}^D$	Elastic stiffness at constant displacement Field	PA
$c_{i,j}^E$	Elastic stiffness at constant electric Field	PA
c_w	Longitudinal wave velocity for width resonance	m/s
D	Displacement Field	C/m^2
$d_{i,j}$	Piezoelectric strain constant	C/N
E	Young's modulus	Pa
$e_{i,j}$	Piezoelectric stress constant	C/m^2
f_a	Antiresonance	Hz
f_r	Resonance	Hz
$h_{i,j}$	Piezoelectric stiffness constant	V/m
I	Current	A
k_t	Electromechanical coupling coefficient of thin plate	—
k_{33}	Electromechanical coupling coefficient of free rod	—

k'_{33}	Electromechanical coupling coefficient of narrow beam/slender bar	–
L	Length	m
Q_m	Mechanical quality factor	–
S	Strain	–
$s^D_{i,j}$	Compliance at constant displacement Field	$1/PA$
$s^E_{i,j}$	Compliance at constant electric Field	$1/PA$
T	Stress	Pa
t	Thickness	m
V	Voltage	V
$V.F.$	Volume fraction	–
w	Width	m
Z	Acoustic impedance	$MRayl$

List of Figures

1.1	Illustration of a completed piezocomposite array.	4
2.1	Two phased material classified by the connectivity.	15
2.2	Piezoelectric slender bar for a single array element.	17
2.3	Equivalent circuit for piezoelectric element at thickness extensional mode operation in Mason Model.	18
2.4	KLM equivalent circuit model for a piezoelectric element operating in the thickness extensional mode	18
3.1	Process flow for the fabrication of the 2-2 piezocomposite.	20
3.2	Effective electromechanical coupling coefficient as a function of aspect ratio of a pure slender bar with no kerf filler	23
3.3	Theoretical electromechanical coupling coefficient and effective acoustic impedance as a function of piezoceramic volume fraction V_c	26
3.4	Top view of the 2-2 dicing scheme of a piezocomposite.	28
3.5	COMSOL Model and the meshed result of a bulk Pz27 plate.	31
3.6	COMSOL model of a shallow-diced air kerf Pz27.	32
3.7	COMSOL model of a composite plate.	33
3.8	COMSOL model of a composite array element.	34
3.9	Oblique dicing at different deviation angles.	35
3.10	Set up for the electrical impedance measurement. The network analyzer was calibrated for the medical needle probe.	37
4.1	EpoTek 3012-filled composite showing the front side and the back side.	39
4.2	SEM image of the EpoTek 3012-filled composite.	39
4.3	SAM image of the front face of the composite structure. Red area marks surface defects.	40
4.4	Electroded composite of PZ-27 and RTV 3140	40
4.5	RTV 3140 composite	41

4.6	Condition of the filled kerf with RTV 3140	41
4.7	EpoTek 3012-filled piezocomposite array	42
4.8	Piezocomposite of Pz27 and RTV 3140	43
4.9	Electrical impedance magnitude and phase of bulk Pz27 disk. Black line indicates the measured electrical impedance.	44
4.10	Electrical impedance and phase angle of the measured result and two-dimensional COMSOL FEM simulation results with three different set of material data in the frequency range of 1.5 to 2.5 MHz.	45
4.11	Electrical impedance and phase angle measured on diced Pz27 with two-dimensional FEM simulations.	46
4.12	Electrical impedance and phase of the EpoTek 3012-filled composite plate.	47
4.13	Electrical impedance and phase of the EpoTek 3012-filled composite in the range of 1 MHz to 4 MHz.	48
4.14	Electrical impedance and phase of the RTV 3140-filled composite.	49
4.15	Electrical impedance and phase of the EpoTek 3012-filled composite array elements	51
4.16	Resonance and antiresonance frequency across the composite array	52
4.17	Electrical impedance and phase of the RTV 3140-filled composite array elements.	53
4.18	Resonance and antiresonance frequency across the composite array	54
4.19	Electrical impedance and phase angle of the composite structure with oblique dicing at an angle of 0° to 1.5°	55
5.1	Dicing result at different feed speed.	63
A.1	Bulk PZ-27 disk with diameter of 3 cm supplied from manufacturer FerroPerm A/S	70
A.2	Side view of the dicing regime showing the total width, thickness, depth of cuts and the sacrificial layer.	71
A.3	Top view of the dicing schemes to separate two piezoceramic samples on the bulk PZ-27 disk	71
A.4	Diced PZ-27 with air kerf and Kapton tape on the bottom. Feedspeed = 1 mm/s. Shower rate = 0.75 L/mm.	72
A.5	Breaking and shorting of elements near the edge of the diced sample after dicing.	73
A.6	Mixing of epoxy with Speed Mixer DAC 150 FVZ-K	74
A.7	Degassing setup for epoxy.	75
A.8	Filling Epoxy on the diced PZT sample and repeatedly degassed before curing in oven.	75

A.9 Filled samples sandwiched by insulating tapes and metal brick to avoid bending of the sample.	76
A.10 Filled sampled after curing within the epoxy dam.	76
A.11 Degassing equipment for RTV 3140	77
A.12 RTV 3140 after degassing with multiple pockets of voids, indicating a poor degassing quality.	77
A.13 Filled composite prior to lapping. The diced and filled composite was taped with the yellow Kapton tape at the bottom.	78
A.14 Iezoceramic and kerf width on the top and the bottom of the diced showing a non-vertical dicing.	79
A.15 Cross section of the lapped composite	82
A.16 Surface condition of the lapped composite	82
A.17 Top surface of the composite to be scratch diced with the element width and pitch. .	84

List of Tables

1.1	Comparison of the performance of piezoceramics and piezocomposites.	3
2.1	List of independent material parameters of a piezoelectric material	11
3.1	Material parameter of the piezoceramic Pz27	21
3.2	Fitting of material parameters of bulk Pz27 disk for one-dimensional modelling . . .	22
3.3	Material Parameter of passive polymer filler EpoTek 3012 & RTV 3140 silicon rubber	25
3.4	Fitting of material parameters of the bulk Pz27, EpoTek 3012-filled and RTV 3140- filled piezocomposite	27
3.5	Early design goal of the 2-2 piezocomposite array	29
3.6	FEM model properties for a shallow diced air kerf Pz27	32
3.7	FEM model properties for the composite plate	33
3.8	General procedure for fabricating a 2-2 piezocomposite plate.	36
4.1	The resonance, antiresonance and coupling coefficient of the measured Pz27 and FEM results from three sets of parameters and the percentage difference to the measured value.	45
4.2	Resonance, antiresonance frequency and the coupling coefficient of the piezocomposite with EpoTek 3012	47
4.3	Measured and modelled resonance and antiresonance of piezocomposite of Pz27 and EpoTek 3012 from three different material data sets.	48
4.4	Resonance, antiresonance frequency and the coupling coefficient of the RTV 3140- filled composite calculated by Eq. 2.24.	49
4.5	Measured properties of the fabricated 2-2 piezocomposite plate	50
4.6	Measured properties of the 40-element Pz27 and EpoTek 3012 composite array . . .	51
4.7	Statistics of the resonance and antiresonance frequency of the composite array ele- ments of Pz27 with EpoTek 3012 as polymer filler	52
4.8	Measured properties of the 18-element Pz27 and RTV 3140 composite array	53

4.9	Statistics of the resonance and antiresonance frequency of the composite array elements of Pz27 with RTV 3140 as polymer filler	54
4.10	Comparison of the coupling coefficients calculated from the impedance spectra.	55
A.1	Pure EpoTek 301-2 filler epoxy mixing recipes	74
A.2	Procedures for fabricating a 2-2 piezocomposite plate	80
A.3	Parameters for electrode sputtering.	83

Contents

Abstract	i
Acknowledgement	ii
List of Symbols	iii
List of Figures	ix
List of Tables	ix
1 Introduction	1
1.1 Motivation	1
1.2 Thesis Objective	5
1.3 Thesis Structure	6
2 Theoretical Background	7
2.1 Acoustics and Ultrasound	7
2.2 Piezoelectricity	10
2.2.1 Piezoelectric Constitutive Equation	10
2.2.2 Resonance, Antiresonance and Electromechanical Coupling Coefficient	12
2.2.3 Quality Factor and Losses	13
2.3 Polymer Material	13
2.4 Piezocomposite Material	14
2.5 Effective Electromechanical Coupling Coefficient and Aspect Ratio	16
2.6 One-dimensional Modelling – Xtrans	17
2.7 Finite Element Modelling	19
3 Materials and Methods	20
3.1 Material Parameters	21
3.1.1 Active Piezoceramic - Pz27	21

3.1.2	Electromechanical Coupling Coefficient and Aspect Ratio of Pz27	22
3.1.3	Passive Filler Polymer - EpoTek 3012 and RTV 3140	24
3.2	Piezocomposite Design	26
3.3	Finite Element Modelling	30
3.3.1	Bulk Plate Pz27	30
3.3.2	Diced Pz27 with Air Kerf	31
3.3.3	Composite Plate	32
3.3.4	Composite Array	33
3.3.5	Oblique Dicing	34
3.4	Composite Plate and Array Fabrication	36
3.5	Characterization Methods	37
4	Results	38
4.1	Fabrication Result	38
4.1.1	Composite Plate - Pz27 & EpoTek 3012	38
4.1.2	Composite Plate - Pz27 & RTV 3140	40
4.1.3	Composite Array - Pz27 & EpoTek 3012	42
4.1.4	Composite Array - Pz27 & RTV 3140	43
4.2	Characterization - Composite Plate	44
4.2.1	Electrical Characterization of Bulk Disk of Pz27	44
4.2.2	Electrical Characterization of Diced Pz27 with Bottom Support	45
4.2.3	Electrical Characterization of Piezocomposite Plate - Pz27 and EpoTek 3012	46
4.2.4	Electrical Characterization of Piezocomposite Plate - Pz27 and RTV 3140	48
4.3	Summary of Measured Properties of the Fabricated Composite Plates	50
4.4	Characterization - Composite Array	51
4.4.1	Electrical Characterization of the Composite Array - Pz27 and EpoTek 3012	51
4.4.2	Electrical Characterization of the Composite Array - Pz27 and RTV 3140	53
4.5	Electromechanical Coupling Coefficient	54
4.6	Oblique Dicing	55
5	Discussion	57
5.1	Fitting of Material Parameters	57
5.2	Electrical Characterization of the Diced Pz27 Pillars with Bottom Support	58
5.3	2-2 Piezocomposite Plate	58
5.4	2-2 Piezocomposite Array	59

5.5	Comparison of Hard (EpoTek 3012) and Soft (RTV 3140) Polymer Filler	60
5.6	Electromechanical Coupling Coefficient	61
5.7	Mechanical Challenges	62
5.7.1	Mechanical Dicing	62
5.7.2	Filler Condition of the Composite Structure	63
5.7.3	Separation and Characterization of Array Element	64
6	Conclusion	65
6.1	Conclusion	65
6.2	Future work	66
A	Fabrication of the 2-2 Piezocomposite	70
A.1	Step 1 - Sample Preparation	70
A.2	Step 2 - First Shallow Dicing	71
A.3	Step 3 - Kerf Filling, Degassing and Curing	74
A.4	Step 4 - Sample Inspection	78
A.5	Step 5 - Lapping	80
A.6	Step 6 - Sputtering	83
A.7	Step 7 - Composite Array Fabrication	84

Chapter 1

Introduction

1.1 Motivation

In the study of sound, ultrasound is defined as sound waves with a frequency higher than the hearing limit of human ears. Ultrasound is widely utilized in medical diagnostics, particularly in the pulse echo mode. When an ultrasonic pulse is transmitted into the human body, it will reflect off the tissues along the propagation path, and these echoes will carry information about the tissue's inhomogeneous acoustic and structural properties. The amplitude, frequency, and time of flight characteristics of these echoes are captured, and the internal structures of the target may be examined to generate a comprehensive image for diagnostics.

An ultrasonic transducer is a device that generates and receives ultrasound pulses, by converting electrical signals to and from mechanical vibrations. It is typically constructed of a piezoelectric material that oscillates to create ultrasonic waves when voltage is applied. Ultrasound transducers are commonly manufactured as either a single element transducer or an array transducer. To transmit and receive ultrasonic signals, a single element transducer vibrates its surface by electrical or mechanical stimulation. An array transducer is constructed by combining more than one element and exciting each array element independently. In comparison to traditional radiography, MRI, and X-ray CT scan, ultrasound is a safer, less expensive, and more portable option for medical diagnostic imaging [1].

The operating center frequency of a medical transducer typically ranges from 1 MHz to 20 MHz. Other application that make use of ultrasonic transducer is ultrasound cleaner, non-destructive testing (NDT), liquid level, flow and concentration control in chemical and process industries. Ultrasonic waves are also widely utilized in underwater applications such as sonars and echo-sounders for contouring the ocean floor, underwater communication systems and fishing. Despite the fact that these applications utilize lower frequencies to scan across greater distances, the fundamental ideas are the

same as in medical ultrasonography.

For efficient acoustic wave transmission, the piezoelectric material used in medical ultrasonic transducers should have a high electromechanical coupling coefficient and be acoustically matched to human tissue as well as low electrical losses (i.e. low dielectric loss tangent or low $\tan \delta_e$ and low mechanical losses (i.e. high mechanical quality factor or high Q_m) [2], [3]. Low $\tan \delta_e$ reduces the signal loss due to the internal dissipation of electromagnetic energy. High Q_m reduces energy loss due to internal heat generation. Both of these characteristics are desirable in order to facilitate an effective transmission of ultrasonic energy [4].

Although conventional monolithic piezoceramics have a high coupling factor, low $\tan \delta_e$ and high Q_m , the major drawbacks are the high characteristic acoustic impedance in comparison to the normal load medium and the presence of lateral modes. The large impedance mismatch between the piezoelectric material and the load medium results in a high Q-factor for the device, which is not suitable for operation with broad bandwidth. Specifically, mechanical quality factor Q_m of a piezoelectric material describe the energy losses within the piezoelectric material while device Q-factor describe the frequency response of the overall transducer. High mechanical quality factor Q_m is desired for minimal internal energy losses within the piezoelectric material and a low device Q-factor of the transducer is desired for broad brand operation.

Alternatively, the use of a piezocomposite material can mitigate some of the disadvantages of a piezoelectric transducer. Piezocomposite materials are made up of periodic piezoceramic and polymer phases. For two-phase composites, the material properties can be tailored by fine tuning the volume fractions of each material phase. For example, 60% volume fraction of piezoelectric material means that the material has 60% of the volume occupied by the piezoelectric material and the other 40% by a softer polymer filler. The volume fraction of piezoceramic and polymer filler changes the acoustic and electrical characteristics of the piezocomposite, which may be fine tuned and modified to meet the criteria for a medical ultrasound transducer.

The benefits of using a piezocomposite include a high electromechanical coupling factor, low acoustic impedance allowing for good matching with water or human tissue, good mechanical flexibility, and broad bandwidth operation with a low mechanical quality factor [3], [4]. Piezocomposite offers better energy conversion since its coupling coefficient is typically higher than that of a piezoceramic as the softer polymer phase reduces lateral restriction of piezoelectric material's vibration, the piezocomposite's thickness-mode electromechanical coupling can surpass the constituent piezoceramic's k_t (0.40–0.50) and reach the value of the ceramic's free rod-mode electromechanical coupling, k_{33} (0.70–0.80) [3]. The acoustic impedance of a material is defined as the square root of the product of the material's density and elastic stiffness. Piezocomposite has a lower acoustic impedance since

Table 1.1: Comparison of the performance of piezoceramics and piezocomposites. Blue and red denotes the advantage and disadvantage for medical transducer application. Adapted from [5]

Parameter	Piezoceramics	Piezocomposites
Electromechanical coupling coefficient	High	High
Acoustic Impedance	High	Low
Dielectric constant	High	Intermediate
Transmission band	Narrow	Broadband
Lateral Modes	Numerous	Reduced

some of the heavy and stiff piezoceramics are replaced with a lighter and softer polymer, this allow a better acoustic matching to human tissue or water (1.5 MRayl) by lowering the acoustic impedance of typical piezoceramics (20–30 MRayl) to that of piezocomposite ($Z < 10$ MRayl). By filling the active piezoceramic with a passive soft polymer, the piezocomposite can behave like a homogeneous material if the resonances of the lateral waves are moved outside the operating frequency range, reducing unwanted coupling of lateral modes. A qualitative comparison of the advantages and disadvantages of monolithic piezoceramics and piezocomposite was summarized in [5] and shown in Table 1.1. These advantages showed that piezoelectric composite materials are especially useful for underwater sonar and medical diagnostic ultrasonic transducer applications.

Note that a piezocomposite and a conventional transducer array are visually alike. The major distinction between the two is that each element of a piezocomposite is linked to the same terminal, but an array is made up of many single transducer elements with individual terminations and may thus be regulated individually.

In short, the motivation for using a piezocomposite over a homogeneous piezoelectric material is that since ultrasound imaging depends on the conversion between electrical and mechanical energy, a piezocomposite can achieve a greater coupling efficiency than a bulk piezoelectric material and a piezocomposite is capable of reducing lateral resonances.

Previous research in [2], [6] has demonstrated how a dual frequency hybrid transducer (DHUT) was developed with a PZT stack with matching and backing layers operating with a center frequency at 7 MHz as the transmitter (TX) while a CMUT layer on top operates at twice the operating frequency to the transmitter as the receiver (RX) to capture the second harmonic. Second harmonic comes from the non-linearity of material properties. When an acoustic beam is propagates through the tissue, the tissue generates harmonic frequencies due to the non-linearity of the medium. In a linear medium, the pulse shape may change as the pulse propagates, i.e. due to frequency dependent attenuation, but no new frequencies are generated in the transmitted pressure pulse. On the contrary,

in a non-linear medium, the peaks of the pressure wave travel faster than the troughs since the propagation in the compressed high-pressure region is faster than that in the expanded low-pressure region, the waveform becomes distorted and additional harmonics are generated. Subsequently, the higher harmonics are damped in the medium. For example, conventionally when a 2 MHz transducer transmits a frequency band around 2 MHz, the returning echoes from the tissue will also be frequencies around 2 MHz. In harmonic imaging, transmitting the frequency band around the 2 MHz, the returning echoes will also comprise harmonics at 4 MHz, 8 MHz, etc. By capturing these higher harmonics, greater image clarity, contrast, resolution and reduced reverberation and beam aberration are achieved. Imaging techniques utilizing such a mechanism are called Tissue Harmonic Imaging (THI) and the most commonly used harmonic is the second harmonic [1], [7].

This thesis focuses on the low frequency piezoelectric component of the DHUT technology by establishing manufacturing and characterization methodologies in USN's laboratory. The high frequency CMUT part is not investigated in this thesis. The DHUT concept is to combine the advantages of piezoelectric/piezocomposite in transmit (i.e. linearity and high transmit amplitude) with the advantages of CMUT in receive (i.e. large bandwidth, configurable, suitable for high frequency operation). The design, fabrication and characterization of a 2-MHz 40-element and a 2-2 piezocomposite array is presented in this thesis. The purpose was to develop fabrication and characterization methods for composites and arrays in the USN transducer lab. A cut-away view of the DHUT with a LF piezocomposite array is illustrated in Fig 1.1.

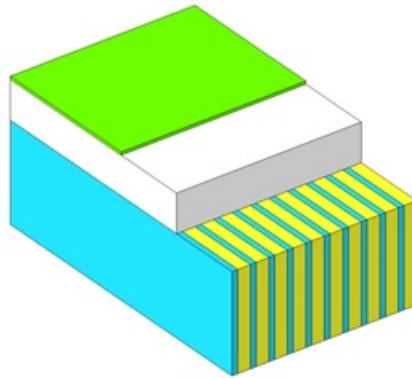


Figure 1.1: Illustration of a completed piezocomposite array with matching layer and CMUT. Yellow is the piezoceramic, cyan is the kerf filler, white is the matching layer, and green is the CMUT silicon layer.

Each array element consists of two piezoceramic layers and three polymer layers. The array elements are covered with Cr/Au plated electrodes on top and bottom surfaces. The composite is acoustically matched with a matching layer and a silicon layer is on top to mimic the CMUT layer. The composite array elements were separated by a $375 \mu\text{m}$ pitch (0.51λ in water at the operating frequency) and the

kerf for electrode separation was $125\ \mu\text{m}$. This work focuses on the fabrication of the piezocomposite and the composite was modelled in 1D and 2D finite element analysis and fabricated by mechanical dicing from a plate of piezoelectric ceramic and polymer filling. The electrical impedance and phase angle were characterized to study the electrical behaviour.

1.2 Thesis Objective

This thesis aims to provide a complete overview of the fabrication and characterization of the low frequency (LF) piezoelectric array to be used as the transmitter in a hybrid PZT-CMUT transducer. The objectives are as follows:

1. Fabricate the LF stack of the DHUT, a 2 MHz piezocomposite 2-2 array
2. Establish fabrication procedures for piezocomposites and piezocomposite arrays to be used in USN's transducer laboratory
3. Provide the understanding and basis for the fabrication processes
4. Evaluate any challenges arising from the fabrication procedures

The following presents the overview of the tasks that are performed for the thesis.

1. Design and Modelling
 - (a) Calculate effective medium parameters for the composite using models from the literature
 - (b) 1D modelling in Mason equivalent circuit model
 - (c) Finite element modelling in COMSOL
2. Fabrication
 - (a) Determine the material parameters
 - (b) Fabricate the LF stack of the DHUT, a 2 MHz piezocomposite 2-2 array
 - (c) Establish the fabrication process for piezocomposite plate
 - (d) Establish the fabrication process for piezocomposite array
3. Characterization
 - (a) Electrical impedance and phase measurement of the composite plate
 - (b) Electrical impedance and phase measurement of the composite array
4. Others
 - (a) Evaluate possible challenges during the fabrication procedures

1.3 Thesis Structure

The theoretical foundation of this investigation is presented in Chapter 2. Section 2.1 discusses the related acoustics and ultrasound theories. Section 2.2 explains the fundamentals of piezoelectricity. Section 2.3 describes the polymer material parameters. The formulation for the piezocomposite material's parameters is presented in section 2.4 and 2.5. The background description of the one-dimensional and two dimensional modelling methods is briefly described in section 2.6 and 2.7.

The process flow of piezocomposite manufacturing and modeling methodologies are presented in Chapter 3. Section 3.1 contains a list of all the material parameters utilized in this investigation. The 1D modelling is presented in section 3.2. The finite element technique is discussed in section 3.3. The composite fabrication processes are covered in section 3.4. The Characterization methods and instruments used in this study are outlined in section 3.5.

The results and findings are presented in Chapter 4. Section 4.1 shows the composites samples' fabrication results. Section 4.2 present the findings of the composite plate characterization, whereas section 4.3 covers the results of the composite array characterization.

Chapter 5 discusses the measurement results and the difficulties encountered throughout the fabrication process, while Chapter 6 gives the conclusion and future work.

Chapter 2

Theoretical Background

2.1 Acoustics and Ultrasound

In ultrasound imaging, acoustic waves are generated by a transducer and the waves are transmitted through the propagation medium. Reflected echoes carrying information about the condition of the human body are captured and processed to an imaging system for diagnostics. The frequency of medical diagnostic ultrasound imaging typically ranges from 2 MHz to 15 MHz [1].

The density ρ and stiffness of the propagation medium are the fundamental characteristics determining sound propagation in the science of acoustics, and the wave is characterized by pressure inside the propagation medium p and particle velocity v . The propagation of sound comes in the form of compressional and shear waves. Compressional waves occur in both solid and liquid materials, whereas shear waves occur in solids and other viscous fluid. The main properties of these waves are their speed, namely the longitudinal or transversal wave velocity. In general, the wave velocity c in a medium is given by

$$c = \sqrt{\frac{\text{Elastic Modulus}}{\rho}} \quad (2.1)$$

For a liquid, the longitudinal wave velocity c_L is given by

$$c_L = \sqrt{\frac{B}{\rho}} \quad (2.2)$$

where B is the bulk modulus of elasticity.

For a solid, the longitudinal wave velocity c_L and shear wave velocity c_s are

$$c_l = \sqrt{\frac{E(1-\nu)}{(1+\nu)(1-2\nu)\rho}} \quad (2.3)$$

$$c_s = \sqrt{\frac{G}{\rho}} \quad (2.4)$$

where E , ν , G and ρ are the Young's modulus, Poisson's ratio, shear modulus and density, respectively. These properties are crucial to determine the choice and design of a transducer in the following sections.

Another property is the characteristic acoustic impedance. The characteristic acoustic impedance describes the transmission and reflection of sound waves of the medium at boundaries. Characteristic acoustic impedance Z_A (referred to acoustic impedance hereafter) of a material A for plane sound waves is given by

$$Z_A = \rho c_l. \quad (2.5)$$

The acoustic impedance of solids is typically much greater than that of liquids and gases due to higher density and stiffness in solids (i.e. 38 MRayl in silver versus 1.5 MRayl in water). A typical piezoelectric ceramic has characteristic acoustic impedance of around 30 MRayl.

When sound waves travel through the interface of two different media with different material properties, reflection will occur. With the acoustic impedance, we can determine the transmission coefficient and reflection coefficient of a sound wave propagating from medium 1 to medium 2 at the interface boundary. The transmission coefficient T and reflection coefficient R for plane pressure waves at normal incidence are given as

$$T = \frac{p_t}{p_i} = \frac{2Z_2}{Z_1 + Z_2} \quad (2.6)$$

$$R = \frac{p_r}{p_i} = \frac{Z_2 - Z_1}{Z_1 + Z_2}. \quad (2.7)$$

where p_i is the pressure amplitude of the incident wave, p_t the pressure amplitude of the wave transmitted through the interface, and p_r the pressure amplitude of the reflected wave. From Eq.2.6 and 2.7, when the difference between Z_1 and Z_2 is small (i.e. $Z_1 \approx Z_2$), $T \approx 1$ and $R \approx 0$. However, if the difference is large (i.e. $Z_1 \ll Z_2$ or $Z_1 \gg Z_2$), $T \approx 0$ and $R \approx \pm 1$. Thus, strong reflection is due to large impedance mismatch. One of the goals in this thesis is to minimize this mismatch to facilitate efficient propagation. For example, a PZT material with acoustic impedance in the region of 30 MRayl and human muscle with acoustic impedance of 1.5 MRayl, $T \approx 0.10$ and $R \approx 0.90$. Most of the waves will be reflected at the interface, limiting the transmission of waves. Therefore, an intermediate layer is introduced between the two media to enhance the transmission efficiency.

There are two requirements for the matching layer to improve the transmission. Its layer thickness and its acoustic impedance. The layer thickness follows the same analogy as in transmission line theory and the thickness should normally be around a quarter of the acoustic wavelength in the layer,

$$t_{ML} = \frac{\lambda_{ML}}{4} = \frac{c_{ML}}{4f} \quad (2.8)$$

where λ_{ML} is the wavelength and c_{ML} is the longitudinal speed of sound inside the matching layer. The definition of optimal performance of an ultrasound transducer depends on the application, and this definition influences the choice of matching layer impedance and thickness. Maximum transmission of acoustic energy between two media for a single matching layer is [1]

$$Z_{ML} = \sqrt{Z_1 Z_2}. \quad (2.9)$$

For an ultrasound transducer $Z_1 = Z_p$ and $Z_2 = Z_l$ where Z_p and Z_l are the acoustic impedance of piezoelectric material and load medium, respectively.

Bandwidth is essential in medical ultrasound imaging, and medical ultrasound transducers are often optimized for wide-band transmission. Desilets [8] has given guidelines for how to optimize acoustic matching layer properties for maximum bandwidth. The resulting acoustic impedance for a single matching layer is according to this

$$Z_{ML} = (Z_p Z_l^2)^{1/3}. \quad (2.10)$$

For two matching layers, the acoustic impedance for the first and second layer should be

$$Z_{ML1} = (Z_p^4 Z_l^3)^{1/7} \quad (2.11)$$

$$Z_{ML2} = (Z_p Z_l^6)^{1/7}. \quad (2.12)$$

The backing layer for the transducer also has an important role in the performance of the transduction. Backing layer can be used to adjust the mechanical quality factor, bandwidth and sensitivity.

2.2 Piezoelectricity

2.2.1 Piezoelectric Constitutive Equation

The piezoelectric effect describes the conversion mechanism from mechanical energy to electrical energy and vice versa. Such a material is called piezoelectric material. A piezoelectric material is made up of molecules that have dipoles that oriented in the same direction. When a piezoelectric material is mechanically deformed as a result of an applied mechanical load, the electric polarization changes macroscopically [9]. Such interaction converts energy to and from mechanical domain (i.e. mechanical strain S and mechanical stress T) and electrical domain (i.e. electric field intensity E and electric displacement D). If the material is covered with electrode, the electrical voltages can be measured or applied to detect or create mechanical deformation. For anisotropic solids, its mechanical properties can be described by its stiffness matrix from Hooke's law and its dielectric properties can be expressed with Voigt notation, also called matrix notation, as

$$\begin{bmatrix} T_1 \\ T_2 \\ T_3 \\ T_4 \\ T_5 \\ T_6 \end{bmatrix} = \begin{bmatrix} c_{11}^E & c_{12}^E & c_{13}^E & c_{14}^E & c_{15}^E & c_{16}^E \\ c_{21}^E & c_{22}^E & c_{23}^E & c_{24}^E & c_{25}^E & c_{26}^E \\ c_{31}^E & c_{32}^E & c_{33}^E & c_{34}^E & c_{35}^E & c_{36}^E \\ c_{41}^E & c_{42}^E & c_{43}^E & c_{44}^E & c_{45}^E & c_{46}^E \\ c_{51}^E & c_{52}^E & c_{53}^E & c_{54}^E & c_{55}^E & c_{56}^E \\ c_{61}^E & c_{62}^E & c_{63}^E & c_{64}^E & c_{65}^E & c_{66}^E \end{bmatrix} \begin{bmatrix} S_1 \\ S_2 \\ S_3 \\ S_4 \\ S_5 \\ S_6 \end{bmatrix} \quad (2.13)$$

$$\begin{bmatrix} D_1 \\ D_2 \\ D_3 \end{bmatrix} = \begin{bmatrix} \varepsilon_{11}^S & \varepsilon_{12}^S & \varepsilon_{13}^S \\ \varepsilon_{21}^S & \varepsilon_{22}^S & \varepsilon_{23}^S \\ \varepsilon_{31}^S & \varepsilon_{32}^S & \varepsilon_{33}^S \end{bmatrix} \begin{bmatrix} E_1 \\ E_2 \\ E_3 \end{bmatrix}$$

where T_i is the rank 2 mechanical stress tensor written as a 6×1 column vector, S_i is the rank 2 mechanical strain tensor written on the same format, $c_{i,j}^E$ is the elastic stiffness constants at constant electric field, $D_{1,2,3}$ is the electric displacement field, E_i is the electric field and $\varepsilon_{i,j}^S$ is the relative permittivity at constant strain, i.e. clamped conditions. Detailed explanations of all parameters can be found in [9].

Under the effect of piezoelectricity, the electric field and displacement induces mechanical stress and strain and vice versa, thus, the piezoelectric material is given by the piezoelectric constitutive equations. This creates a coupling between the mechanical and electrical domains. The separate mechanical and electrical equations above are coupled, giving the following constitutive equations in stress charge form

$$\begin{aligned} T &= [c^E]S - e^t E \\ D &= eS + [\varepsilon^S E] \end{aligned} \quad (2.14)$$

and c^E , e and ε^S are the stiffness matrix at constant electric field, piezoelectric stress coefficient (superscript t indicates matrix transpose) and clamped permittivity. For a piezoelectric material with a crystalline structure of class 6mm and the crystal symmetry relationship, the component notation results in reduction of independent components [9]. The resultant matrices from Eq. 2.13 are

$$\begin{aligned}
 \begin{bmatrix} T_1 \\ T_2 \\ T_3 \\ T_4 \\ T_5 \\ T_6 \end{bmatrix} &= \begin{bmatrix} c_{11}^E & c_{12}^E & c_{13}^E & 0 & 0 & 0 \\ c_{12}^E & c_{11}^E & c_{13}^E & 0 & 0 & 0 \\ c_{13}^E & c_{12}^E & c_{33}^E & 0 & 0 & 0 \\ 0 & 0 & 0 & c_{44}^E & 0 & 0 \\ 0 & 0 & 0 & 0 & c_{44}^E & 0 \\ 0 & 0 & 0 & 0 & 0 & \frac{c_{11}^E - c_{12}^E}{2} \end{bmatrix} \begin{bmatrix} S_1 \\ S_2 \\ S_3 \\ S_4 \\ S_5 \\ S_6 \end{bmatrix} - \begin{bmatrix} 0 & 0 & e_{31} \\ 0 & 0 & e_{31} \\ 0 & 0 & e_{33} \\ 0 & e_{15} & 0 \\ e_{15} & 0 & 0 \\ 0 & 0 & 0 \end{bmatrix} \begin{bmatrix} E_1 \\ E_2 \\ E_3 \end{bmatrix} \\
 \begin{bmatrix} D_1 \\ D_2 \\ D_3 \end{bmatrix} &= \begin{bmatrix} 0 & 0 & 0 & 0 & e_{15} & 0 \\ 0 & 0 & 0 & e_{15} & 0 & 0 \\ e_{31} & e_{31} & e_{33} & 0 & 0 & 0 \end{bmatrix} \begin{bmatrix} S_1 \\ S_2 \\ S_3 \\ S_4 \\ S_5 \\ S_6 \end{bmatrix} + \begin{bmatrix} \varepsilon_{11}^S & 0 & 0 \\ 0 & \varepsilon_{11}^S & 0 \\ 0 & 0 & \varepsilon_{33}^S \end{bmatrix} \begin{bmatrix} E_1 \\ E_2 \\ E_3 \end{bmatrix}
 \end{aligned} \tag{2.15}$$

The independent components on Eq.2.15 are listed below:

Table 2.1: List of independent material parameters of a piezoelectric material

Parameter	Symbol	Unit
Elastic Stiffness	c_{11}^E c_{12}^E c_{13}^E c_{33}^E c_{44}^E	Pa
Relative Permittivity	ε_{11}^S ε_{33}^S	-
Piezoelectric Stress Constants	e_{15} e_{31} e_{33}	C/m^2

Next, the electromechanical coupling factor k_t describes the efficiency of energy conversion of the piezoelectric material. For a thin disk or plate operating in thickness mode, the coupling factor is

$$k_t = \frac{e_{33}}{\sqrt{c_{33}^D \varepsilon_{33}^S}} \tag{2.16}$$

and for a free long rod operating in thickness mode, the coupling factor is commonly expressed in d form and it is defined as

$$k_{33} = \frac{d_{33}}{\sqrt{s_{33}^D \varepsilon_{33}^S}} . \tag{2.17}$$

and k_{33} is also the maximum coupling factor of the piezoelectric material, hence, $k_{33} > k_t$. d_{33} is the piezoelectric strain constant and s_{33}^E is the compliance constant. c_{33}^D is the elastic stiffness along the thickness direction at constant electric displacement D , i.e. constant charge or open circuit conditions. The value of c_{33}^D relates to the value of the longitudinal wave velocity and it defined as

$$c_t = \sqrt{\frac{c_{33}^D}{\rho_p}} \quad (2.18)$$

where ρ_p is the density of piezoelectric material, and thus, the acoustic impedance

$$Z_p = \sqrt{\rho_p c_{33}^D}. \quad (2.19)$$

The thickness mode piezoelectric coupling coefficient h_{33} is given by [10] as

$$h_{33} = k_t \sqrt{\frac{c_{33}^D}{\varepsilon_{33}^S}} \quad (2.20)$$

Additional relations are

$$e_{33} = h_{33} \varepsilon_{33}^S \quad (2.21)$$

$$c_{33}^E = c_{33}^D (1 - k_t^2) = c_{33}^D - \frac{e_{33}^2}{\varepsilon_{33}^S} \quad (2.22)$$

and the values of c_{33}^D , c_{33}^E and ε_{33}^S are readily available from manufacturer's technical data sheet.

2.2.2 Resonance, Antiresonance and Electromechanical Coupling Coefficient

For an ultrasound transducer, the energy is typically generated by the mechanical vibration due to the piezoelectric material operating in the thickness extension mode. For a circular plate, thickness extensional modes means that mechanical deformation and thus vibration occurs along the thickness direction with the diameter much larger than the thickness of the plate (i.e. diameter > 10 times plate thickness). Operation around the resonance frequency of the thickness mode is preferred since the sound pressure, surface normal velocity and electrical outputs is large around the resonance frequency f_r [9]. The mechanical resonance of the piezoelectric element occurs when the thickness of the piezoelectric material is

$$t_{PZT} = \frac{\lambda_L}{2} = \frac{c_L}{2f_a} \quad (2.23)$$

If the resonance f_r and anti-resonance frequency f_a is obtained, the thickness mode electromechanical coupling constant can be found from [10] as

$$k_t^2 = \frac{\pi f_r}{2f_a} \tan \frac{\pi}{2} \left(1 - \frac{f_r}{f_a} \right) \quad (2.24)$$

2.2.3 Quality Factor and Losses

All materials are lossy and losses can be classified into mechanical, dielectric and piezoelectric losses as complex parameter: c^* , e^* and ε^* . The losses can be summarized as complex parameters from [11]

$$\begin{aligned} c^* &= c' + jc'' = c'(1 - j \tan \delta_m) = c' \left(1 - \frac{j}{Q_m}\right) \\ e^* &= e' + je'' = e'(1 - j \tan \delta_p) = e' \left(1 - \frac{j}{Q_e}\right) \\ \varepsilon^* &= \varepsilon' + j\varepsilon'' = \varepsilon'(1 - j \tan \delta_d) = \varepsilon' \left(1 - \frac{j}{Q_d}\right) \end{aligned} \quad (2.25)$$

where c' and c'' are the real and imaginary elastic stiffness parameters.

For piezoelectric material, it is common to express the loss tangent as

$$\tan \delta_m = \frac{1}{Q_m} \quad (2.26)$$

A high mechanical quality factor Q_m of the piezoceramic indicates low internal energy losses as heat and the ultrasonic output is maximized at resonance frequency, however a pure piezoceramic as a transducer can only operate at a single narrow frequency range. For medical transducers, the overall transducer device Q-factor should be low since a low Q allows large bandwidth operation. The device Q-factor is limited by the acoustic matching to the target medium and attenuation of the waves inside the transducer.

2.3 Polymer Material

The polymer material for composite design is an important factor determining the final performance of the fabricated composite transducer. Numerous polymers have been used as the filler and a number of polymers and their material properties can be found summarized in [5]. The lateral clamping condition for the vibrating piezoceramic material is determined by the elastic stiffness of the polymer material. The ideal condition for achieving the maximum coupling factor is with air, since piezoceramics may vibrate without limitation, however this results in a mechanically weak structure. As a result, a soft polymer with low elastic stiffness decreases the lateral restriction of vibrating piezoceramics while also still offering certain mechanical support to the microstructure.

For an isotropic homogeneous material, the relevant elastic stiffness constants are

$$c_{11} = \frac{1 - \nu}{\nu} \frac{Ev}{(1 + \nu)(1 - 2\nu)} \quad (2.27)$$

$$c_{12} = \frac{Ev}{(1 + \nu)(1 - 2\nu)} \quad (2.28)$$

where the Young's modulus E and Poisson's ratio ν can be obtained from literature or from speed of sound measurement of longitudinal wave velocity c_l and shear wave velocity c_s and they are related as [12]

$$\begin{aligned} E &= \rho_{filler} c_s^2 \left(\frac{3c_l^2 - 4c_s^2}{c_l^2 - c_s^2} \right) \\ \nu &= \frac{1 - 2(c_s/c_l)^2}{2 - 2(c_s/c_l)^2} \end{aligned} \quad (2.29)$$

and the shear wave velocity inside the polymer can be approximated by [13]

$$c_s = 0.45c_l \quad (2.30)$$

2.4 Piezocomposite Material

The theory of piezocomposite materials are widely studied and this section presents the model of a piezocomposite material with 2-2 connectivity and the resulting effective material parameters of the electromechanical coupling coefficient k_t , acoustic impedance Z and the dielectric permittivity ε^S as a function of volume fraction of the piezoceramic material.

A piezocomposite material is a material comprised of piezoelectric ceramics and a passive polymer material such as epoxies. There are several advantages to use piezocomposite materials [3], [9]. First, the total acoustic impedance of a piezocomposite is smaller than that of a bulk piezoelectric ceramics. The polymer with a low acoustic impedance effectively lowers the combined acoustic impedance from around 30 MRayl of the bulk piezoceramic down to $Z \approx 10$ MRayl for the piezocomposite depending on the configuration of the composite. This provides better acoustic matching with human tissue with $Z \approx 1.6$ MRayl. Second, the coupling coefficient of a composite can be made larger than that of the piezoceramic material ($k_t \approx 0.7$)[3]. Third, the passive polymer reduces undesired vibration modes [9]. Lastly, its high mechanical flexibility allows the material to be optimized and tailored with the target application.

Connectivity is described by Newnham et al. into two numbers i,j. Both numbers can have values of 0, 1, 2, 3 and together creating 10 sets of connectivity patterns. The first digit states the degree of freedom of the active piezoceramics and the second digit states the degree of freedom of the passive polymer. For example, when a material is only continuous in one direction, it is called '1', in two direction it is called '2', etc. An example is a 3-1 composite has piezoceramic rods being continuous in one direction a polymer phase being continuous in three direction. For 2-2 composite, both the active and passive phase are continuous in two direction and stacked on each other, creating an alternating stack of materials.

When the polymer is embedded in the piezoceramics, effective material parameters are required to model a piezocomposite material accurately. The main variable here is the volume fraction or the

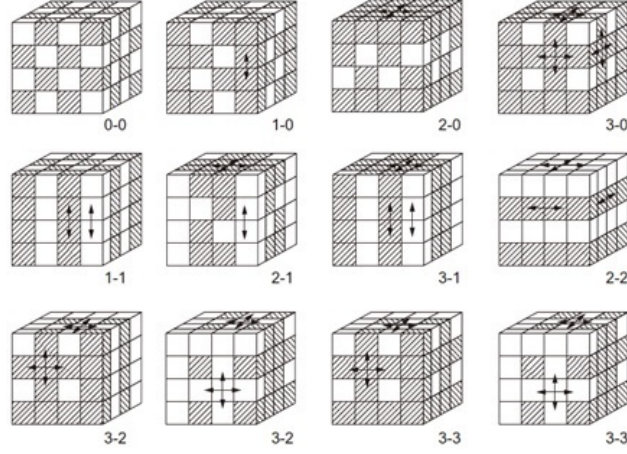


Figure 2.1: Two phased material classified by the connectivity. 3-2 and 3-3 has two configurations. (Taken directly from [4])

volume percentage of piezoceramics or the polymer and their sum is

$$V_c + V_p = 1 \quad (2.31)$$

where V_c and V_p are the volume percentage of the ceramic material and the polymer material.

The composite can be treated like one effective medium provided the composite dimensions are much smaller than the acoustic wavelengths involved. The most well-known effective medium theory is from Smith and Auld [3] for a 1-3 piezocomposite. The composites studied in this thesis are of 2-2 connectivity and with the volume percentage of the ceramics and the polymer, the three principal effective material parameters (denoted by the asterisk $*$) for 2-2 composites are given by the following the formulation developed in [14], [15]

1. effective stiffness at constant electric field

$$c_{33}^{E*} = V_c \left(c_{33}^E - \frac{V_p (c_{12} - c_{13}^E)^2}{V_p c_{11}^E + V_c c_{11}} \right) + V_p c_{11} \quad (2.32)$$

2. effective dielectric permittivity ε_{33}^*

$$\varepsilon_{33}^{s*} = V_c \left(\varepsilon_{33}^s + \frac{e_{31}^2 V_p}{V_p c_{11}^E + V_c c_{11}} \right) + V_p \varepsilon_{11} \quad (2.33)$$

3. effective piezoelectric stress coefficient e_{33}^*

$$e_{33}^* = V_c \left(e_{33} - \frac{V_p e_{31} (c_{13}^E - c_{12})}{V_p c_{11}^E + V_c c_{11}} \right) \quad (2.34)$$

where c_{12} , c_{12} and c_{13} are the stiffness constant and ε_{11} is the permittivity of the passive filler polymer. The parameters of c_{11}^E , c_{13}^E and c_{33}^E are the stiffness constants, e_{31} and e_{33} are the piezoelectric stress coefficient and ε_{33}^s is the dielectric permittivity of the active piezoelectric material.

Other effective parameters can be calculated and they are defined as

1. stiffness at constant electric displacement field

$$c_{33}^{D*} = c_{33}^{E*} + \frac{e_{33}^{*2}}{\epsilon_{33}^{s*}} \quad (2.35)$$

2. effective density

$$\rho^* = \rho_c V_c + \rho_p V_p \quad (2.36)$$

3. effective longitudinal speed of sound along the thickness direction

$$c_L^* = \sqrt{\frac{c_{33}^{D*}}{\rho^*}} \quad (2.37)$$

4. effective acoustic impedance

$$Z^* = \sqrt{\rho^* c_{33}^{D*}} = \rho^* c_L^* \quad (2.38)$$

5. effective piezoelectric stiffness constant

$$h_{33}^* = \frac{e_{33}^*}{\epsilon_{33}^{s*}} \quad (2.39)$$

6. thickness mode electromechanical coupling coefficient for the composite plate

$$k_t^* = \frac{e_{33}^*}{\sqrt{c_{33}^{D*} \epsilon_{33}^{s*}}} = h_{33}^* \sqrt{\frac{\epsilon_{33}^{s*}}{c_{33}^{D*}}} \quad (2.40)$$

From above the behaviour of the effective acoustic impedance and electromechanical coupling coefficient can be controlled by modifying the volume fraction V_c .

2.5 Effective Electromechanical Coupling Coefficient and Aspect Ratio

The electromechanical coupling coefficient of the piezoceramics are also affected by other factors that showed the practical limitation of the highest coupling coefficient. The theoretical modelling for a slender bar of piezoceramic material was studied extensively in [16], [17]. They stated that the first factor is the intrinsic coupling coefficient factor defined by the material parameters as in Eq.2.16 and 2.17. The intrinsic factor leads to the common values for the coupling coefficients which are the the maximum coupling coefficient k_{33} for the long rod and the minimum coupling coefficient k_t for a thin plate. The second factor is the extrinsic aspect ratio factor and this introduces an intermediate coupling coefficient k_{33}' for a tall slab of piezoceramics which is smaller than k_{33} but larger than k_t . The third factor is the stiffness of the kerf filler material.

In Fig 2.2, l_1 is elevation, l_2 is the element width and l_3 is the element thickness. The aspect ratio is defined as the ratio between element thickness to the element width

$$G = \frac{l_3}{l_2} \quad (2.41)$$

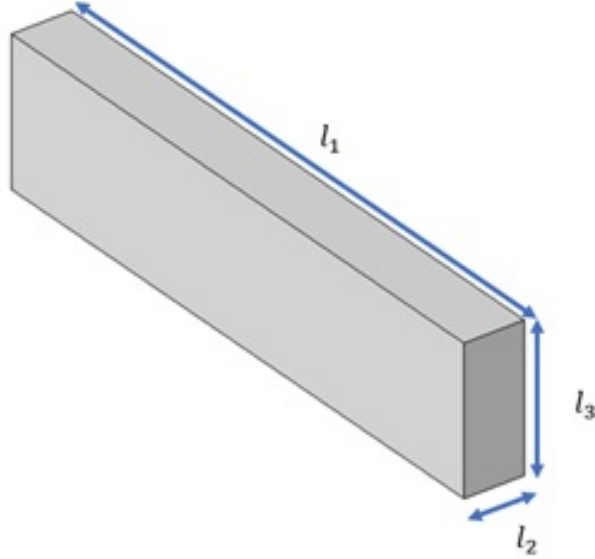


Figure 2.2: Piezoelectric slender bar for a single array element.

The electromechanical coupling coefficient as a function of aspect ratio is given by [16], [17]

$$k = \frac{U_m}{\sqrt{U_e U_d}} \quad (2.42)$$

where U_m , U_e , U_d are the mutual, elastic and dielectric energies and the full expression is:

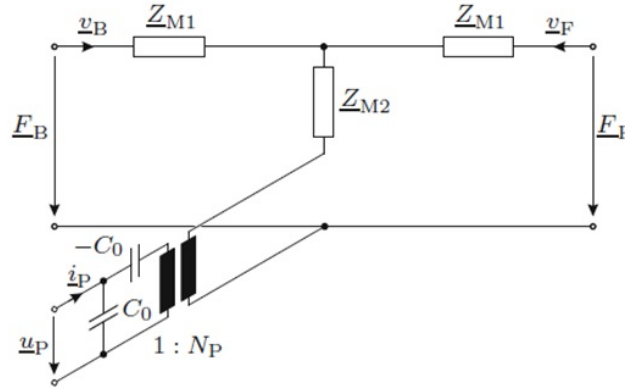
$$k = \frac{\frac{1+\sigma}{1-\sigma}(g^2(G) - 1) \frac{s_{13}^E}{s_{11}^E} d_{31} + \left(d_{33} - \frac{s_{13}^E}{s_{11}^E} d_{31} \right)}{\sqrt{\left[\frac{1+\sigma}{1-\sigma}(g^2(G) - 1) \frac{s_{13}^E{}^2}{s_{11}^E} + \left(s_{33}^E - \frac{s_{13}^E{}^2}{s_{11}^E} \right) \right] \left[\frac{1+\sigma}{1-\sigma}(g^2(G) - 1) \frac{d_{31}^2}{s_{11}^E} + \left(\varepsilon_{33}^T - d_{31}^2/s_{11}^E \right) \right]}} \quad (2.43)$$

where $\sigma = -s_{12}^E/s_{11}^E$ is the Poisson's ratio, s^E is the compliance and $g(G)$ is function of aspect ratio G . A plot of the resulting coupling coefficient for three different sets of material parameter is shown in Fig. 3.2.

2.6 One-dimensional Modelling – Xtrans

Several equivalent circuits models exist for piezoelectric transducers, the most common are the Mason model and the KLM model. In this thesis, the Xtrans package, a MATLAB program developed by the department of Circulation and Medical Imaging at NTNU is used to perform one

dimensional modelling. It is based on the equivalent circuit for the Mason model for one piezoelectric element operating in thickness mode.

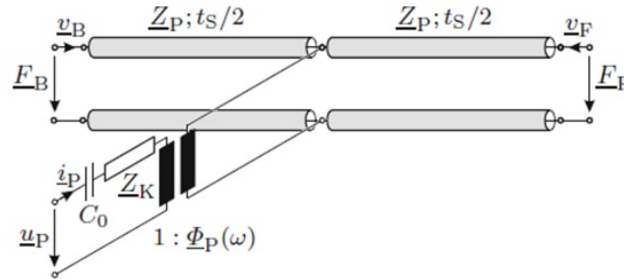


$$Z_{M1} = jZ_p \tan \frac{kt_s}{2} \qquad N_p = h_{33}C_0$$

$$Z_{M2} = -jZ_p \csc kt_s \qquad h_{33} = kt \sqrt{\frac{c_{33}^D}{\epsilon_{33}^s}}$$

$$C_0 = \frac{\epsilon_{33}^s A}{t_s}$$

Figure 2.3: Equivalent circuit for piezoelectric element at thickness extensional mode operation in Mason Model. t_s is the piezoelectric element thickness, k is the wave number. Adapted from [9]



$$\phi_p(\omega) = \frac{\omega Z_p}{2h_{33}} \csc \frac{kt_s}{2} \qquad Z_K = \frac{jh_{33}^2}{\omega^2 Z_P} \sin kt_s$$

Figure 2.4: The KLM equivalent circuit model for a piezoelectric element operating in the thickness extensional mode. Adapted from [9]

In Mason's model as shown in Fig. 2.3, the constant transmission ratio $N_p = h_{33}C_0$ and the negative capacitance $-C_0$ serves as an ideal transformer and couples the electrical port to the mechanical ports. In the KLM equivalent circuit as shown in Fig. 2.4, instead of a constant of $N_p = h_{33}C_0$, the transmission ratio is $\phi_p(\omega)$ and it is a function of frequency.

With the clamped capacitance C_0 at the electrical port of the Mason's model, Mason's model is

suites to study the electrical behaviour of the designed transducer. The KLM model can be even more suited to study the effects of additional layers in the front and back of the piezoelectric material (i.e. matching layers) since the model is based on mechanical transmission lines [9]. However, the two models are equivalent, i.e. give the same results. The effective material data for one-dimensional simulation is then calculated and put into the Xtrans package. This model represents the analytic modelling of the transducer stack. The result of acoustic impedance and electromechanical coupling coefficient becomes a function of piezoceramic volume fraction.

2.7 Finite Element Modelling

Finite element modelling (FEM) is a numerical method in solving partial differential equations (PDEs) within the relevant physics problem in two or three spatial coordinate when the physical phenomena can not be solved analytically. FEM begins by solving a set of PDEs that govern the physical processes with boundary and initial conditions. Then, using spatial discretisation, FEM deconstructs the model body's complex geometry into smaller bodies as finite elements. These finite points result in a simultaneous algebraic system of equations that can be approximated to the true solution. In this work, a 2D model of the design transducer was developed and simulated using FEM. When compared to the one-dimensional Mason model, it allowed for the investigation of any 2D effects, most notably lateral modes within the composite structure.

The steps of finite element modelling are as follow:

- Define the physics involved in the problem. In this study, the physics involved are piezoelectricity, solid mechanics and electrostatics. This is illustrated in the constitutive equation in Eq. 2.14 which couples the all three of these physics domain.
- Define the geometric properties of the model according to the transducer design as mention in previous section.
- Define the material properties of every model elements. For piezoelectric material, it was described as the stiffness matrix as in Eq. 2.15. For polymer material, it was described by Young's modulus and Poisson's ratio as in Eq. 2.29.
- Define the boundary conditions that describes the modelling phenomena.
- Define the mesh of the model. High solution accuracy requires convergence of the solution. This is affected by the mesh shape and density.
- Compute and derive relevant variables and quantities

Chapter 3

Materials and Methods

This chapter introduces the relevant calculations of all the materials and the subsequent modelling methods with a summary of all material used in this work. Fig. 3.1 presents the entire process flow of piezocomposite fabrication. Section 3.1 covers all essential piezoceramic and filler polymer material parameters. Sections 3.2 and 3.3 outline the one-dimensional and two-dimensional, finite element modeling techniques. Sec 3.4 presents general composite manufacturing processes using USN laboratory equipment, which is further described in Appendix A. Sec 3.5 provides a brief description of the Characterization approach.

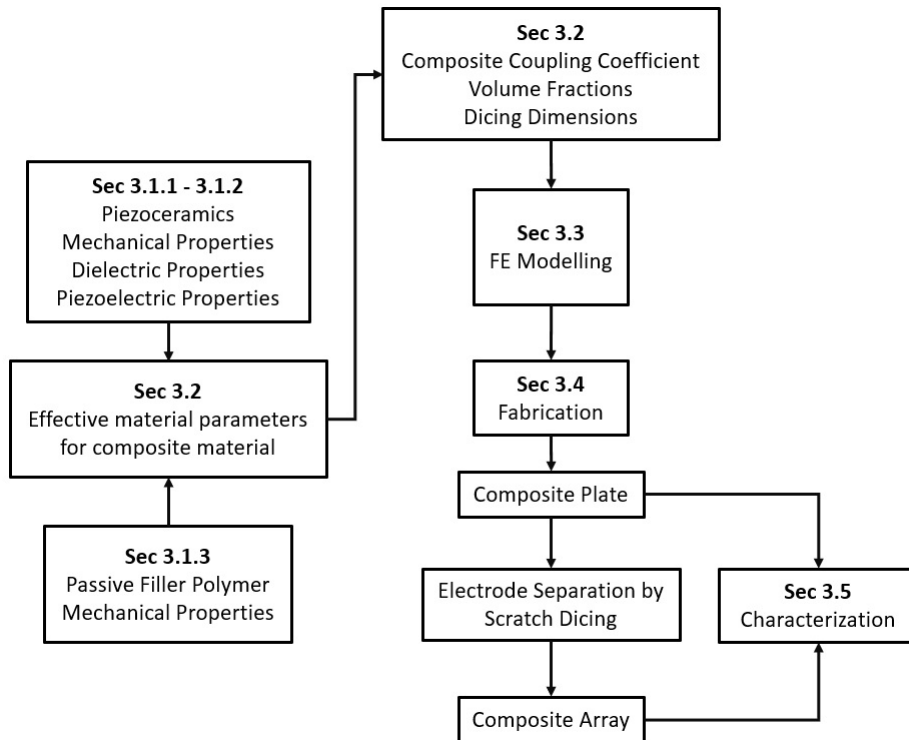


Figure 3.1: Process flow for the fabrication of the 2-2 piezocomposite.

3.1 Material Parameters

3.1.1 Active Piezoceramic - Pz27

In this thesis, the active piezoceramics was chosen as Pz27 disks (FerroPerm A/S) with a radius of 5 mm and a thickness of 1 mm. Its resonant frequency at this stage was 2 MHz. Pz27 is often found in acoustic transducers, accelerometers and other applications as it provides good coupling and stable performance. The material parameters are often readily available from the manufacturer; however, a more accurate value should be obtained by curve fitting to closely model the fabricated samples. Table 3.1 lists all relevant material parameters of Pz27.

Table 3.1: Material parameter of the piezoceramic Pz27 obtained from three different sources. The last lines give the electromechanical coupling constant k for a slender bar for different values of the aspect ratio G .

Parameter	FerroPerm A/S [18]	Perez et al.[19]	Storheim et al. [20]
c_{11}^E [$10^{10} N/m^2$]	14.7	$11.8(1 + 0.0474i)$	$11.875(1 + 0.0104i)$
c_{12}^E [$10^{10} N/m^2$]	10.5	$7.49(1 + 0.0005i)$	$7.43(1 + 0.0140i)$
c_{13}^E [$10^{10} N/m^2$]	9.37	$7.38(1 + 0.0003i)$	$7.425(1 + 0.083i)$
c_{33}^E [$10^{10} N/m^2$]	11.3	$11.04(1 + 0.043i)$	$11.205(1 + 0.056i)$
c_{44}^E [$10^{10} N/m^2$]	2.3	$2.03(1 + 0.0178i)$	$2.11(1 + 0.0133i)$
e_{13} [C/m^2]	-3.09	$-5.1(1 - 0.0001i)$	$-5.4(1 - 0.0060i)$
e_{33} [C/m^2]	16.02	$16.0(1 - 0.0024i)$	$16.04(1 - 0.0031i)$
e_{15} [C/m^2]	11.64	$11.2(1 - 0.0089i)$	$11.2(1 - 0.0050i)$
$\varepsilon_{11}^S/\varepsilon_0$	1130	$984(1 - 0.0001i)$	$916(1 - 0.0200i)$
$\varepsilon_{33}^S/\varepsilon_0$	914	$830(1 - 0.0133i)$	$920(1 - 0.0116i)$
Q_m	73	—	—
$\tan \delta$	0.017	—	—
ρ_{piezo} [kg/m^3]	7700	7707	7700
k_{33}	0.699	0.700	0.684
k at $G = 8.5$	0.652	0.655	0.636
k'_{33} or k at $G \rightarrow \infty$	0.653	0.655	0.637
k_t or k at $G \rightarrow 0$	0.468	0.490	0.469

c_{ij}^E are the stiffness constants at constant electric field, e_{ij} are the piezoelectric stress constants, ε_{ij}^S are the relative permittivities, and ρ_{piezo} is the density of the piezoceramic. Mechanical and dielectric losses from the FerroPerm A/S are represented by the mechanical quality factor Q_m and

the loss tangent. G denotes the aspect ratio of a slender bar material(i.e. thickness to width ratio)

Three sets of material parameters were tested. The first set of data was based on the material data sheet from the manufacturer FerroPerm A/S [18]. The second set of data was based on the results published by Perez et al. [19]. The last set of data was based on the data from the research group in University of Bergen published by Storheim et al.[20]. These data were used for fitting our measurement results. Relevant values of the electromechanical coupling coefficients of the Pz27 obtained from [18] and contribution due to aspect ratio from Sec. 2.5 are also listed in Table 3.1.

Losses for Perez et al. and Storheim et al. are represented by the complex value. For this thesis, the parameters from Perez et al. were used as the main material fitting parameters, as these are results from a well-conducted study published in *Ultrasonics* in 2014, and were assumed to be the most reliable and verified data set. The data from Storheim et al. was part of a master thesis done in UiB, 2010 and were added here for comparison. Note that there are a 20% to 30% difference in the elastic stiffness between the manufacturer's data to the other two sets of parameters. The difference between each set of parameters is discussed in the following chapters. The resulting electromechanical coupling coefficients from three sets of data are also calculated from Fig. 3.2 and tabulated in Table 3.1. k_{33} is the coupling of a free rod, k is the coupling of a slender bar as a function of its aspect ratio G , k'_{33} or k at $G \rightarrow \infty$ is the coupling when aspect ratio G approaches infinity (i.e. infinitely slender bar) and k_t is the coupling of a thin plate (i.e. $G \rightarrow 0$). The slender bar model is of special interest in this thesis as can represent one element in a one-dimensional linear array or one line in a 2-2 connectivity piezocomposite.

From the parameters as listed in 3.1, the relevant parameters for one-dimensional Xtrans modelling of the bulk Pz27 disk are listed below in Table 3.2.

Table 3.2: Fitting of material parameters of bulk Pz27 disk for one-dimensional modelling

Parameter	FerroPerm A/S [18]	Perez et al.[19]	Storheim et al.[20]
A [mm^2]	706	706	706
h_{33} [$10^8 V/m$]	19.8	21.8	19.7
$\varepsilon^S/\varepsilon_0$	914	913.7	920
Z [$MRayls$]	33.37	33.46	33.26
c_l [m/s]	4334	4341	4319

3.1.2 Electromechanical Coupling Coefficient and Aspect Ratio of Pz27

For the Pz27 in use, a plot of its electromechanical coupling coefficient as a function of aspect ratio is illustrated in Fig. 3.2 and the relevant coupling values are listed in Table 3.1. The highest and lowest coupling are also illustrated by the dashed asymptotes. For Pz27, the highest coupling for

a slender bar is therefore at the range of 0.64 to 0.66 depending on the set of the material parameters. For Pz27 FerroPerm A/S, the highest achievable coupling is thus 0.653 for an infinitely slender bar.

Based on the dicing dimensions as described above, the sample to be fabricated has an aspect ratio of:

$$G = \frac{l_3}{l_2} = \frac{724\mu\text{m}}{85\mu\text{m}} = 8.5 \quad (3.1)$$

resulting in effective electromechanical coupling of 0.652 for Pz27 as shown in Fig. 3.2 with the material parameters of Pz27 FerroPerm A/S.

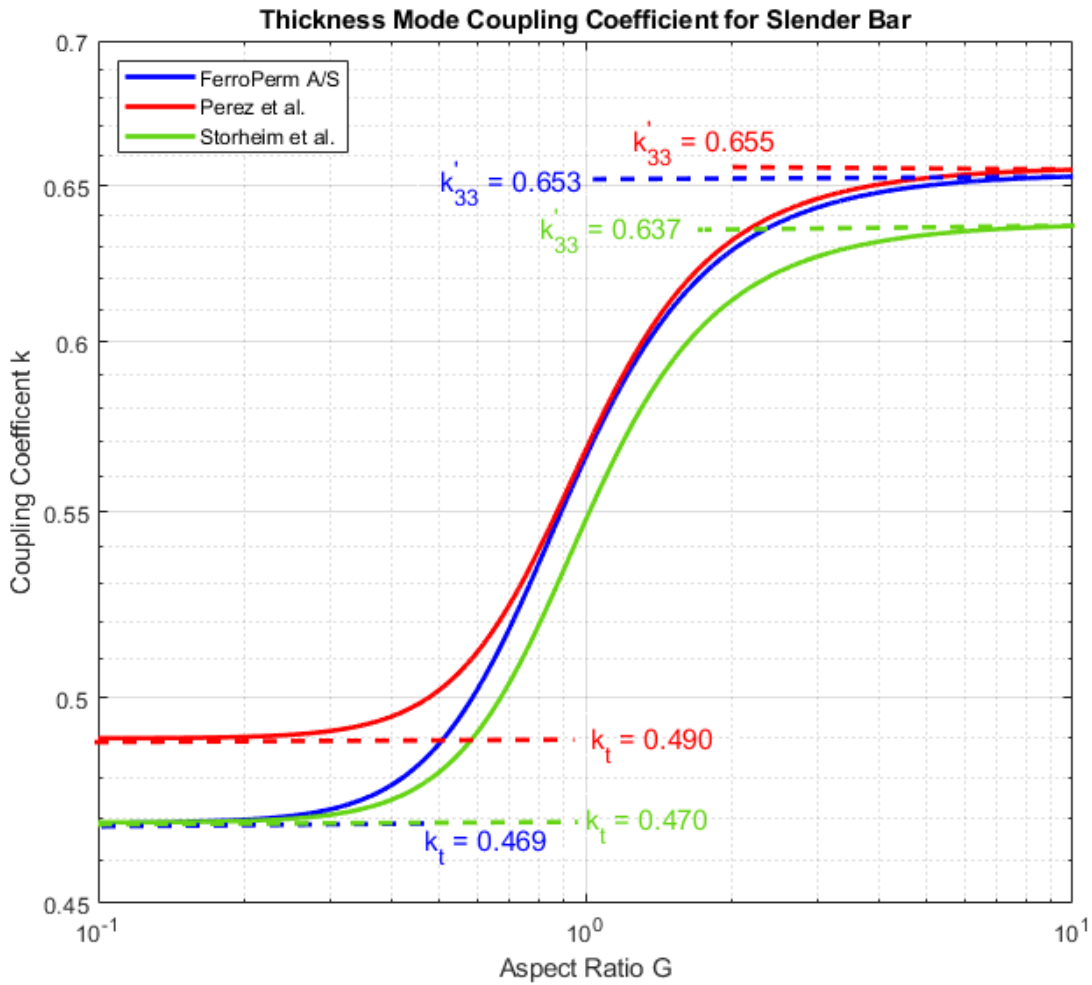


Figure 3.2: Effective electromechanical coupling coefficient as a function of aspect ratio of a pure slender bar with no kerf filler. The slender bar coupling k'_{33} and thin plate coupling k_t are calculated for three different set of material parameters. The blue curve indicates coupling with the material parameter set of FerroPerm A/S. The red curve indicates coupling with the material parameter set of Perez et al. The green curve indicates the coupling with the material parameter set of Storheim et al. The values approaching to the infinite slender bar are listed in Table 3.1 for comparison.

In comparison, the coupling for a free long rod is 0.69, as specified by the manufacturer, while the coupling for a slender bar is 0.652 at $G = 8.5$, which is almost 96% of the coupling for a free long rod. The slender bar coupling in this transducer design can therefore obtain a value that approaches the value of an infinitely slender bar ($k_t' = 0.653$) with an aspect ratio of 8.5. Note that on the opposite side where $G \rightarrow 0$, the coupling approaches the values of k_t which corresponds to the thin plate coupling and Eq. 2.24 becomes 2.16 as stated in [16]. In Chapter 4 and 5, the final measured coupling coefficient of the manufactured sample, as well as the comparison of all theoretical and experimental values, will be explained.

3.1.3 Passive Filler Polymer - EpoTek 3012 and RTV 3140

For this thesis, a non-conductive epoxy EpoTek 3012 (Epoxy Technology Inc. Billerica, MA, United States) [21] and RTV 3140 Silicone Rubber RTV Coating, Non-Corrosive Silicone Rubber (DOW CORNING®), Midland, MI, United States) [22] are selected as the polymer fillers. The materials were chosen as examples of two representatives of material types used in kerf fillers in piezocomposites. EpoTek 3012 is an epoxy that provides high structural stability but suppresses piezoelectric material motion. It's also a well-studied kerf filling material for ultrasonic transducers that's easily available at USN's lab. RTV 3140 is a softer silicone substance that allows the piezoelectric to move more freely, but it lacks structural stability and is relatively lossy. By comparing the composite with two material with different mechanical properties (i.e. stiffness, longitudinal and shear velocity), we can analyse its effect on the transducer performance (i.e. electrical behaviour) qualitatively and quantitatively.

In order to obtain the material parameters of the two polymers, two approaches were used. The manufacturer provided the material specifications for EpoTek 3012, which are described in Table 3.3. The material parameters of RTV 3140 Silicone were found to be more difficult to acquire, and the original technique for obtaining the values was to perform a speed of sound measurement in USN's measuring setup, as described in Tran's master's thesis [23].

The material parameters of EpoTek 3012 and RTV 3140 are listed in Table 3.3. For Epotek 3012, the value of longitudinal velocity were measured using the Speed of Sound measurement setup at USN ultrasound lab and the shear velocity are approximated to be 45% as described in [13]. The longitudinal and shear velocity were then used to calculate the Young's modulus and Poisson's ratio required to obtain the effective material parameters for the one-dimensional Mason model. For RTV 3140, the longitudinal and shear velocity can not be measured effectively due to the limitation in lab equipment for degassing. Therefore, the Young's modulus E , Poisson's ratio ν longitudinal velocity c_l and shear velocity c_s are obtained from typical values of published literature in [24] and [25].

Table 3.3: Material Parameter of passive polymer filler EpoTek 3012 & RTV 3140 silicon rubber

Properties	Symbols	EpoTek 3012	RTV 3140
Density	$\rho_{filler} [kg/m^3]$	1147*	1050 [22]
Young's Modulus	$E [GPa]$	4.10***	0.0018***
Poisson's Ratio	ν	0.37 [13]	0.49 [26]
Long. Velocity	$c_l [m/s]$	2587*	1000***
Shear Velocity	$c_s [m/s]$	1164**	90***
Rel. Permittivity	ϵ	3.8 [21]	2.57 [22]

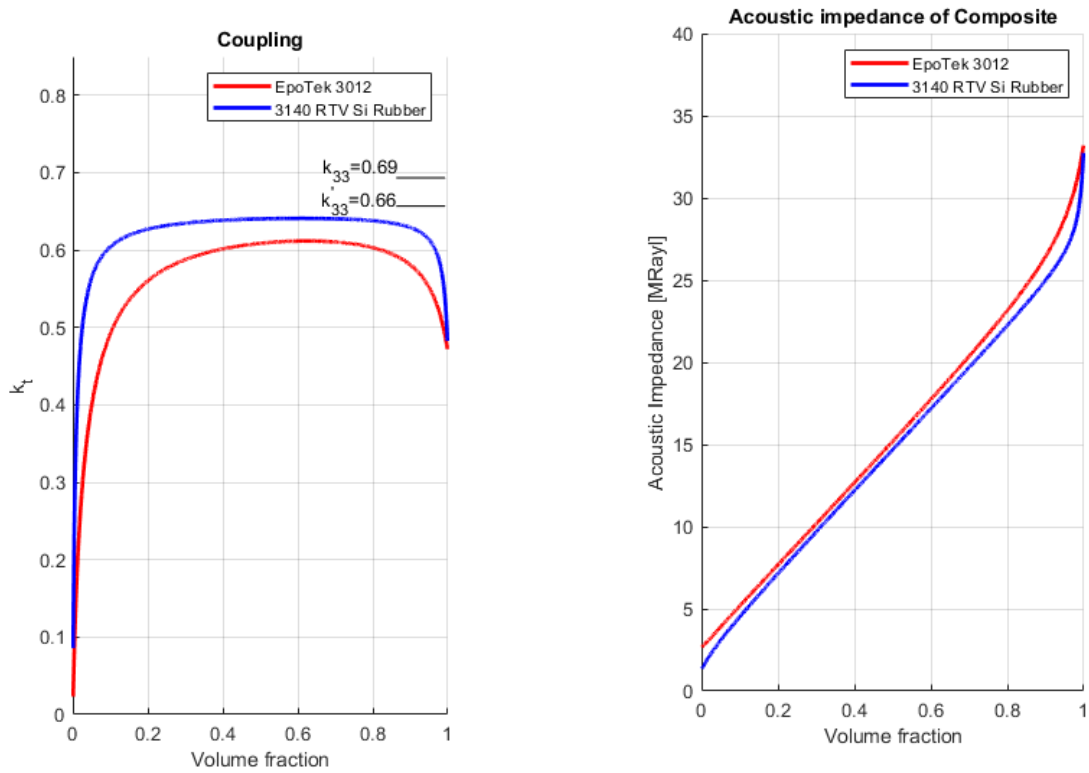
* Measured at the USN ultrasound lab.

** The values can be approximated to be 45% of the longitudinal velocity [13].

*** Typical values measured for RTV silicone rubber by [24] and [25]

3.2 Piezocomposite Design

This section presents the composite design of a 2-2 piezocomposite material fabricated by the dice-and-fill method. A piezocomposite material is made up of two parts: active piezoceramics and passive polymer filler. Air backing was chosen for this work due to its ability to achieve high sensitivity. The coupling coefficient and acoustic impedance are key factors in defining the behavior of piezocomposite design, and they are functions of volume fraction based on the analytical model provided by [14], [15] in Sec 2.4. The objective of piezocomposite design is to get the highest thickness mode coupling coefficient by modifying the volume fraction. Fig. 3.3 illustrated the theoretical coupling coefficient with active piezoceramic Pz27 and two passive polymer filler EpoTek 3012 and RTV 3140 were calculated. The curves are calculated using Eq. 2.40 and 2.38 based on the material data given in Table 3.1 and 3.3.



(a) Theoretical coupling coefficient as a function of volume fraction for Pz27 with the two kerf filler materials. (b) Theoretical characteristic acoustic impedance as a function of volume fraction fraction for Pz27 with the two kerf filler materials.

Figure 3.3: Theoretical electromechanical coupling coefficient and effective acoustic impedance as a function of piezoceramic volume fraction V_c . k_{33} is the coupling of the piezoceramic as a thin rod, given by the manufacturer's data sheet [18]. k'_{33} is the coupling of the piezoceramic as a infinitely slender bar and it is also the highest achievable coupling in a 2-2 composite after fabrication.

Fig. 3.3 illustrates that if the volume fraction equals to 1 (i.e. a bulk piezoelectric plate), the coupling coefficient reaches the thin plate coupling coefficient $k_t = 0.47$. If the volume fraction is close to zero, it corresponds to a simple polymer which has no piezoelectric characteristics and thus $k_t \rightarrow 0$. For the epoxy material EpoTek 3012, the coupling coefficient reaches its maximum at approximately 0.61 for a volume fraction of approximately 0.68, as calculated in Fig. 3.3. Similar results are obtained for the composite with a soft silicone polymer, RTV 3140 and the maximum coupling constant with this softer filler is 0.64, somewhat larger than for the epoxy filler, and is seen over a wide range in volume fractions from 0.5 to 0.7. Thus, a volume fraction of 0.68 was chosen for the piezocomposite design with both polymer filler EpoTek 3012 and RTV 3140 so that the dicing dimensions are identical for both fillers which simplifies dicing procedures while at this volume fraction the highest coupling k_t can still be achieved for both polymer filler.

The theoretical characteristic acoustic impedance for both polymers are around 20 MRayl at volume fraction of 0.68. The calculated effective composite material parameter from Sec. 3.1 for one-dimensional Mason model of the piezocomposite material are listed below in Table 3.4 with active piezoceramic Pz27 from Perez et al. in Table 3.1 and polymer filler EpoTek 3012 and RTV 3140 from Table 3.3. The material values for the bulk Pz27 was also listed as a comparison to the composite plate.

Table 3.4: Fitting of material parameters of the bulk Pz27, EpoTek 3012-filled and RTV 3140-filled piezocomposite for one-dimensional Mason modelling in Xtrans.

Parameter	Bulk Pz27	Pz27 w/ EpoTek 3012	Pz27 w/ RTV 3140
$A [mm^2]$	706	224	42
$h_{33} [10^8 V/m]$	21.8	24.6	25.2
$\varepsilon^S/\varepsilon_0$	913.7	583	582
$Z [MRayls]$	33.46	21.7	20.9
$c_l [m/s]$	4341	3880	3745

Next, the design of the dicing dimension depends on resonance frequency and volume fraction. Frequency determines the final thickness of the piezocomposite using the half-wave resonance in Eq. 2.23. Volume fraction determines the width of polymer filler and width of piezoceramic. Fig. 3.4 shows the top view of the dimensions of piezoceramics and polymer filler with the kerf filler width (i.e. w_{filler}) and piezoceramic width (i.e. w_{piezo}).

Since the thickness mode vibration should be the only excited mode, other undesired vibrational modes will negatively affect the thickness mode vibration as they produce unwanted mechanical and

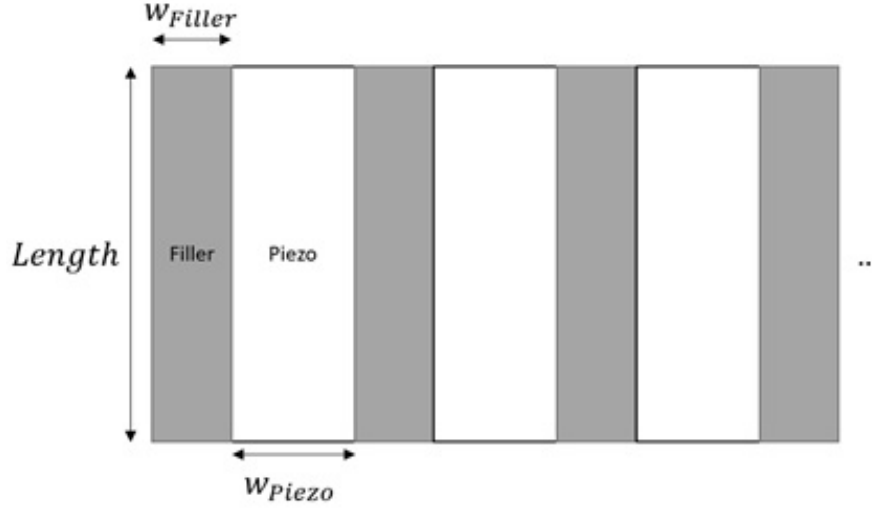


Figure 3.4: Top view of the 2-2 dicing scheme of a piezocomposite. This is visually similar to a transducer array, but it is important to distinguish that for a piezocomposite, several piezoceramics and kerf filler are excited together. For a transducer array, only a single piezoceramic is excited.

electrical outputs. The lateral periodicity produces lateral resonances by Lamb-type wave reflections from within the microstructure.

To reduce the effect of lateral resonances within the periodic composite structure, there are two conditions. First, the lateral resonances are kept above twice the center frequency since the composite is assumed to be operating in a broadband bandwidth as stated in the guidelines provided by Ritter et al. in [27]. Second, for a 2-2 composite with high volume fraction as in the case of this work, the first lateral resonance is determined by the half wavelength resonance for a longitudinal wave across the width of the ceramic. As a result, to minimize the lateral coupling, the initial design width requirement for a 2-2 composite array follows the guidelines in [27] where the lateral resonance are above twice the center frequency and are thus the maximum allowable spatial dimension of a periodic composite are defined as

$$\text{Ceramic Width} \leq \frac{c_w}{2 \times 2 \times f_c} \quad (3.2)$$

where f_c is the device center frequency and c_w is the longitudinal wave velocity for width resonance of the piezoceramic and it is

$$c_w = \sqrt{\frac{c_{11}^E}{\rho_{piezo}}}. \quad (3.3)$$

where c_{11}^E and ρ_{piezo} are the stiffness and density of the piezoceramic. As stated in the guideline of [27] with c_w obtained from equation 2.30 and 3.3, the requirement for the maximum width size are

$$\text{Ceramic Width} \leq \frac{c_w}{2 \times 2 \times f_c} = \frac{4369 \text{ m/s}}{4 \times 2 \text{ MHz}} \approx 546 \mu\text{m} \quad (3.4)$$

where f_c is the device center frequency.

The kerf width is dictated by the availability of dicing blades, the thinnest available in USN's lab was the 40 μm diamond blade (Z09-SD1700-Y1-60, 53.4 \times 0.033AS \times 40) resulting in a kerf width of 40 μm , giving the following composite width dimensions

$$\begin{aligned} \text{Kerf width} &= 40 \mu\text{m} \\ \text{Ceramic Width} &= \frac{V_c}{V_p} \times \text{Kerf width} = \frac{0.68}{0.32} \times 40\mu\text{m} = 85 \mu\text{m} \end{aligned} \quad (3.5)$$

These cut dimensions were well below the threshold as calculated in Eq. 3.4 and lead to a volume fraction of 0.68 ideally but one should perform test cuts on dummy samples to obtain the actual cutting widths produced by the dicing saw. w_{filler} was designed to have a width of 40 μm as in the dicing blade available in the laboratory, which gives the value of w_{piezo} to be 85 μm . The final dicing dimension tested on a dummy sample produced a kerf close to 40 μm and a pitch of 85 μm and making the final volume fraction as 0.68. The initial design parameters of the 2-2 piezocomposite array are listed in Table 3.5.

Table 3.5: Early design goal of the 2-2 piezocomposite array

Active Piezoceramic	Pz27
Passive Polymer Filler	EpoTek 3012 and RTV 3140
Center Frequency	2 MHz
Thickness	0.724 mm
Volume fraction	0.68
Kerf	40 μm
Piezo Width	85 μm
Pitch	250 μm (0.51 λ in water)
Dimension	15 \times 20 mm ²

3.3 Finite Element Modelling

This section presents the finite element modelling of the transducer structure at each fabrication step , 1) Bulk Plate, 2) Air Kerf, 3) Composite Plate, 4) Composite Array, 5) DHUT, and an addition study 6) Oblique Dicing. Finite element modeling was done with COMSOL Multiphysics 5.5 (COMSOL AB, Stockholm, Sweden). The Acoustic-Piezoelectric Interaction Physics Package solves interaction between acoustic pressure and structural deformation in solid and piezoelectric domains with *Pressure Acoustics*, *Solid Mechanics* and *Electrostatics* interfaces. In this study, only *Solid Mechanics* and *Electrostatics* were used to model the transducer behaviour.

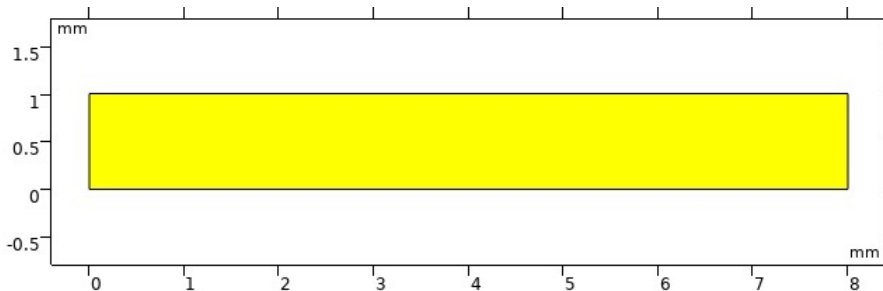
The main material parameters for all modelling methods were listed in Chapter 3. The electrical impedance Z was calculated by dividing the potential difference V between the top and bottom electrodes and the current I . Current I was calculated by:

$$I = L \int_0^{w_{piezo}} j_y dx \quad (3.6)$$

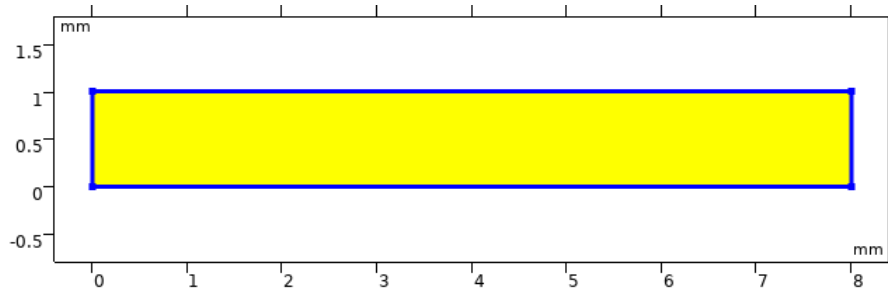
where j_y is the y-component current density, w_{piezo} is the piezoelectric material width, and $L = 16$ mm is the length of the active element.

3.3.1 Bulk Plate Pz27

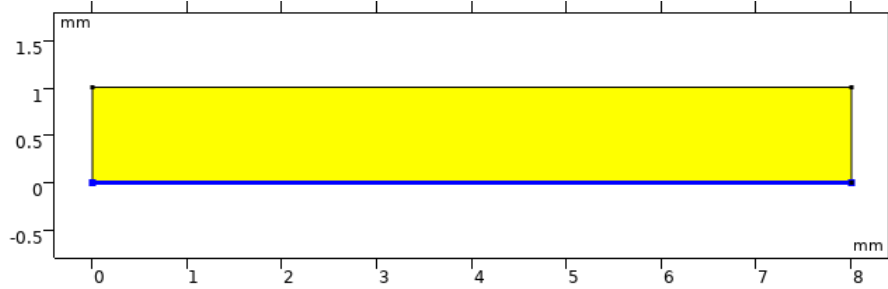
In this section, the model presents a simple structure of a Pz27 sample as shown in Fig. 3.5. Colour yellow indicates Pz27 material. The COMSOL physics domains of *Solid Mechanics (Piezoelectric Effect)* and *Electrostatics* were selected to the entire structure. In the *Solid Mechanics* domain, the boundary condition *Free* was selected for top and bottom and *Periodic Condition* was selected on the sides. In the *Electrostatics* domain, one element on top was connected to the *Terminal* with 1V setting and the plate bottom was connected to *Ground*. The mapped mesh was selected with *Extra Fine* setting. The model was computed in the frequency domain from 0.1 to 10 MHz with a step frequency of 0.01 MHz. The dimensions are shown in Table 3.6.



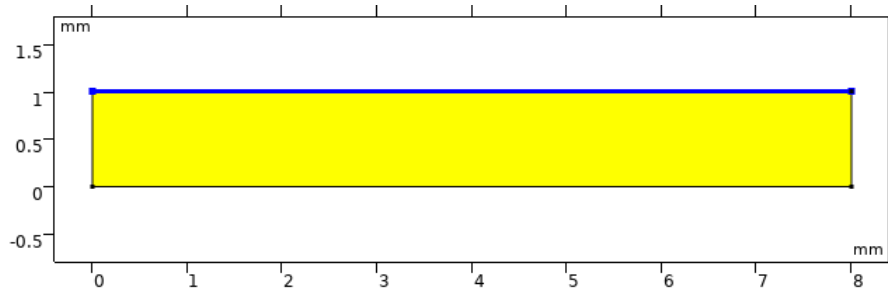
(a) Model structure



(b) Free - Solid Mechanics



(c) Terminal



(d) Ground

Figure 3.5: COMSOL Model and the meshed result of a bulk Pz27 plate.

3.3.2 Diced Pz27 with Air Kerf

In this section, the model represents a structure of a shallow diced Pz27 sample with repeating diced elements connected by a base support as shown in Fig. 3.6. The complete model structure has 160 individual piezoceramic fingers but only a section of the model is shown in Fig. 3.6 for illustration purposes. Table 3-1 shows the relevant features for this model. Physics domains of *Solid Mechanics (Piezoelectric Effect)* and *Electrostatics* were selected to all structure. In the *Solid Mechanics* domain, the *Free* boundary condition was selected for all boundaries. In *Electrostatics* domain, one element on top was connected to the *Terminal* and the plate bottom was connected to *Ground*. Mapped mesh was selected with *Extra Fine* setting. Model was computed in frequency domain from 0.1 to 10 MHz with step frequency of 0.01 MHz.

Table 3.6: FEM model properties for a shallow diced air kerf Pz27

Material	Pz27
Thickness – Element	0.85 <i>mm</i>
Thickness – Plate	0.15 <i>mm</i>
No. of Pillars	160
Element Width	85 μm

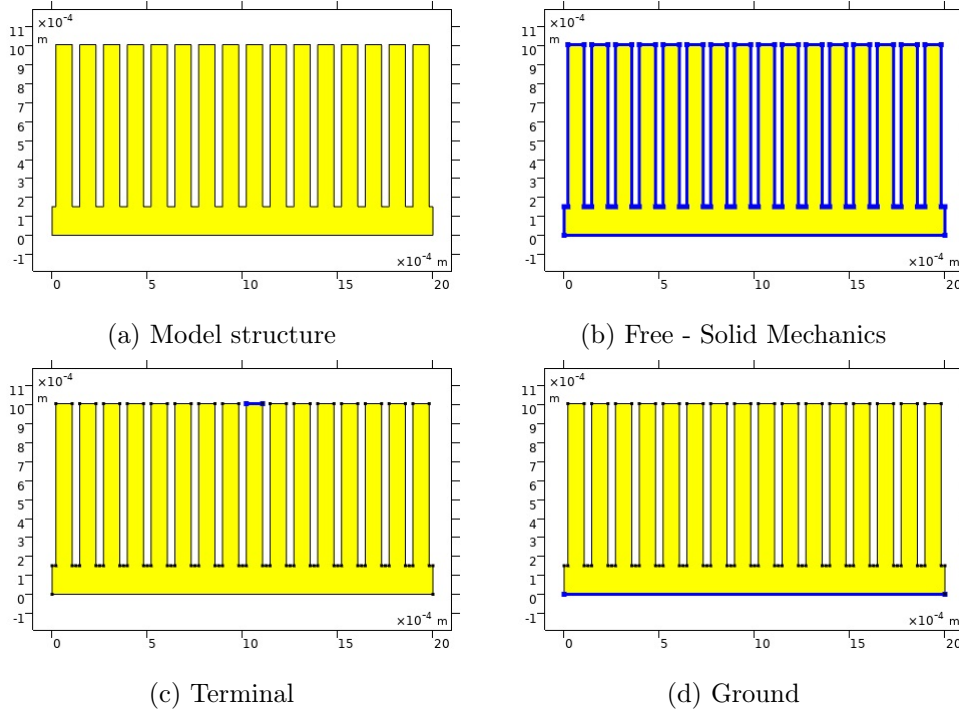


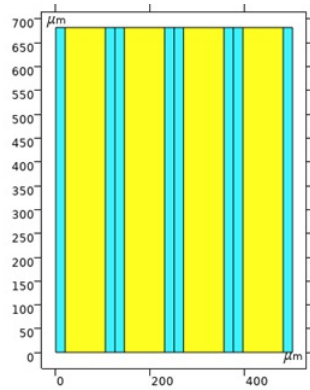
Figure 3.6: COMSOL model of a shallow-diced air kerf Pz27. The simulation model has 160 individual pillars and only part of the complete model is shown here for illustration

3.3.3 Composite Plate

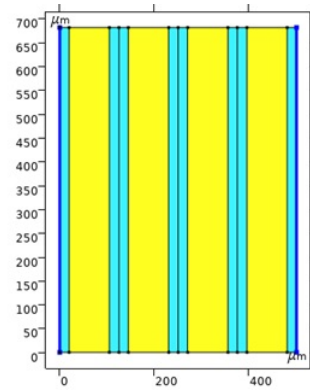
In this section, the model presents the structure of the lapped and filled composite fingers as shown in Fig. 3.7. Colour cyan indicates filler material (i.e. EpoTek 3012 & RTV 3140). Table 3-2 shows the relevant features. For a transducer loaded by air, the physics domains of *Solid Mechanics* (*Piezoelectric Effect*) and *Electrostatics* were selected to both materials. In the *Solid Mechanics* domain, the *Free* boundary condition was selected for the top and bottom boundary and *Periodic Condition* was selected to the sides of the structure. In *Electrostatics* domain, the top boundaries of Pz27 and filler were connected to the *Terminal* and the bottom was connected to the *ground*. The mesh was mapped with the *Extra Fine* setting. The model was computed in the frequency domain from 0.1 to 6 MHz with step frequency of 0.01 MHz.

Table 3.7: FEM model properties for the composite plate

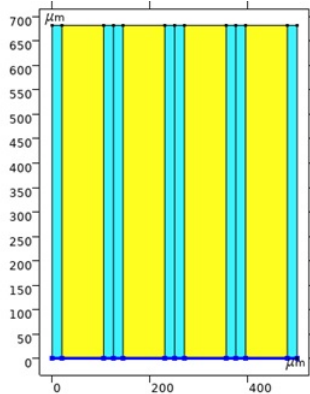
Piezoceramic Width	85 μm
Piezoceramic Thickness	724 μm
Kerf Width	40 μm
Kerf Thickness	724 μm



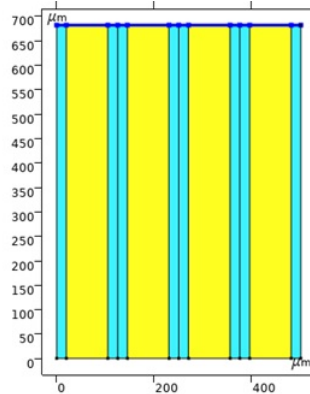
(a) Model structure



(b) Periodic Condition in Solid Mechanics



(c) Terminal



(d) Ground

Figure 3.7: COMSOL model of a composite plate.

3.3.4 Composite Array

The physical structures of a 2-2 composite plate and a one-dimensional linear array are very similar, the main difference is the electrode arrangement. The model for the composite array shown in Fig. 3.8, and is similar to that of a composite plate, except for the electrode. One single composite element is defined as two piezoelectric layers of Pz27 sandwiched by layers of kerf filler layers (EpoTek 3012 or RTV 3140) as shown in Fig. 3.8. The total width of a single composite element is 250 μm and the electrode separation is 125 μm , and the pitch is therefore 375 μm , corresponding to 0.51λ in water at 2 MHz.

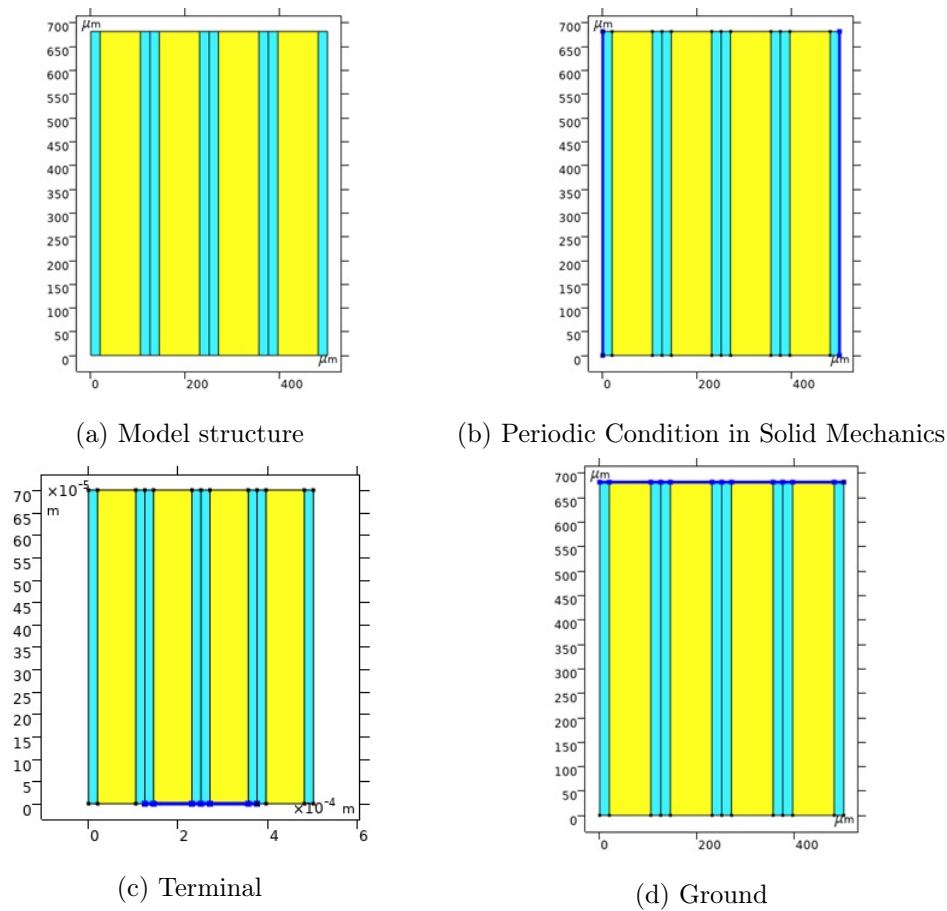


Figure 3.8: COMSOL model of a composite array element.

The transducer was assumed to be operated as a phased array with minimal grating lobes, so that the pitch is about or less than one-half of a wavelength in water at 2 MHz; thus, a pitch of $375 \mu\text{m}$ is desired. Furthermore, because the size of two piezoelectric bars with three kerf layers is approximately $250 \mu\text{m}$, and because of the ease of manufacturing and access to the $120 \mu\text{m}$ dicing blade at USN's laboratory, an array element with a size of approximately $250 \mu\text{m}$ and a separation distance of $120 \mu\text{m}$, resulting in a pitch of $375 \mu\text{m}$, may be readily produced by using a dicing blade of $120 \mu\text{m}$.

3.3.5 Oblique Dicing

In this additional section, the model represents an oblique dicing variation leading to non-vertical side walls of piezoceramic fingers. This section is added since minor oblique dicing effect was observed during fabrication and this study serves to identify if this effect will influence the behaviour of the piezocomposite. Fig. 3.9 shows the trapezoidal structures by increasing the deviation angles from vertical 0° to 3° deviation. The volume fraction was kept constant by keeping the area of the structure constant. Physics domains, mesh and frequency domain study were similar as in Sec 3.2.1.

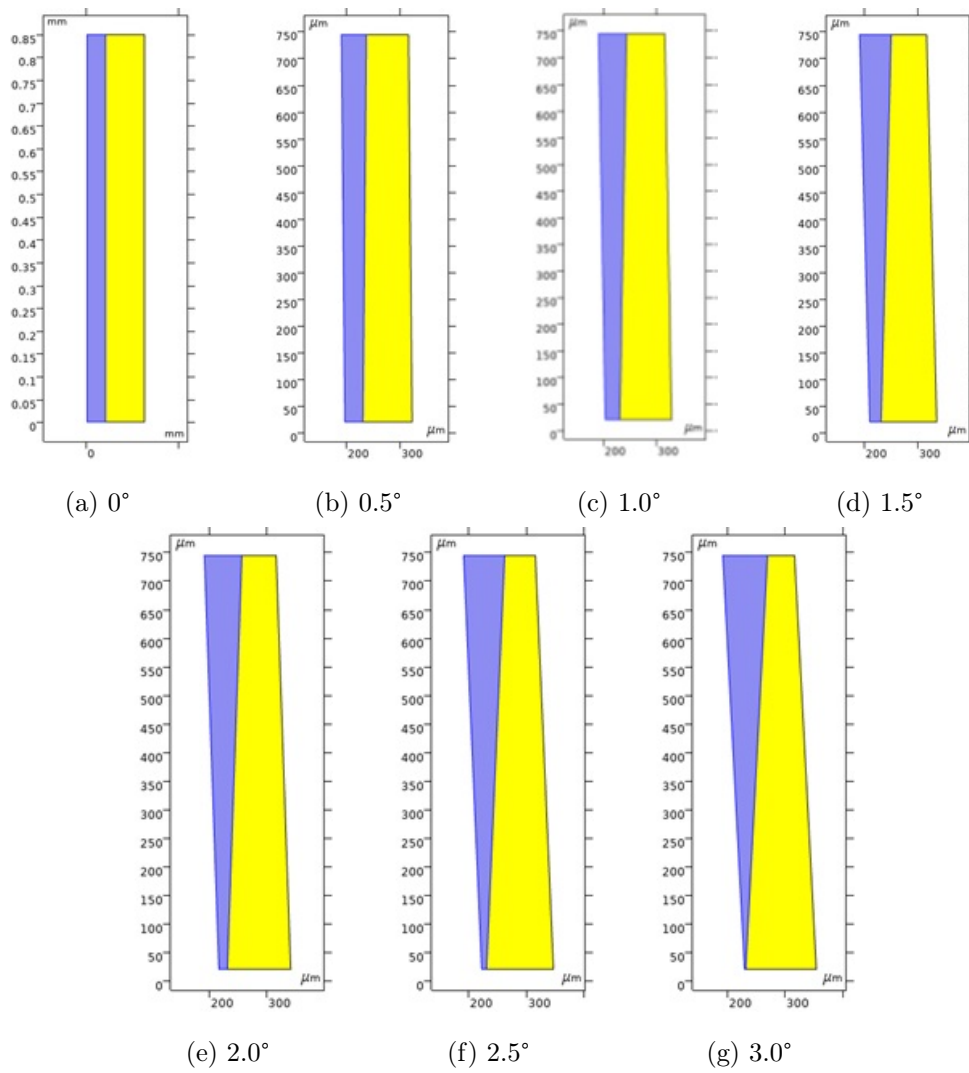
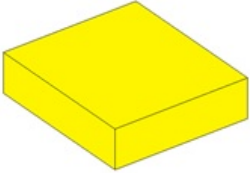
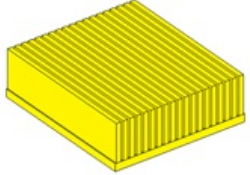
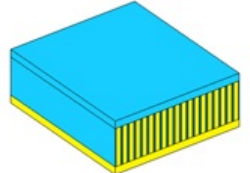
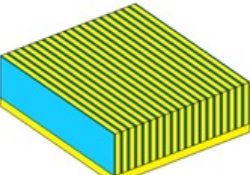
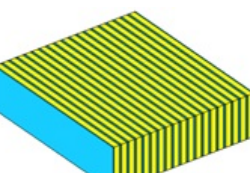


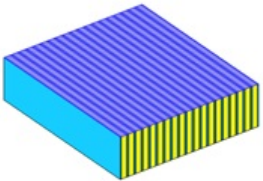
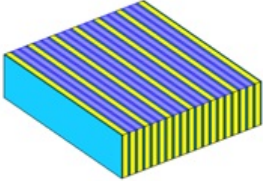
Figure 3.9: Oblique dicing at different deviation angles. Yellow is piezoceramics, blue is kerf.

3.4 Composite Plate and Array Fabrication

The general steps of composite manufacture are illustrated in Table 3.8 and. A detailed step by step procedures are described in the Appendix. The composite was fabricated by a dice and fill method. The piezoceramics was diced by Disco DAD 3220 dicing saw, (Disco Corporation, Tokyo, Japan). The composite was lapped with MultiPrep™ System, Allied High Tech Products Inc., CA, United States). Sample surface inspection throughout the fabrication was done using optical microscope Leica DM4000M (Leica Camera AG, Wetzlar, Germany), optical microscope Neophot 32 (Carl Zeiss AG, Jena, Germany), scanning electron microscope SU 3500 (Hitachi, Tokyo, Japan) and scanning acoustic microscope SAM 300 (PVA TePLA, Wetztenberg, Germany).

Table 3.8: General procedure for fabricating a 2-2 piezocomposite plate.

Steps	Process	Illustration
Step 1	PZT sample. Clean the surface with isopropyl alcohol (Yellow – Pz27)	
Step 2	Dice a shallow thickness. Do not dice through, but leave the plate intact at the bottom for support. Performed with Disco DAD 3220, (Disco Corporation, Tokyo, Japan).	
Step 3	Fill the kerf with polymer filler, degas and cure (Cyan – Kerf filler)	
Step 4	Inspect the cross section to identify the uniform region inside the filled kerf and Remove excess epoxy.	
Step 5	Lap the bottom PZT support layer to reach final thickness. Performed with MultiPrep™ System, Allied High Tech Products Inc., CA, United States)	

Step 6	Electrode metallization by sputtering on the top and bottom face (Blue – Metallization). Perform with Sputter AJA (AJA International Inc., MA, United States)	
Step 7	Array element separation by scratch dicing the electrode away (Blue - Metallization)	

3.5 Characterization Methods

The electrical impedance magnitude and phase angle of the composite plate were measured in air using a network analyser (Rohde & Schwarz ZVL, Munich, Germany) with a medical needle probe as shown in Fig 3.10. The frequency range was calibrated to 0.1 to 10 MHz or 0.1 to 6 MHz with 1600 data points. The measurement data were acquired by a PC-type computer running LabVIEW (National Instruments Corp. Austin, TX) and saved to disk. Further analysis was done offline using MATLAB. The measurements were done in air, corresponding to no loading. The network analyser was calibrated at the probe tip under in open, short and 50Ω load termination.

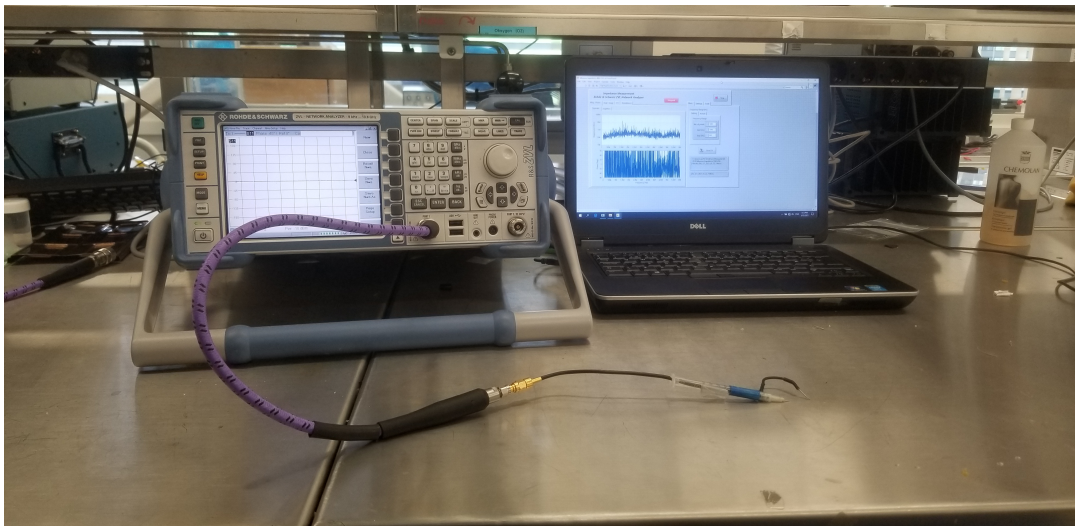


Figure 3.10: Set up for the electrical impedance measurement. The network analyzer was calibrated for the medical needle probe.

Chapter 4

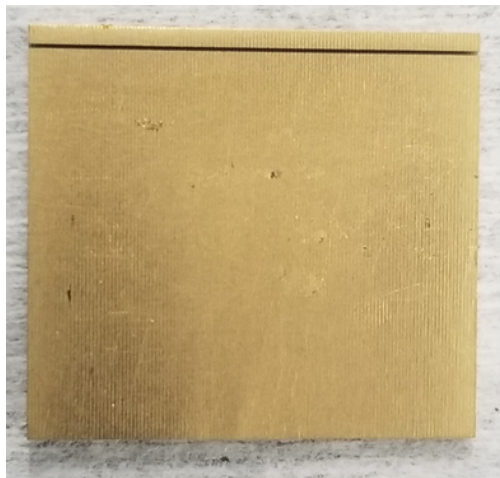
Results

This chapter describes the fabrication and characterization result of the fabricated composites. Sec. 4.1 shows fabrication results. The findings of the Characterization of the manufactured composite plate are presented in Sec. 4.2. The findings of the characterization of the manufactured composite array are presented in Sec. 4.3. Sec. 4.4 compares the measured and theoretical values of the electromechanical coupling coefficients.

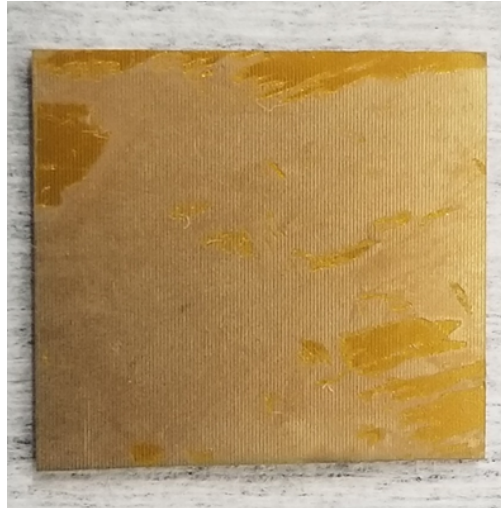
4.1 Fabrication Result

4.1.1 Composite Plate - Pz27 & EpoTek 3012

The fabricated composite of Pz27 with EpoTek 3012 is shown in Fig 4.1. The dimension (Length× Width× Thickness) of this composite are $14\text{ mm} \times 16\text{ mm} \times 0.731\text{ mm}$. The thickness variations across the composite were measured to be less than $20\text{ }\mu\text{m}$. A wrap around was made to separate the electrode between the active area and the back electrode as the additional diced line in Fig 4.1.



(a) Front face of the composite. A wrap around structure was made by dicing a shallow line to separate the top and bottom electrodes.



(b) Back face of the composite. Residue adhesive of Kapton tape from the adhesion test remained on the back side and was cleaned afterwards.

Figure 4.1: EpoTek 3012-filled composite showing the front side and the back side.

SEM imaging was used to detect any fractures, voids, or composite delamination. The SEM picture of the cross section of the composite was obtained by SEM SU 3500 (Hitachi, Tokyo, Japan) as shown in Fig. 4.2 and indicated little to no voids or fractures.

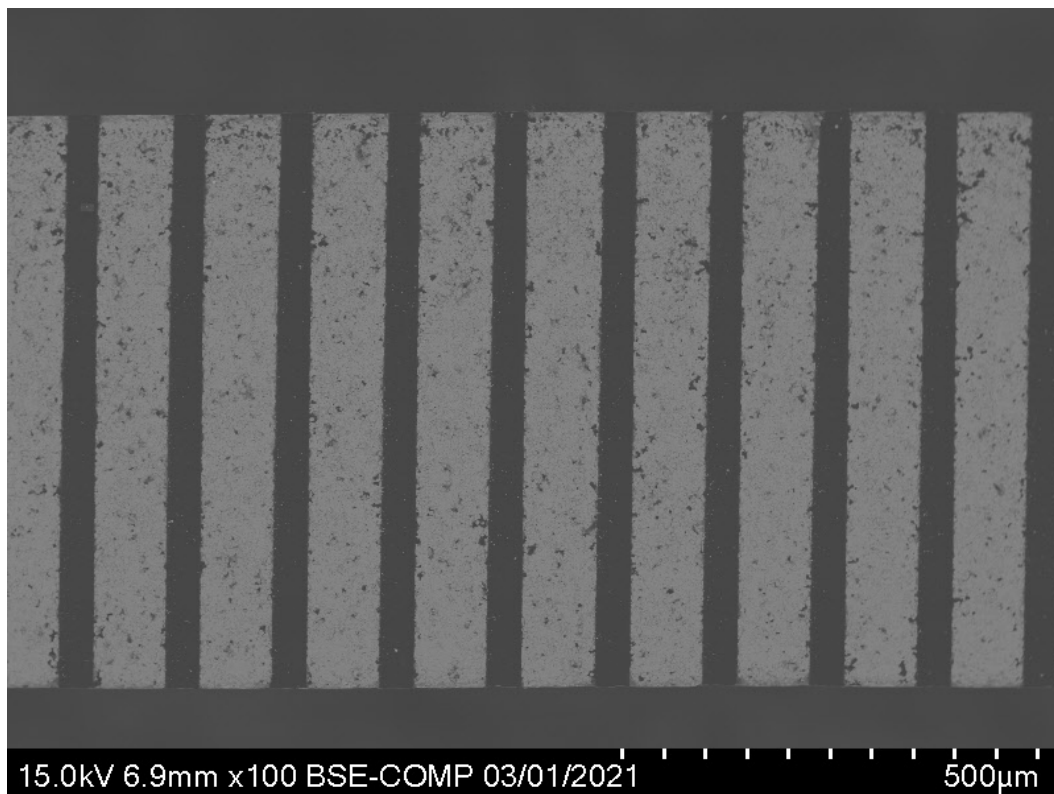


Figure 4.2: SEM image of the EpoTek 3012-filled composite. The brighter portion of the image are the piezoceramics whereas the darker portions are polymer filler.

A SAM picture was also acquired in Fig. 4.3 to the front face of the composite with scanning acoustic microscope SAM 300 (PVA TePLA, Wetttenberg, Germany). However, due to SAM software limitations, information from the image is minimal and is included here solely as a example.

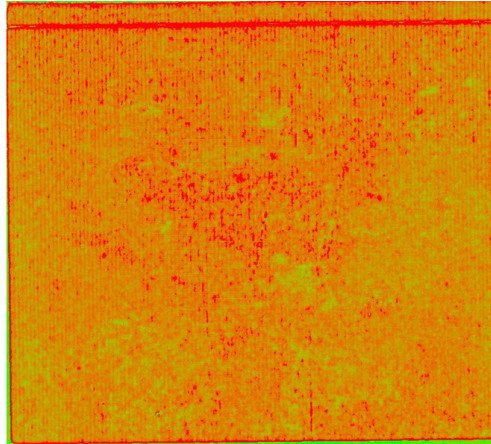


Figure 4.3: SAM image of the front face of the composite structure. Red area marks surface defects.

4.1.2 Composite Plate - Pz27 & RTV 3140

Same fabrication procedures were done with another kerf filler RTV 3140 and the results of the RTV 3140-filled composite is shown in Fig. 4.4. The dimension (Length \times Width) of this composite are $11\text{ mm} \times 16\text{ mm}$, however, the thickness variation for this sample was larger than 0.05 mm .

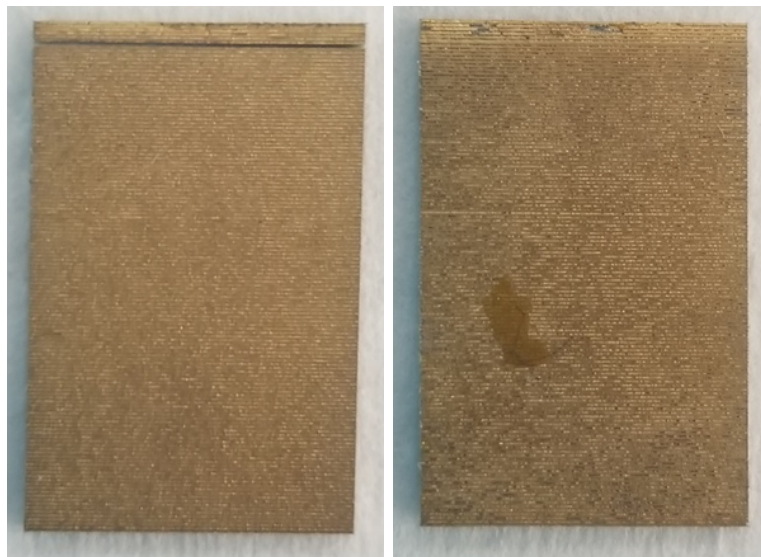


Figure 4.4: Electroded composite of PZ-27 and RTV 3140 showing the front side (left) and the back side (middle). Residue adhesive of Kapton tape from the adhesion test remains on the back side and is cleaned afterwards.

As a result, the composite in Fig. 4.4 was diced further into a smaller composite to produce a more consistent thickness, as seen in Fig. 4.5 and it has a dimension (Length \times Width \times Thickness)

of $6\text{ mm} \times 7\text{ mm} \times 0.701\text{ mm}$, with a thickness variation of approximately $14\ \mu\text{m}$.

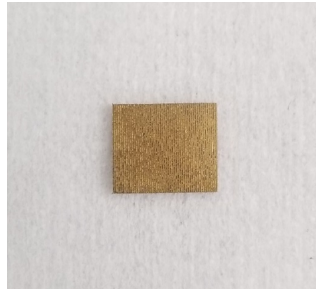


Figure 4.5: RTV 3140-filled composite after further dicing. Due the large thickness variation, the sample is further diced in the region of low thickness variations of approximately $14\ \mu\text{m}$.

Fig. 4.6 shows the kerf filler condition of RTV 3140, with numerous voids, tears and filler inconsistencies. This is largely due to RTV 3140's poor degassing. Some dark-coloured debris can also be observed within the kerf, which is most likely caused by the silicon carbide of the grinding paper during the lapping process.

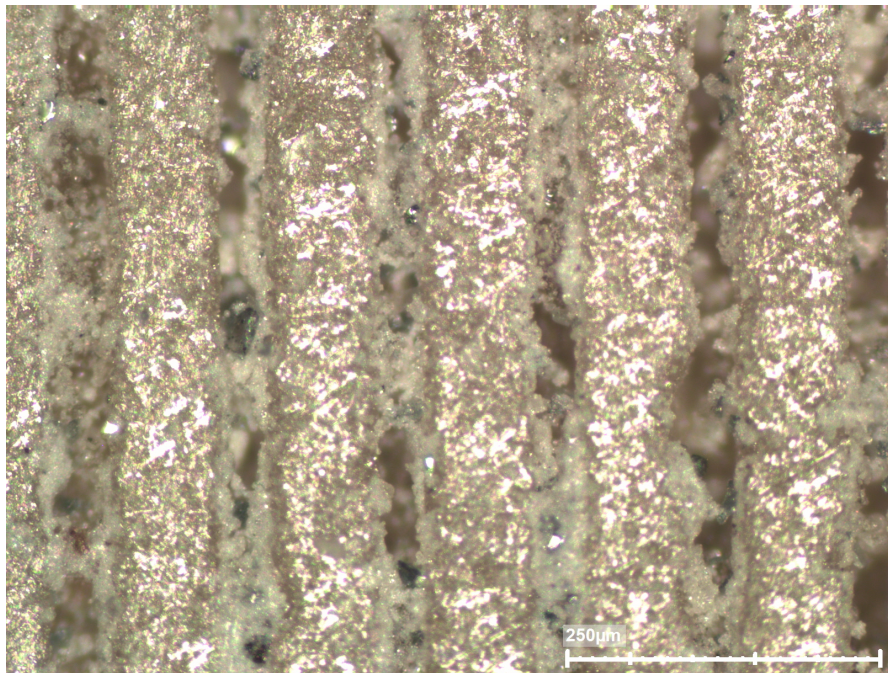
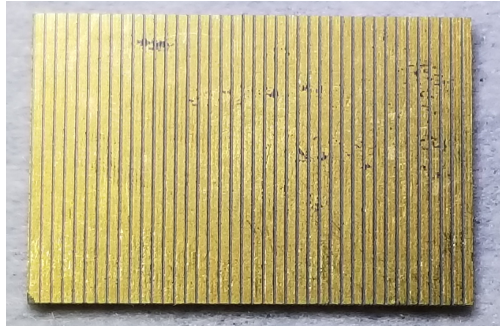


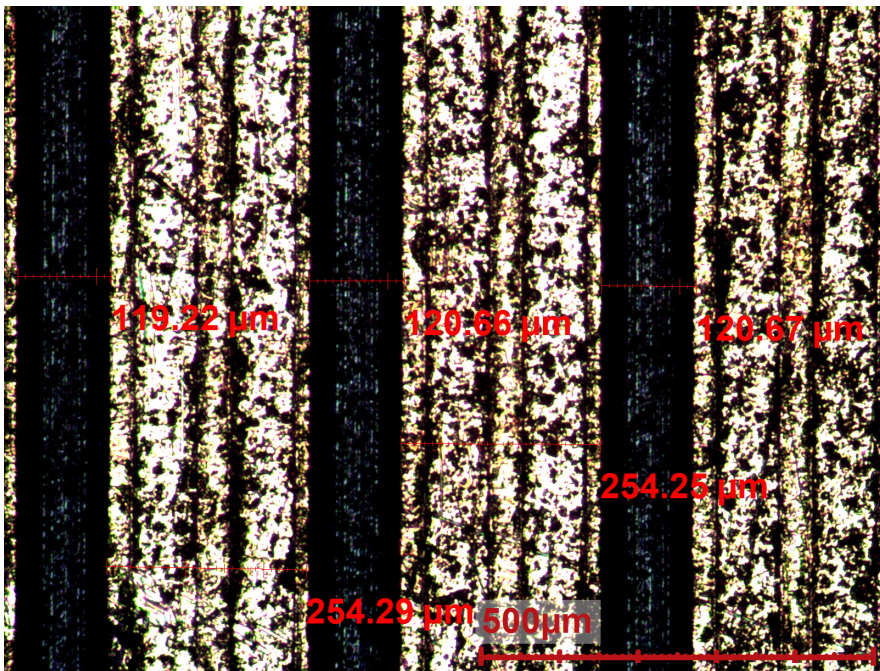
Figure 4.6: The kerf filler condition before sputtering of electrode under microscope. Voids and debris can be found within the kerf. Bright lines are the diced Pz27 fingers. The white and grayish materials are the RTV 3140 silicone. Voids and tearing of the silicone can be observed in this image and showing the limitation for using RTV 3140 as a kerf filler with current equipment at USN's laboratory. Black debris located at the middle of the second kerf line could originates from the silicon carbide particles from the grinding paper lodged inside during lapping.

4.1.3 Composite Array - Pz27 & EpoTek 3012

Fig. 4.7 showed the EpoTek 3012-filled composite array fabricated with further dicing the composite plate. The final dimension (Length \times Width) of this EpoTek 3012-filled composite array is $10.5\text{ mm} \times 15\text{ mm}$ with the same thickness to that of the composite plate of 0.701 mm and the same thickness variation of approximately $14\text{ }\mu\text{m}$. The average separation width produced by the dicing saw is approximately $120\text{ }\mu\text{m}$ and the width of an active array element is approximately $254\text{ }\mu\text{m}$. In Fig 4.7 and Fig. 4.8, for the EpoTek 3012-filled composite, the piezo widths and the kerf widths are in average $254\text{ }\mu\text{m}$ and $120\text{ }\mu\text{m}$ respectively.



(a) Composite array of PZ-27 and EpoTek 3012 as the polymer filler with 40 composite elements

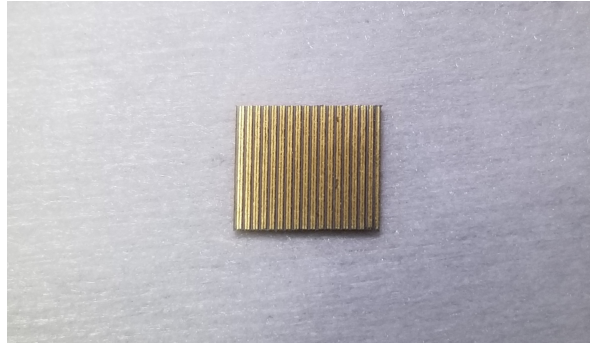


(b) Microscopic image of a section showing typical active composite elements and scratched kerf

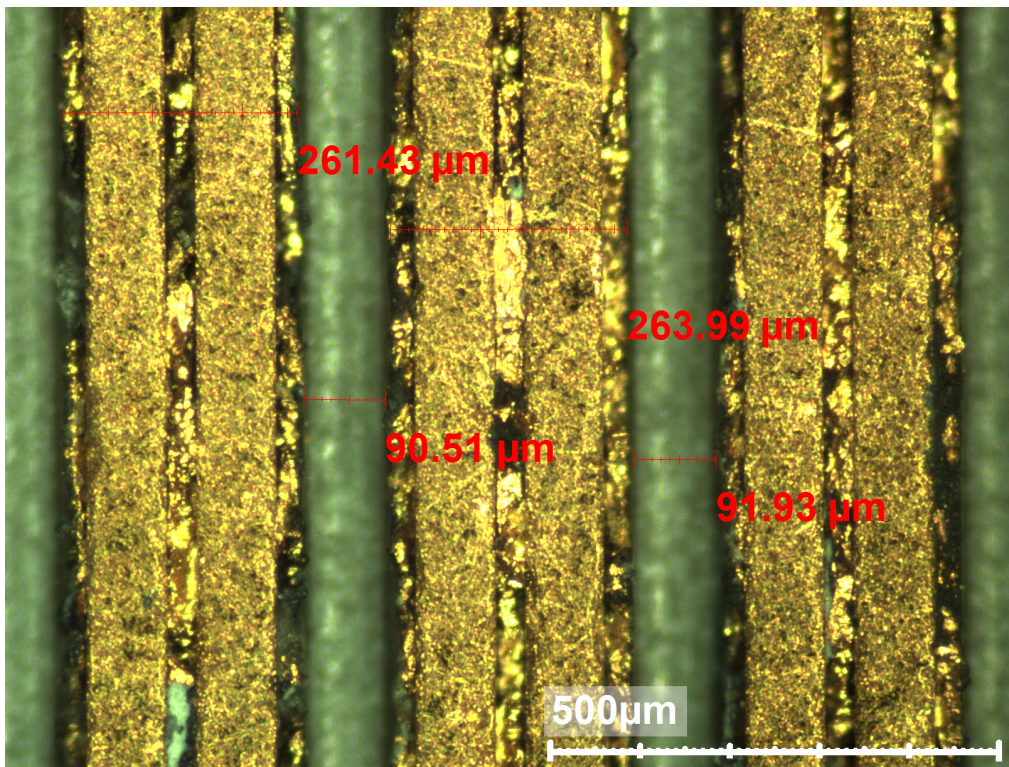
Figure 4.7: EpoTek 3012-filled piezocomposite array. The golden portions are the array elements and the dark lines are the scratch diced composite lines. The red lines are the width measurement of the kerf and array element. The size of the kerfs and array element widths are around $120\text{ }\mu\text{m}$ and $254\text{ }\mu\text{m}$ in average, respectively.

4.1.4 Composite Array - Pz27 & RTV 3140

For the RTV 3140-filled composite as seen in Fig. 4.5, the 18 electrodes were diced on the composite plate and it has a dimension (Length \times Width \times Thickness) of $6\text{ mm} \times 7\text{ mm} \times 0.701\text{ mm}$, with a thickness variation of approximately $14\text{ }\mu\text{m}$.



(a) Composite array of PZ-27 and RTV 3140 with 18 composite elements.



(b) Microscopic image of a section showing typical active composite elements and scratched kerf of the piezocomposite array of Pz27 and RTV 3140. The golden area is the composite array element and the green lines are the scratch diced region for electrode separation. Red lines are the width measurement. The kerfs and array element widths are about $91\text{ }\mu\text{m}$ and $262\text{ }\mu\text{m}$ in average, respectively.

Figure 4.8: The fabricated RTV 3140-filled piezocomposite.

The width measurement as seen in Fig. 4.5 of the active composite array element and the

separation widths are approximately $262 \mu\text{m}$ and $91 \mu\text{m}$ in average, respectively. Thus the pitch of this composite array is approximately $353 \mu\text{m}$. The piezoceramic fingers appear to be in good condition, however the kerfs have visible defects. As visible at the bottom of the first array element, the transducer surface is comprised of many holes and a non-electroded area. The impact of these surface detectors is explored in the next chapter.

4.2 Characterization - Composite Plate

4.2.1 Electrical Characterization of Bulk Disk of Pz27

The electrical impedance measured on the the bulk Pz27 plate is shown in Fig. 4.9. This curve was used to estimate the material parameters that most closely matched the actual piezoceramic used in this thesis. The measurements are plotted together with results of one-dimensional analytical calculations (Mason-model implemented in Xtrans) and two-dimensional FEM simulations using COMSOL, using material parameter data from the manufacturer Ferroperm A/S and from the published data sets by Perez et al. [19] and from Storheim et al. [20].

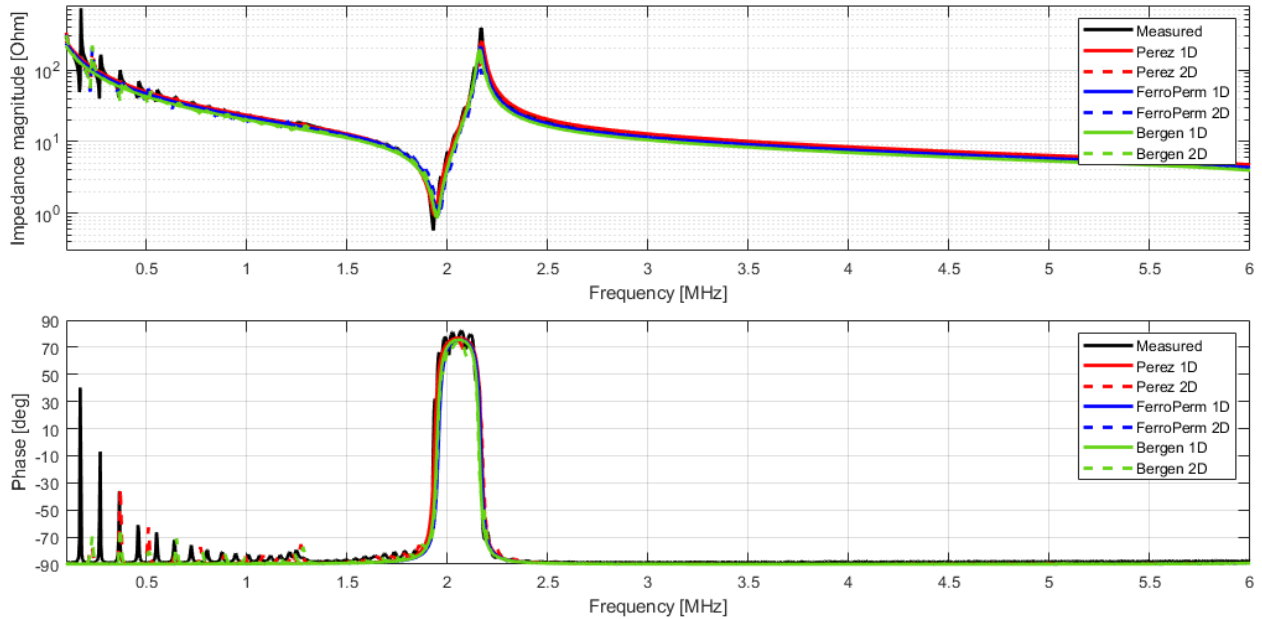


Figure 4.9: Electrical impedance magnitude and phase of bulk Pz27 disk. Black line indicates the measured electrical impedance. Red line indicates simulation result with material parameters from Perez et al.[21]. Blue line indicates simulation result with material parameters from FerroPerm A/S [18]. Green line indicates simulation result with material parameters from Storheim et al.[20].

Fig. 4.10 shows the same data as Fig. 4.9 zoomed in on the resonance and antiresonance frequencies, but only keeping the measured and two-dimensional COMSOL simulations with the measured data set from the manufacturer Ferroperm A/S and from the published data sets by Perez et al. [19]

and from Storheim et al. [20].

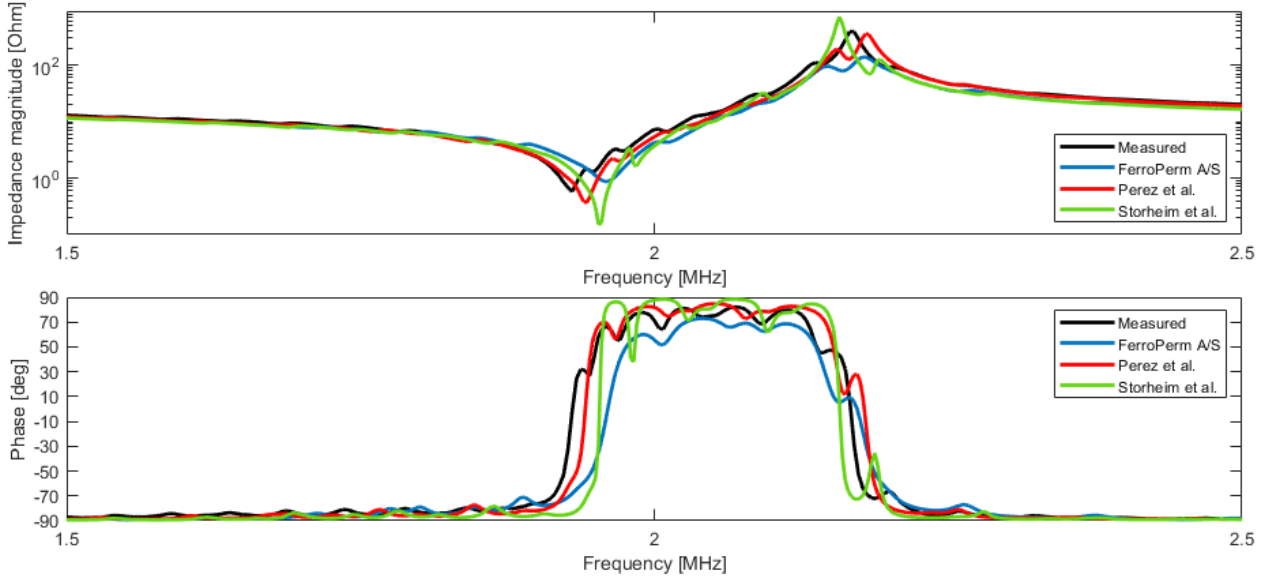


Figure 4.10: Electrical impedance and phase angle of the measured result and two-dimensional COMSOL FEM simulation results with three different set of material data in the frequency range of 1.5 to 2.5 MHz.

All material parameter sets fits the measurement well, and the resonance and antiresonance from all three sets of parameters showed a difference less than 6%, with the parameters of Perez et al. showing the smallest deviation to the measurement result as seen in Table 4.1. However, the differences of these parameters was measured to be more pronounced when the Pz27 was diced and filled to a composite material and it is discussed in the later section.

Table 4.1: The resonance, antiresonance and coupling coefficient of the measured Pz27 and FEM results from three sets of parameters and the percentage difference to the measured value.

Parameter	Measured	Perez et al.	FerroPerm A/S	Storheim et al.
f_r [MHz]	1.930	1.943 (0.6%)	1.960 (1.5%)	1.953 (1.2%)
f_a [MHz]	2.166	2.180 (0.6%)	2.180 (-0.6%)	2.158 (-0.4%)
k_t	0.492	0.492 (0%)	0.475 (-3.4%)	0.462 (-6.0%)

4.2.2 Electrical Characterization of Diced Pz27 with Bottom Support

Fig. 4.11 shows the measured and modelled electrical impedance and phase angle of eight diced Pz27 pillars with a bottom support structure. The first resonance and antiresonance pair occurred about 1 MHz, while the second pair occurred in the 1.5 to 1.7 MHz range. The measured impedance spectra from all 8 pillars agree well with each other, but deviate clearly from the curve simulated in

FEM. The resonance peak positions are the same for both measurements simulations, but the width of the resonance regions deviate, by the distance between the resonance and antiresonance peaks being much smaller in the measured spectra compared to the simulated spectra. This indicates a much lower electromechanical coupling k in the fabricated samples than what is predicted from the simulations. The simulated spectra show the first resonance and antiresonance pair at 0.8 MHz and 1.1 MHz and the second pair at 1.4 MHz and 1.8 MHz. The reason for this deviation cannot be identified at this time, but it will be discussed in the following chapter.

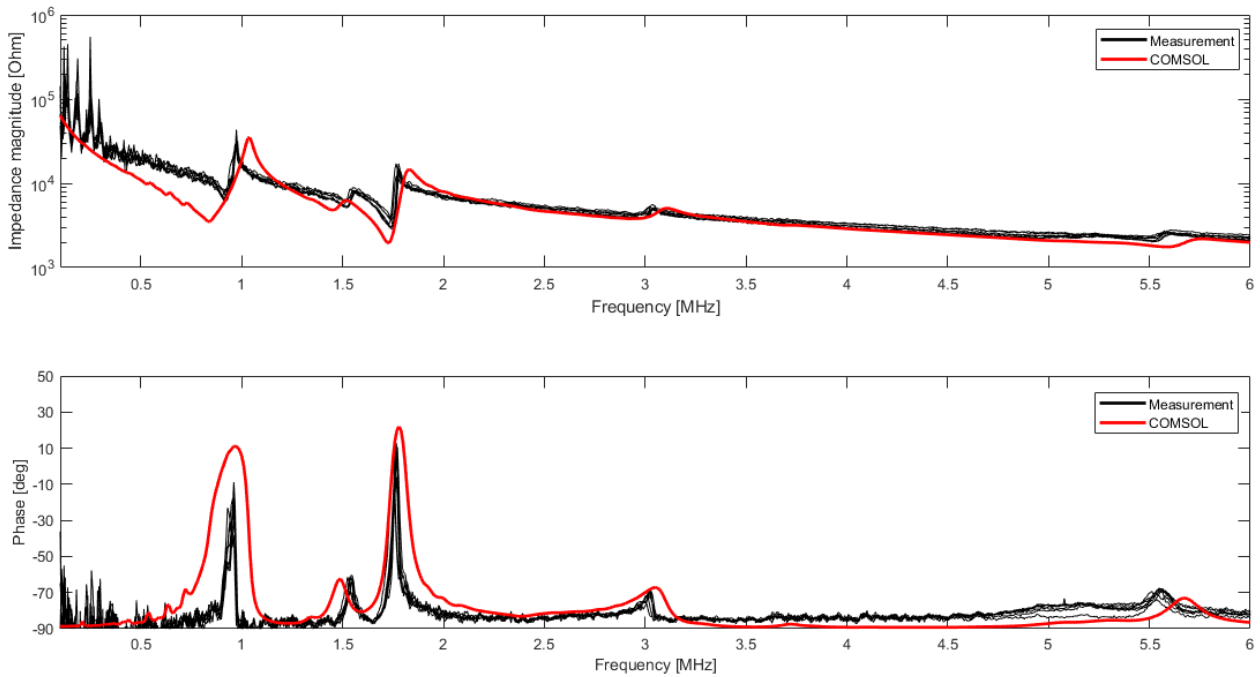


Figure 4.11: Electrical impedance and phase angle measured on diced Pz27, together with two-dimensional FEM simulations. The results show measurements on 8 of the 140 elements. Diced Pz27 with air kerf is very fragile, making it difficult to efficiently measure each individual element using the current laboratory setup.

4.2.3 Electrical Characterization of Piezocomposite Plate - Pz27 and EpoTek 3012

The electrical impedance magnitude and phase of Pz27 and EpoTek 3012 composite are shown in Fig. 4.12. The measured and simulated results agree very well. However, the antiresonance of the measurement result is slightly lower than that of the modelled result by 2.6%, thus the coupling coefficient of the fabricated composite is about 3% lower than the expected modeling result as shown in Table 4.2. Several lateral modes can be observed at the low frequencies, but these are of little interest.

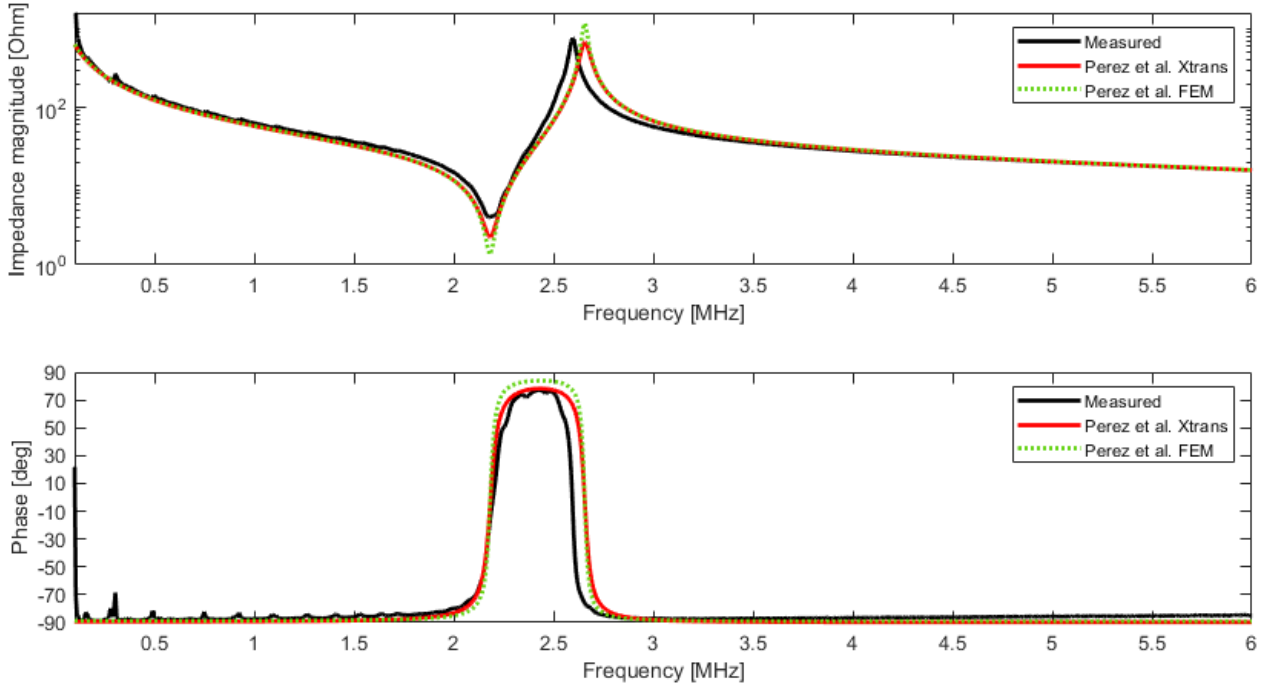


Figure 4.12: Electrical impedance and phase of the EpoTek 3012-filled composite plate.

Table 4.2: Resonance, antiresonance frequency and the coupling coefficient of the piezocomposite with EpoTek 3012 calculated by Eq. 2.24

Parameter	Measured	One-dimensional Xtrans	Two-dimensional COMSOL [MHz]
f_r [MHz]	2.17	2.1827	2.18
f_a [MHz]	2.60	2.6582	2.66
k_t	0.59	0.61	0.61

To investigate which of the three material parameters sets fit best to the measured data, i.e. Perez et al., Storheim et al., or the data from the manufacturer, in Fig. 4.13, the measured results are shown and compared to the simulation result with all three sets of parameter data. Only two-dimensional simulation is presented as they have previously been shown to agree with analytical results from one-dimensional Xtrans modeling. The general trends of the measured and simulation result are similar. However, the impedance curve from Fig. 4.13 and the resonance and antiresonance values as shown in Table 4.3, the manufacturer's data for composite modeling in COMSOL showed the largest discrepancy compared to the measurement among all sets while with parameters from Perez et al. and Storheim et al. the deviation is low. This result demonstrated that the use of published values for material parameters fitting offers an improvement for piezocomposite modeling over the manufacturer's data for this fabricated sample.

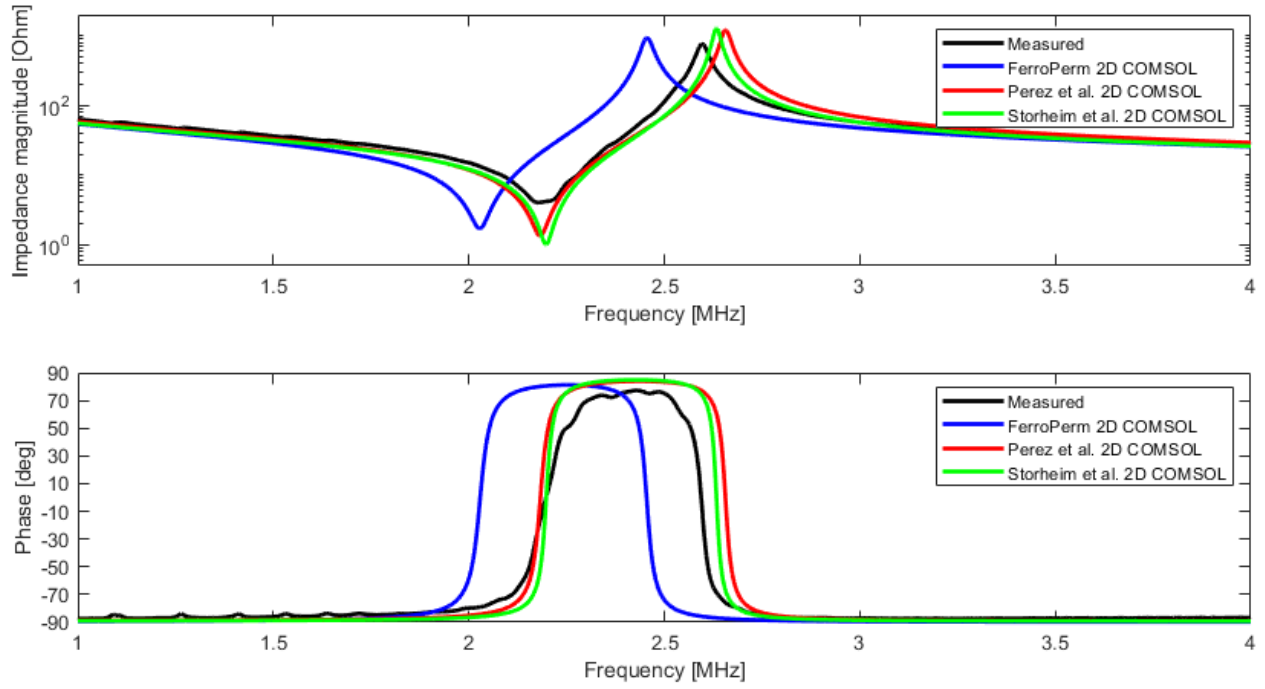


Figure 4.13: Electrical impedance and phase of the EpoTek 3012-filled composite in the range of 1 MHz to 4 MHz. Black line is the measurement. Blue line is the modelled result with FerroPerm A/S data set. Red line is the modelled result with Perez et al. data set. Green line is the modelled result with Storheim et al. data set. Black, red and green line are close to each other while the blue line showed a large deviation.

Table 4.3: The resonance and antiresonance of the measured piezocomposite of Pz27 and EpoTek 3012 with two-dimensional COMSOL modeling results from three sets of parameters and the percentage difference to the measured value.

Parameter	Measured	Perez et al.	FerroPerm A/S cite{pz27}	Storheim et al.
f_r [Mhz]	2.174	2.182 (0.4%)	2.028 (-6.7%)	2.198 (1.1%)
f_a [Mhz]	2.595	2.658 (2.4%)	2.456 (-5.4%)	2.634 (1.5%)

4.2.4 Electrical Characterization of Piezocomposite Plate - Pz27 and RTV 3140

The measured, modelled and fitting values of the electrical impedance magnitude and phase of Pz27 and RTV 3140 composite are shown in Fig. 4.14. The general trend of the measurement agrees with the models. The resonance and antiresonance between the measured and modelled result matches with each other with a difference in magnitude due to different value of energy losses. The resonance also appeared to be less pronounced and smooth compared to the modelled result with a small variation near 2.5 MHz. Several low frequency lateral modes can also be observed below 2 MHz, but they are of little interest. From the values of the resonance and antiresonance as shown in

Table 4.4, the measured results showed a slightly lower coupling coefficient of -3% than the modelled values.

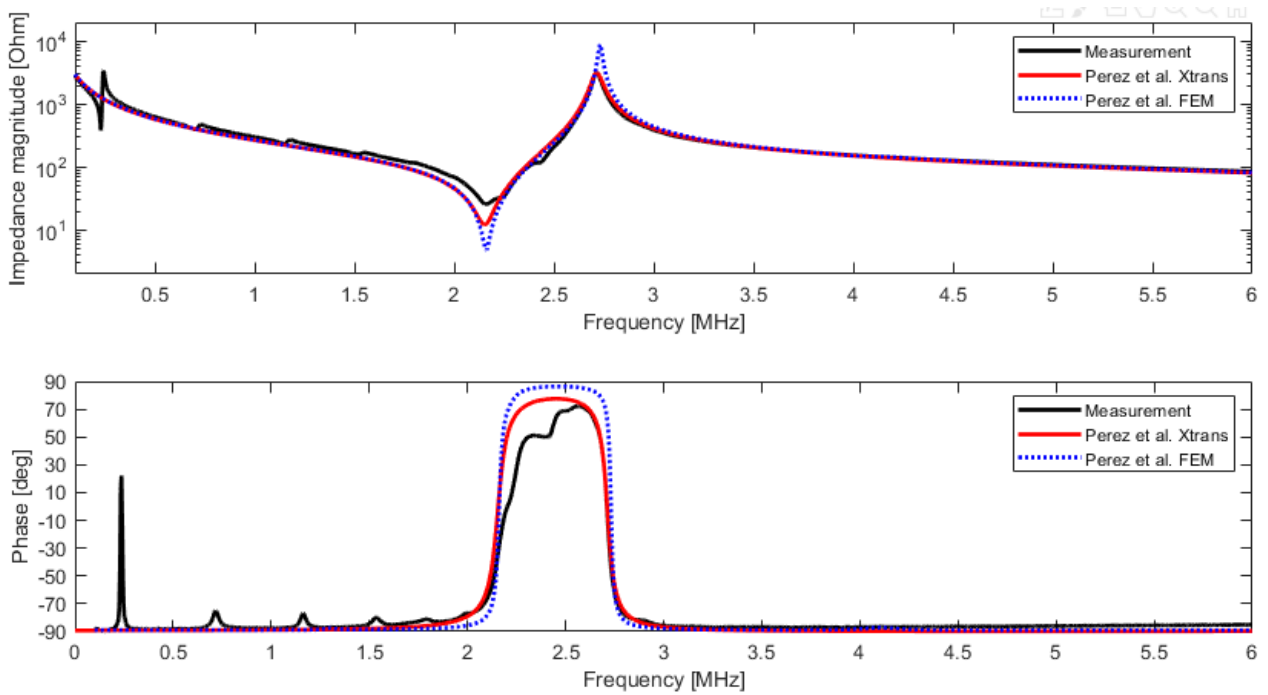


Figure 4.14: Electrical impedance and phase of the RTV 3140-filled composite. Black line is the measurement. Red line is the result of one-dimensional modeling. Blue dashed line is the two-dimensional FEM result.

Table 4.4: Resonance, antiresonance frequency and the coupling coefficient of the RTV 3140-filled composite calculated by Eq. 2.24.

Parameter	Measured	One-dimensional Xtrans	Two-dimensional COMSOL [MHz]
f_r [MHz]	2.159	2.153	2.162
f_a [MHz]	2.712	2.715	2.732
k_t	0.644	0.648	0.650

4.3 Summary of Measured Properties of the Fabricated Composite Plates

Table 4.5 summarizes the overview of the measured properties of the produced composite plates with polymer filler of EpoTek 3012 and RTV 3140 and related parameters.

Table 4.5: Measured properties of the fabricated 2-2 piezocomposite plate

Active Piezoceramic	Pz27	
Passive Polymer Filler	EpoTek 3012	RTV 3140
Resonance Frequency	2.21 MHz	2.16 MHz
Antiresonance Frequency	2.65 MHz	2.71 MHz
Electromechanical Coupling Coefficient	0.59	0.64
Thickness	0.731 <i>mm</i>	0.701 <i>mm</i>
Volume fraction	0.68	0.68
Filler Kerf	40 μm	
Ceramic Width	85 μm	
Active Area Length	14 <i>mm</i>	6 <i>mm</i>
Active Area Width	16 <i>mm</i>	7 <i>mm</i>
Active Area	224 <i>mm</i> ²	42 <i>mm</i> ²

4.4 Characterization - Composite Array

4.4.1 Electrical Characterization of the Composite Array - Pz27 and EpoTek 3012

The piezocomposite plate was made into a one-dimensional array by dicing kerfs into the electrodes at the top face, with a electrode spacing of $125 \mu\text{m}$, as described in Chapter 3. and the properties of the fabricated array is summarized in Table 4.6. The electrical impedance and phase angle of all the composite elements with two-dimensional modeling is shown in Fig. 4.15.

Table 4.6: Measured properties of the 40-element Pz27 and EpoTek 3012 composite array

Properties	Value
Number of elements	40
Number of open elements	0
Number of shorted elements	0
Average resonance frequency	2.43
Average antiresonance frequency	2.57

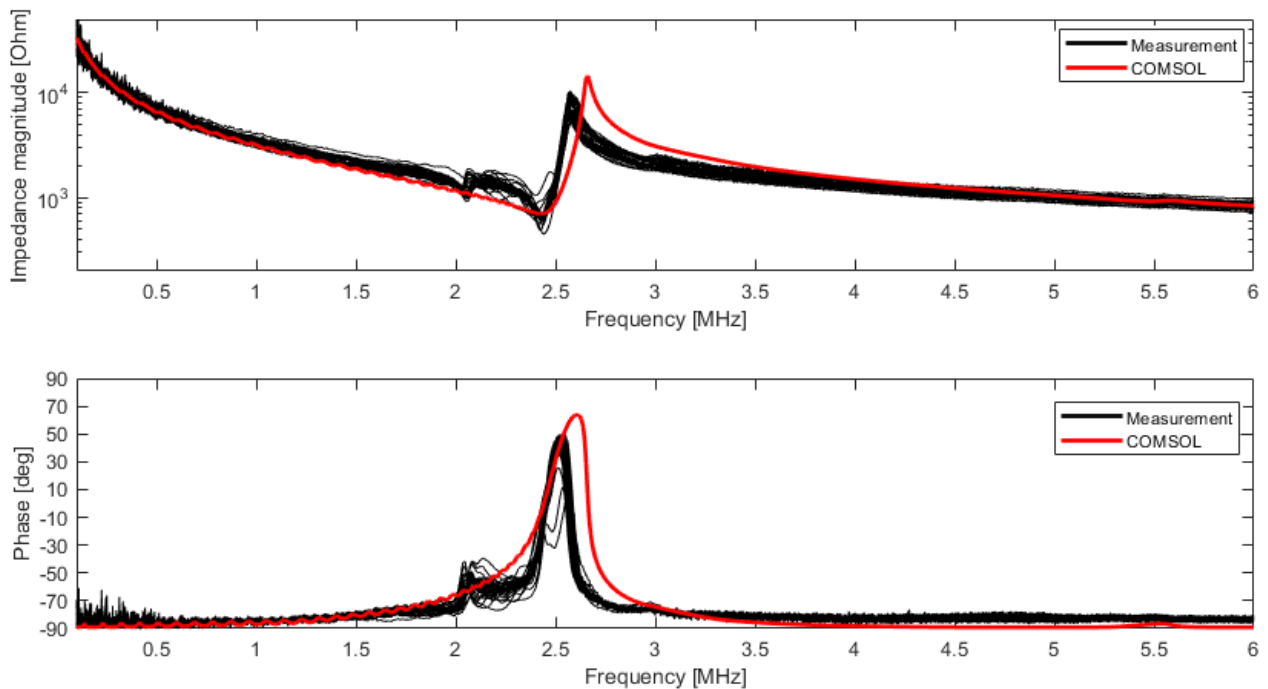


Figure 4.15: Electrical impedance and phase of the EpoTek 3012-filled composite array elements. Black lines are the measurement of all composite elements. Red line is the COMSOL FEM result.

One-dimensional modeling is not applicable here since the lateral coupling boundary conditions are not considered in XTrans, therefore only two-dimensional modeling results are shown here. All

impedance measurement between the individual elements are consistent with each other. Comparing the measured results to the modelled results, the general trend agrees, but differ in the region of 2 to 2.5 MHz with the measured result showing extra modes.

When compared to the piezocomposite, a substantial reduction in electromechanical coupling was observed in In Fig. 4.15, as demonstrated by the reduced separation between the resonance and antiresonance frequencies. The resonance and antiresonance frequency of all individual elements are shown in Fig. 4.16 with high consistency. The average resonance and antiresonance frequency shown in Table 4.7 lead to the electromechanical coupling coefficient of 0.37 for the composite elements which around 37% lower than the coupling for composite plate. The cause for this decrease could be due to the separation kerf at this stage consists of kerf filler and piezoceramics itself as shown in Fig. A.17 leading to an increase of stiffness of the separation which limits the cross coupling reduction ability.

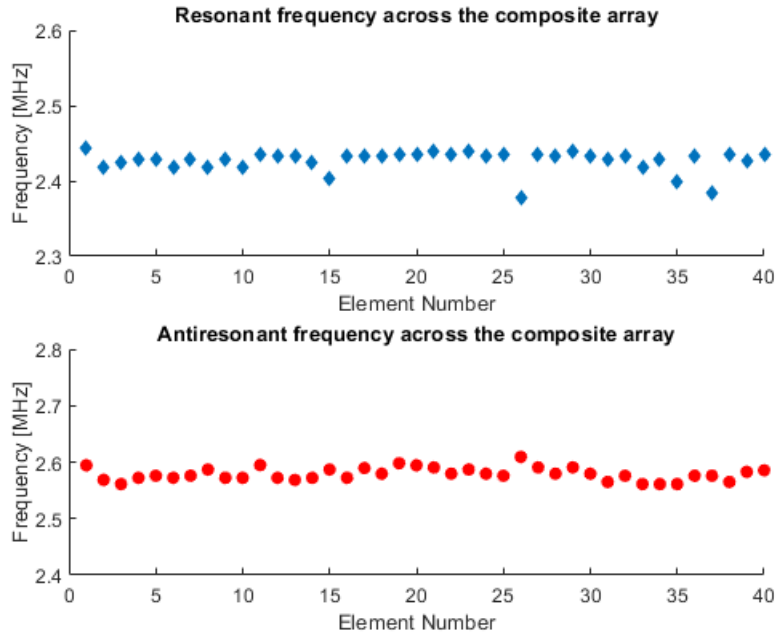


Figure 4.16: Resonance and antiresonance frequency across the composite array

Table 4.7: Statistics of the resonance and antiresonance frequency of the composite array elements of Pz27 with EpoTek 3012 as polymer filler

Parameter	Average	Standard Deviation
Resonance Frequency f_r	2.43 MHz	0.01 MHz
Antiresonance frequency f_a	2.57 MHz	0.01 MHz
Coupling Coefficient	0.37	0.019

4.4.2 Electrical Characterization of the Composite Array - Pz27 and RTV 3140

Similar to the previous section, the properties of the composite array of Pz27 with RTV 3140 are summarized in Fig. 4.8. The electrical impedance and phase angle of all the composite elements with one-dimensional modeling is shown in Fig. 4.17. The general trend of the measurement fits with the two-dimensional modeling result and a small resonance-antiresonance pair at around 3 MHz originates from the diced part of the electrode separation.

Table 4.8: Measured properties of the 18-element Pz27 and RTV 3140 composite array

Properties	Value
Number of elements	18
Number of open elements	0
Number of shorted elements	0
Average resonance frequency	2.16
Average antiresonance frequency	2.60

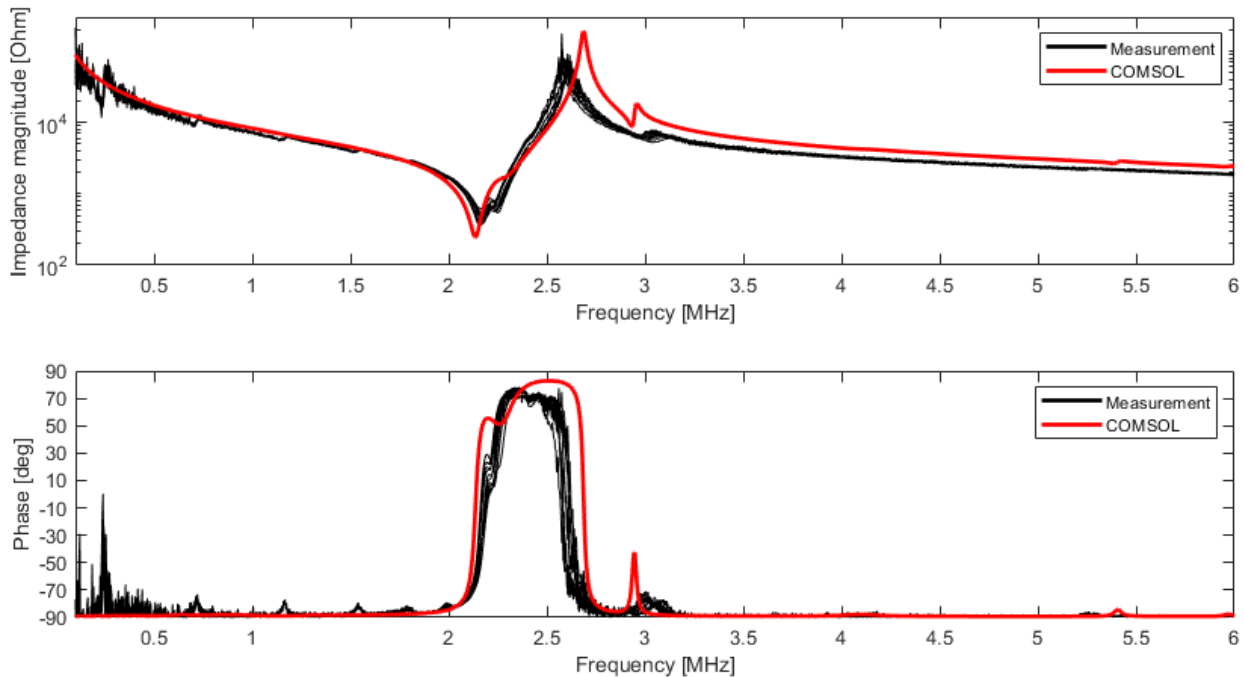


Figure 4.17: Electrical impedance and phase of the RTV 3140-filled composite array elements. Black lines are the measurement of all composite elements. Red line is the COMSOL FEM result.

One key result can be made. The impedance measurement of the RTV 3140-filled piezocomposite array element in Fig. 4.17 still deviate from the RTV 3140-filled piezocomposite plate in Fig. 4.14, most notably by a reduced coupling coefficient as also seen in the case with EpoTek 3012-filled samples. However, the reduction between the piezocomposite plate and the piezocomposite array

element for RTV 3140-filled kerf is much smaller than between the EpoTek-filled piezocomposite and array. For the RTV 3140-filled kerf, the reduction in the coupling is from 0.64 (plate) to 0.59 (array element). For the Epotek 3012-filled kerf, the reduction in the coupling is 0.59 (plate) to 0.37 (array element)

The resonance and antiresonance frequency of the individual composite elements as shown in 4.18 also showed little deviation. The average resonance and antiresonance frequency of the individual composite elements are 2.16 and 2.60 MHz and thus the effective electromechanical coupling coefficient is 0.60 as shown in Table 4.9.

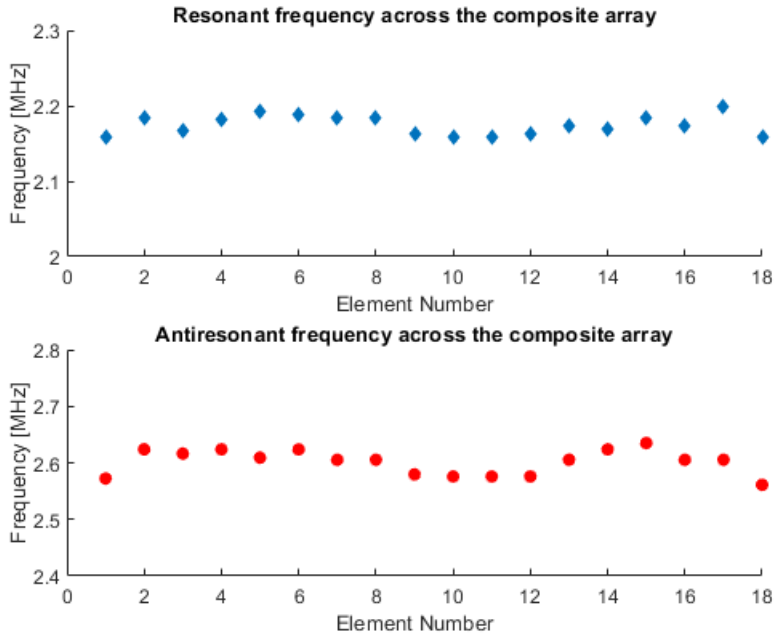


Figure 4.18: Resonance and antiresonance frequency across the composite array

Table 4.9: Statistics of the resonance and antiresonance frequency of the composite array elements of Pz27 with RTV 3140 as polymer filler

Parameter	Average	Standard Deviation
Resonance Frequency f_r	2.17 MHz	0.01 MHz
Antiresonance frequency f_a	2.60 MHz	0.02 MHz
Coupling Coefficient	0.59	0.008

4.5 Electromechanical Coupling Coefficient

The electromechanical coupling coefficients for all fabricated samples and the modelled values are summarized in Table 4.10. The measured coupling constant was calculated with Eq. 2.24 from the resonance and antiresonance of the impedance spectra as shown in Fig. 4.10, 4.12, 4.14, 4.15

and 4.17. The modelled coupling values of k_{33} , k'_{33} and k_t were obtained from Table 3.1 and Fig. 3.2.

Table 4.10: Comparison of the coupling coefficients calculated from the impedance spectra. k_{33} is the ideal thin rod coupling and k_t the plate coupling, both calculated from the material data. k'_{33} is the coupling constant for the slender bar, either calculated material data or found from the impedance measurements.

Piezoceramic	Filler Polymer		k_{33}	k'_{33}	k_t	
Pz27	-	FerroPerm A/S	0.69	0.65	0.47	
		Perez et al.	0.70	0.66	0.49	
		Storheim et al.	0.68	0.64	0.47	
	EpoTek 3012	modelled 2-2 Composite [14], [15]			0.61	
		Measured Composite Plate			0.59	
		Measured Composite Array Element			0.37	
	RTV 3140	modelled 2-2 Composite [14], [15]			0.65	
		Measured Composite Plate			0.64	
		Measured Composite Array Element			0.60	

4.6 Oblique Dicing

The electrical impedance and phase angle of the simulated composite model with oblique dicing walls are shown in Fig. 4.19.

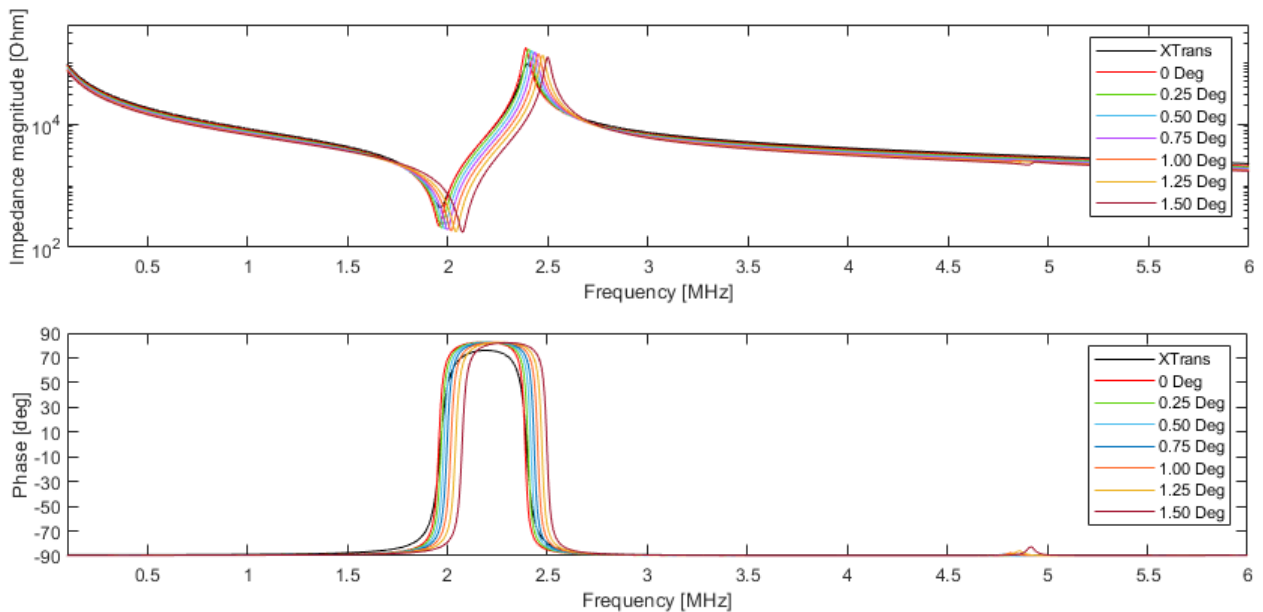


Figure 4.19: Electrical impedance and phase angle of the composite structure with oblique dicing at an angle of 0° to 1.5° .

The change in resonance per degree is 0.08 MHz and the change in antiresonance per degree is 0.02 MHz. The actual dicing of the fabricated composites was not perfectly vertical, but the deviation from vertical was observed to be less than 0.1° as seen in A.14. According to the results in 4.19 this deviation should not cause any measurable changes in the resonance and antiresonance frequencies.

Chapter 5

Discussion

This is the first successful attempt at piezocomposite manufacturing using the equipment available at the USN ultrasound laboratory. With minor variations, the performance of the manufactured piezocomposite samples closely matches that of the predicted behavior. This work was carried out during the Covid-19 pandemic in 2020-2021, when availability and access to laboratories was intermittently limited. This has had an impact on laboratory work, specifically the ability to repeat and verify manufacturing methods and measurements, and thus limiting the ability to further add confidence to the results and the ability to conduct additional tests and modelling. However, this thesis's objectives have all been accomplished. Using USN laboratory equipment, a production procedure for piezocomposites and piezocomposite arrays was established. This thesis provided the theoretical understanding and fabrication basis for future USN users to refer to. Some of the fabrication challenges encountered throughout the fabrication processes have been documented and discussed.

5.1 Fitting of Material Parameters

In the material parameters of Table 3.1, the elastic stiffness c_{11} , c_{12} and c_{13} from Perez et al. and Storheim et al. are lower than the values given from the manufacturer's data by 20% to 30% difference. This difference in stiffness did not affect the electrical impedance for the modeling of the bulk plate. However, for the modeling of a composite, the electrical impedance with manufacturer's data deviates to the measured result by 0.15 MHz (-7%) in resonance and 0.14 MHz (-5%) in antiresonance as shown in Fig. 4.13 while the difference of the resonance and antiresonance from Perez et al. [19] and Storheim et al. [20] is between 0.4% to 2.4%.

The improved fitting obtained when using material parameters from either Perez et al. [19] or Storheim et al. [20] illustrates that the stiffness of the the diced piezoceramic Pz27 in the periodic structure was in fact softer than the values given by the manufacturer. Note that, due to the high

number of parameters involved, there might be multiple set of parameters that leads to the same electrical impedance.

5.2 Electrical Characterization of the Diced Pz27 Pillars with Bottom Support

The behavior of the measured and modelled diced Pz27 pillars with a bottom piezoceramic support as shown in Fig. 4.11 at this intermediate fabrication stage was analysed, but the results are not fully explained.

There are two points of interest. To begin, the difference in coupling between the measured and modelled impedances, as shown in Fig. 4.11, cannot be explained by material losses, given the behavior of the manufactured piezocomposite from the same material sample exhibited negligible losses, and the electromechanical coupling is not strongly influenced by losses. Second, the origins of the resonance and antiresonance pair positions are unclear at the moment. The first pair may be created by the thickness or lateral modes of the bottom support, while the second pair could be generated by the thickness mode of the sliced pillars. Furthermore, the interaction between the diced pillars and the bottom support may impact the final impedance output, making it difficult to establish where the resonance and antiresonance pairs originate at this stage.

As these findings are still confusing and incompletely understood, they were omitted from the modeling. The results for this structure contrast sharply with the results obtained after filling the kerfs, since the results obtained after filling the kerfs are in considerably better agreement between the measurements and the simulations.

5.3 2-2 Piezocomposite Plate

Two 2-2 piezocomposite plates were successfully fabricated and characterized. The composite material was modelled in one-dimensional Mason model and two-dimensional FEM analysis.

Although the one-dimensional Mason model in Xtrans can capture the general behavior of the piezocomposite as a homogeneous material, the periodic structure inside the composite is not considered in this one-dimensional effective medium model. As a result, a two-dimensional FEM analysis was necessary to better simulate the piezocomposite as well as the electrical and mechanical impacts of the structure's boundary conditions. The simulation results from the one-dimensional and two-dimensional models in Fig. 4.12 of the composite with EpoTek 3012 revealed the same resonance and antiresonance frequency. A small variation in peak amplitude was observed, which was most likely related to different representation of energy loss factors. This confirms that this composite

could be reasonably well described by the effective medium one-dimensional model as it gives similar results from the finite element modeling methods with low computational demand.

The losses in one-dimensional modeling were given with the mechanical quality factor, which was then fitted to the measurement. The losses in two-dimensional were presented with complex losses from the Perez et al. data set. The modeling and measurement results showed a similar resonance peak, however the antiresonance of the modelled values is slightly higher by 0.5 MHz. This is most likely because the manufactured sample is mechanically stiffer than expected. Similarly, the impedance for the composite with RTV 3140 in Fig. 4.14 also showed a similar amplitude differences, but the resonance and antiresonance has only minor differences.

The measured results of both EpoTek 3012-filled and RTV 3140-filled piezocomposite plate largely agrees with the modeling result. This marked the possibility of designing, modeling and fabricating a piezocomposite at USN's laboratory that matches with the theoretical performance. The fabrication procedures developed in this work can be referenced for future applications. Moreover, the measured results for the composite with RTV 3140-filled composite in Fig. 4.14 showed a slightly lower coupling coefficient of -3% than the modelled values, indicating the fabricated composite is slightly stiffer than the ideal modeling methods. The magnitude difference of the resonance and antiresonance peaks also showed that the fabricated sample has higher losses than the FEM modeling. A small dip can be also be observed at around 2.45 MHz and the resonance peak is not as pronounced compared to modeling result.

Note that, despite the fact that the kerf condition for the RTV 3140-filled composite is not ideal with numerous voids, debris and irregularities as shown in Fig. 4.6, the impedance curve in Fig. 4.14 does not have a observable effect on the resonance and antiresonance. This is explained by the fact that the ideal situation for kerf material to achieve the maximum coupling (i.e. larger resonance and antiresonance spacing) is with air since it provides zero clamping [17], and the kerfs in the manufactured sample are largely air pockets. However, it would not be optimal in terms of mechanical stability since the air holes would also detach neighboring ceramic pillars.

5.4 2-2 Piezocomposite Array

The modeling of the piezocomposite array elements were not possible with one-dimensional Xtrans model since the boundary conditions of the individual elements had a greater effect on the clamping of the vibrating elements. Using the epoxy EpoTek as kerf filler showed a strong clamping effect of the array elements, see Fig. 4.15. A significant reduction in the electromechanical coupling was found when compared to the piezocomposite, as evidenced by the reduced spacing between the resonance and antiresonance frequencies. This is an indication of the clamping effect of the

EpoTek kerf material within the kerf structure and it will most likely result in crosstalk between the components, albeit crosstalk was not directly measured in this study. This showed that EpoTek 3012 is a sub-par kerf filling material. Furthermore, COMSOL was unable to capture the influence of additional modes surrounding the resonance frequency in the frequency range of 2 to 2.5 MHz, as seen in 4.15.

Similarly for RTV 3140-filled composite array in Fig. 4.17, the model was modified to account for the scratch diced structure, resulting in artifacts at the resonance and 3 MHz. The measurement and simulation results are mostly similar, and the antiresonance difference suggests that the manufactured composite is stiffer than the simulated one. The resonance and antiresonance frequencies of all the array elements in Fig 4.16 are likewise largely consistent for both array composites.

5.5 Comparison of Hard (EpoTek 3012) and Soft (RTV 3140) Polymer Filler

The immediate effect observed by comparing the hard and soft polymer filler in the composite plate is the coupling coefficient. The coupling coefficient listed in Table 4.10 showed that the coupling for the plate is 0.59 for hard EpoTek 3012 which is lower than the coupling for soft RTV 3140 of 0.64. This result was predicted, and it is consistent with the modelled results.

The effect of hard and soft polymer filler is more pronounced by the comparing the impedance of the composite with hard and soft filler. For the Pz27 and EpoTek 3012 composite, the impedance curves for the composite plate in Fig. 4.12 and for the array element in Fig.4.15 showed a significant difference in the vicinity of resonance. For the composite plate, the impedance showed a sharp resonance and antiresonance. For the array element, the separation between resonance and antiresonance was greatly reduced. This is a sign of a reduced coupling constant, most likely caused by clamping of the element from the polymer, and it would cause crosstalk between the elements.

For the Pz27 with the softer RTV 3140 as filler material, the impedance of the composite plate and the array element in Fig A.12 and Fig. 4.17 were much more similar, with sharp resonance and antiresonance. Thus, the use of RTV 3140 filler will reduce crosstalk compared to the EpoTek filler, explained by RTV 3140 being a much softer material.

As a result, using EpoTek 3012 and RTV 3140 in composite array manufacturing with USN's current laboratory equipment necessitates a trade-off. EpoTek 3012 was degassed easily and has less void, however it produces more cross talk. Although RTV 3140 is difficult to degas with current laboratory equipment, it produces less cross talk.

5.6 Electromechanical Coupling Coefficient

From Table 4.10 of the relevant electromechanical coupling coefficients for all manufactured samples and the modelled values and several points of interests can be obtained.

Firstly, the manufactured composite plate has a greater coupling coefficient than the bulk piezoceramic plate, which is to be expected for a composite material. The coupling of the EpoTek 3012-filled and RTV 3140-filled composite plate are 0.59 and 0.64, respectively. They are both higher than the coupling of the bulk Pz27. This is an expected result from the theories of composite material.

The measured coupling for both of the composite plate are close to the modelled values. For EpoTek 3012-filled composite, the measured coupling is 0.59 and the modelled coupling is 0.61, a difference of 3%. For RTV 3140-filled, the measured coupling is 0.64 and the modelled coupling is 0.65, a difference of 1.5%. This indicated that the fabricated composite has a coupling close to the modelled value with RTV 3140-filled composite being much closer to the modelled value.

The modelled composite plate values predicted that the RTV 3140-filled composite is able reach the maximum achievable value (i.e. Slender bar coupling k'_{33}). The modelled coupling of EpoTek 3012-filled and RTV 3140-filled composite plate is 0.61 and 0.65 as mentioned above and the slender bar coupling is 0.66. This modelled result predicts that the RTV 3140-filled composite can more effectively approach the slender bar coupling than the EpoTek 3012-filled composite. This prediction is confirmed by the measured result. the measured coupling of the EpoTek 3012-filled and RTV 3140-filled composite plate are 0.59 and 0.64, respectively. The slender bar coupling is 0.66. Thus, the measured coupling has difference of 10% and 3% to the slender bar coupling. This result confirmed the prediction that RTV 3140-filled composite can reach to the highest slender bar value more effectively than EpoTek 3012-filled composite.

For the composite plate and array element, a large coupling degradation was measured for EpoTek 3012-filled composite. The coupling of the EpoTek 3012-filled composite plate and array element is 0.59 and 0.37, respectively. The coupling degradation of EpoTek 3012-filled is 37%. The coupling of the RTV 3140-filled composite plate and array element is 0.64 and 0.60, respectively. The coupling degradation of RTV 3140-filled is 6%. This showed that EpoTek 3012-filled composite will have a higher coupling degradation when a composite plate was made into an array element than that of a RTV 3140-filled composite.

The RTV 3140-filled composite has a greater coupling than the EpoTek 3012-filled composite. As anticipated from the study of effective material parameters as a function of volume fraction, the composite with soft polymer has higher coupling than the composite with a hard polymer. The coupling of EpoTek 3012-filled and RTV 3140-filled composite plate is 0.59 and 0.64. The coupling of RTV 3140-filled is approximately 8% higher than that of EpoTek 3012-filled composite

plate. A similar effect can be found for a composite array element; the coupling of an EpoTek 3012-filled composite array and an RTV 3140-filled composite array is 0.37 and 0.60, respectively. The coupling of an RTV 3140-filled composite array is roughly 62% more than that of an EpoTek 3012-filled composite array. Therefore, the coupling is larger in the softer RTV 3140-filled composite than in the EpoTek 3012-filled composite and as RTV 3140 gives better electromechanical coupling, and perhaps more importantly, RTV causes less coupling between the array elements, resulting in much less crosstalk. Note that, that direct measurements of crosstalk could not be done with current available equipment, the conclusions about crosstalk are interpreted from the difference between exciting one array element compared to exciting the entire plate. This demonstrates that acoustically, a soft polymer is a better choice of kerf filler for composite manufacturing than hard polymer. On the other hand, the manufacturability and mechanical stability of RTV 3140 limits its potential to be a kerf filler due to the lack of degassing at this stage compared to EpoTek 3012.

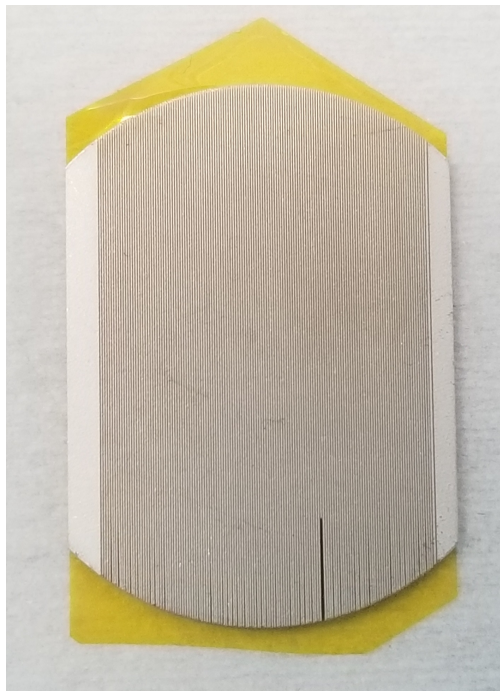
5.7 Mechanical Challenges

5.7.1 Mechanical Dicing

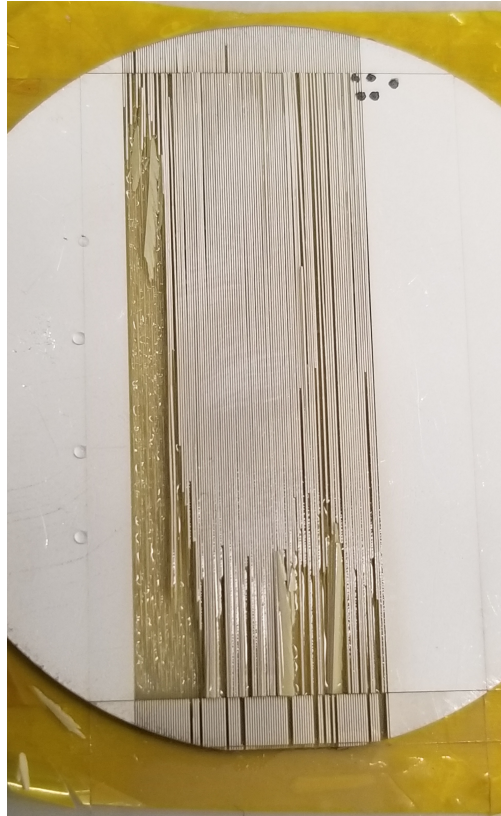
In the dicing of piezoceramics, the final quality of the structure is heavily dependent on the fabricated microstructure. In this work, the feed speed of the dicing blade are the most important parameter in attaining a high quality diced structure. Fig. 5.1 shows the dicing result at difference feed speed.



(a) Feed speed at 0.5 mm/s



(b) Feed speed at 1.0 mm/s



(c) Feed speed at 2.0 mm/s.

Figure 5.1: Dicing result at different feed speed.

At high feed speed, the diced fingers of the piezoceramics broke apart and the resulting sample was unusable. At lower feed speed, the dicing is shown to be more stable with fewer breakage. Other users should take note on maintaining a low feed speed in order to obtain a good sample for subsequent fabrication steps. The water rate was kept at 0.75 L/min for all dicing steps. Higher values of water rate might introduce extra forces that could potentially wash away the fragile structure. The blade quality would also have an effect in the final dicing quality as damaged blade could cause unexpected surface damage along the side walls. Each dicing in Fig 5.1 was performed with a new blade.

5.7.2 Filler Condition of the Composite Structure

The filler quality of the composites with EpoTek 3012 and RTV 3140 can be observed from Fig 4.2 and Fig. 4.6. The fabrication showed that voids, partial filling, or breakage were more often in the RTV 3140 due to the inefficient degassing and possible tearing of RTV 3140 silicone during lapping process as shown in Fig. A.7. However, the behavior of the electrical impedance of the composite plate are not severely affected since the the voids act also as the separation of clamping restriction between each diced active piezoceramics, thus it is still able to reduce the lateral modes.

However, too many voids brings several negative effects. Firstly, too many voids could reduced

the mechanical support of the structure and making it vulnerable to external forces such as during the handling of the sample. Secondly, debris found under optical microscope within the voids could introduce extra lateral coupling. the voids could also allow sputtered gold particles for electrode to be sputtered on the side walls. These negative effects could be the sources the differences of the measurement and the modeling for the composite array element as these imperfections might be magnified due to the small width of the array element as shown in Fig. 4.8.

In addition, due to the limitations of the existing vacuum equipment and the difficulty in achieving the flat surfaces required for speed of sound measurement, performing the speed of sound measurement for the RTV 3140-filled composite was not possible at the moment; therefore, the material parameters were obtained from literature values. The FEM modeling with RTV 3140 was approximated based on literature value and thus obtaining the parameters with speed of sound measurement of the actual silicone could provide a better simulation result.

5.7.3 Separation and Characterization of Array Element

As seen in Fig. 4.7 for the EpoTek 3012-filled composite array, the scratch dicing might not produce a perfectly even separation as the blade was shaped. But the cuts in this method can still provide a consistent volume fraction while some part of the electrode were still connected to the kerfs or piezoceramics. It did not produce any measurable influence as seen from the measurement. Also, the composite tends to bend and it would produce inconsistent dicing pitch for the dicing saw and thus the dicing at this stage with done individually by hand.

For RTV 3140-filled composite array in Fig. 4.8, voids and non-electroded area occurred across the entire sample surface. This reduces the structural integrity as each piezoceramics were only connected to each other by a fraction of the RTV 3140 silicon. The sample were fragile and care must be taken while handling as it may delaminate under small amount of external forces. Environmental dust and debris may also lodge inside these voids. The samples were cleaned with an ultrasound cleaner for 10 minutes prior to sputtering and Characterization. The source of these voids is most likely insufficient degassing. However, these defects did not affect the main resonance and antiresonance severely as seen in Fig. 4.8 but introduced an small peak at around 3 MHz. This was confirmed by the simulation result of 4.17 after adjusting the COMSOL model accordingly.

The characterization of the the composite array element was also laborious due to the lack of Flex circuit. Due to the small size of individual elements $250\ \mu\text{m}$, the electrical Characterization was done using a microscope and this step was challenging since the measurement could done be done with hand and the force on the probe must be kept minimum without creating scratches or damage on the elements. If the size is even smaller, the Characterization will be even more challenging.

Chapter 6

Conclusion

6.1 Conclusion

A step by step fabrication procedure was developed in this work for the manufacture of piezo-composite plate and array. The theoretical background for the fabrication of the 2-2 piezocomposite was presented and it serves as a foundation for designing a piezocomposite. Designers can first determine the choice of the piezoceramics based on the availability and its piezoelectric properties. Then, the choice of polymer filler can be determined based on its mechanical properties (i.e. stiffness). With the material chosen for the transducer, designers can tailor the composite behaviour in the analytical model of the composite based on the piezocomposite theory with fine adjustment of the volume fraction. Next, following the step by step guide of the fabrication procedures, the designer can dice the piezoceramics according to the dimensions needed at the operating frequencies and fill the kerfs with the polymer matrix. This work showed that with the laboratory equipment available at USN it is possible to fabricate a 2-2 piezocomposite material that matches with the modelling result.

Two 2 MHz 2-2 piezocomposite were fabricated with active piezoceramics Pz27 with EpoTek 3012 and RTV 3140 as the polymer filler by dice-and-fill method. Caution was taken for the dicing steps as this step introduces the most imperfections to the samples. The dicing speed for the first dicing must be kept low to reduce the chance of breaking. Calculations for the relevant design and material parameters were presented and modelled in 1D Xtrans and 2D FEM simulation.

It was found that the material data supplied from the manufacturer performed well when modeling the intact piezoelectric plate, but large deviations were found when using this data set to model the diced structures. Material data sets from the literature [REF Prerez, Ref Storheim] were found to fit better to the measured results for both 1D effective medium calculations and 2D FEM simulations. The data from Perez et al. [REF] were shown to have a good fit and were used as the

main data set for the modelling, but differences between Perez et.al and Storheim et al. [REF] in terms of impedance matching and coupling coefficient were not significant.

Several material parameters were used and fitted with the measured values as the it was shown that the manufacturer's material parameters showed a large deviation to the measurement. Data from Perez et al. was shown to have a good fit and was thus used as the main data set for subsequent 1D and 2D finite element modelling. The differences between Perez et.al and Storheim et al. in terms of impedance matching and coupling coefficient were not significant.

The electrical characterization of the fabricated 2-2 piezocomposite plate and array element were performed and compared with 1D and 2D FEM simulation. The measured performance were as expected from theoretical considerations. The fabricated composite plates of Pz27 with EpoTek 3012 and RTV 3140 as the polymer filler have a electromechanical coupling coefficient of 0.59 and 0.64, respectively. The comparison of the impedance between the hard EpoTek 3012 and soft RTV 3140 polymer filler showed that RTV 3140 has a higher ability to reduce lateral coupling than EpoTek 3012 due to being a soft material.

Some of the limitation for this work includes the lack of appropriate degassing equipment for silicone degassing. Silicone requires a dedicated degassing chamber as it tends to contaminate the degassing chamber and reduce the curing quality of other types of epoxies.

6.2 Future work

- Study the pulse echo response and the transmit transfer function of the piezocomposite with a matching layer
- Fabricate the complete DHUT structure with matching layer, silicon or CMUT, flex circuit and a transducer housing for beam profiling and characterisation.
- Investigate the means for RTV 3140 degassing and perform speed of sound measurement for RTV 3140
- Construction of smaller probe for array element characterisation without flex circuit.

Bibliography

- [1] T. L. Szabo and P. A. Lewin, “Ultrasound transducer selection in clinical imaging practice”, *Journal of Ultrasound in Medicine*, vol. 32, 2013.
- [2] A. Stuart Savoia, B. Mauti, T. Manh, L. Hoff, F. Lanteri, J.-F. Gelly, and T. Eggen, “Design, fabrication and characterization of a hybrid piezoelectric-cmut dual-frequency ultrasonic transducer”, pp. 1–4, 2018. DOI: 10.1109/ULTSYM.2018.8580125.
- [3] W. Smith and B. Auld, “Modeling 1-3 composite piezoelectrics: Thickness-mode oscillations”, *IEEE Transactions on Ultrasonics, Ferroelectrics, and Frequency Control*, vol. 38, no. 1, pp. 40–47, 1991. DOI: 10.1109/58.67833.
- [4] K. Uchino, *Advanced Piezoelectric Materials: Science and Technology*. Elsevier, 2017.
- [5] H. J. Lee, S. Zhang, Y. Bar-Cohen, and S. Sherrit, “High temperature, high power piezoelectric composite transducers”, *Sensors (Basel, Switzerland)*, vol. 14, pp. 14 526–14 552, Aug. 2014. DOI: 10.3390/s140814526.
- [6] T. Manh, L. Hoff, T. Eggen, T. F. Johansen, F. Lanteri, and J.-F. Gelly, “Dual frequency hybrid ultrasonic transducers - design and simulations”, pp. 1–4, 2016. DOI: 10.1109/ULTSYM.2016.7728599.
- [7] T. Uppal, “Tissue harmonic imaging”, *Australasian Journal of Ultrasound in Medicine*, vol. 13, no. 2, 2010.
- [8] C. Desilets, J. Fraser, and G. Kino, “The design of efficient broad-band piezoelectric transducers”, *IEEE Transactions on Sonics and Ultrasonics*, vol. 25, no. 3, pp. 115–125, 1978. DOI: 10.1109/T-SU.1978.31001.
- [9] S. J. Rupitsch, “Piezoelectric sensors and actuators”, *Fundamentals and Applications*, 2019.
- [10] S. Sherrit and B. K. Mukherjee, “Characterization of piezoelectric materials for transducers”, *Dielectric and Ferroelectric Reviews*, 2007.

- [11] A. M. González, Á. García, C. Benavente-Peces, and L. Pardo, “Revisiting the characterization of the losses in piezoelectric materials from impedance spectroscopy at resonance”, *Materials*, vol. 9, no. 2, 2016, ISSN: 1996-1944. DOI: 10.3390/ma9020072. [Online]. Available: <https://www.mdpi.com/1996-1944/9/2/72>.
- [12] A. E. Brown, “Rationale and summary of methods for determining ultrasonic properties of materials at Lawrence Livermore National Laboratory”, vol. 1, no. 3, Feb. 1995. DOI: 10.2172/45628. [Online]. Available: <https://www.osti.gov/biblio/45628>.
- [13] J. Cannata, J. Williams, Q. Zhou, T. Ritter, and K. Shung, “Development of a 35-mhz piezo-composite ultrasound array for medical imaging”, *IEEE Transactions on Ultrasonics, Ferroelectrics, and Frequency Control*, vol. 53, no. 1, pp. 224–236, 2006. DOI: 10.1109/TUFFC.2006.1588408.
- [14] K. Nakamura, *Ultrasonic Transducers: Materials and Design for Sensors, Actuators and Medical Applications*. Elsevier, 2012.
- [15] W. Qi and W. Cao, “Finite element analysis and experimental studies on the thickness resonance of piezocomposite transducers”, *Ultrasonic Imaging*, vol. 18, no. 1, pp. 1–9, 1996, ISSN: 0161-7346. DOI: <https://doi.org/10.1006/uimg.1996.0001>.
- [16] M. Kim, J. Kim, and W. Cao, “Electromechanical coupling coefficient of an ultrasonic array element”, *Journal of Applied Physics*, vol. 99, pp. 074102–074102, May 2006. DOI: 10.1063/1.2180487.
- [17] J. Kim, M. Kim, and W. Cao, “Effect of kerf filler on the electromechanical coupling coefficient of an ultrasonic transducer array element”, *Applied Physics Letters*, vol. 91, no. 15, p. 152904, 2007. DOI: 10.1063/1.2795333.
- [18] Meggitt. (2020). “Data for modelling”, [Online]. Available: <https://www.meggittferroperm.com/resources/data-for-modelling/>. (accessed: 01.09.2020).
- [19] N. Perez, R. Carbonari, M. A. Andrade, F. Buiocchi, and J. Adamowski, “A fem-based method to determine the complex material properties of piezoelectric disks”, *Ultrasonics*, vol. 54, Aug. 2014. DOI: 10.1016/j.ultras.2014.03.006.
- [20] E. Storheim, M. Aanesa, M. Vestrheim, and P. Lunde, “Ultrasonic piezoceramic transducers for air,- finite element analysis and measurements”, *33rd Scandinavian Symposium on Physical Acoustics*, Feb. 2010.
- [21] *Epotek 301-2 technical data sheet*, Rev. XVII, EPOXY TECHNOLOGY, Nov. 2019.
- [22] *Dowsil™ 3140 rtv coating technical data sheet*, 11-3214-01 D, DOWSIL™, 2018.

-
- [23] H. T. K. Tran, “Characterization of acoustic material properties using broadband”, M.S. thesis, Høgskolen i Sørøst-Norge, 2016.
- [24] D. Folds, “Speed of sound and transmission loss in silicone rubbers at ultrasonic frequencies”, *Journal of the Acoustical Society of America*, vol. 56, pp. 1295–1296, 1974.
- [25] P. G. Johnson, in *Performance of exterior building walls*. ASTM International, 2003, p. 138.
- [26] *Design manual for potting electronic assemblies*, Sep. 1976. [Online]. Available: <https://www.osti.gov/servlets/purl/12042152>.
- [27] T. Ritter, T. Shrout, R. Tutwiler, and K. Shung, “A 30 MHz piezo-composite ultrasound array for medical imaging applications”, *IEEE Transactions on Ultrasonics, Ferroelectrics, and Frequency Control*, vol. 49, no. 2, pp. 217–230, 2002. DOI: 10.1109/58.985706.

Appendix A

Fabrication of the 2-2 Piezocomposite

A.1 Step 1 - Sample Preparation



Figure A.1: Bulk PZ-27 disk with diameter of 3 cm supplied from manufacturer FerroPerm A/S

The sample was a PZ-27 disk supplied by FerroPerm A/S. It is cheap, readily available and widely used as ultrasound transducers. The surface was cleaned with isopropyl alcohol to remove surface debris. Kapton tape was used to tape the bottom of PZ-27 and it served as a barrier to keep the epoxy away in a later stage. Kapton tape was also easier to remove from the dicing tape at a later stage. It also improved rigidity to the diced piezoceramics. The sample was characterized before the taping of Kapton tape.

A.2 Step 2 - First Shallow Dicing

The fabrication of the dicing was done by DAD 3220 dicing saw (Disco Corp., Tokyo, Japan) and a diamond blade (Z09-SD1700-Y1-60, $53.4 \times 0.033AS \times 40$) to produce kerfs of $40 \mu m$. A detailed description of the dicing dimension in the thickness direction is shown in Fig. A.2.

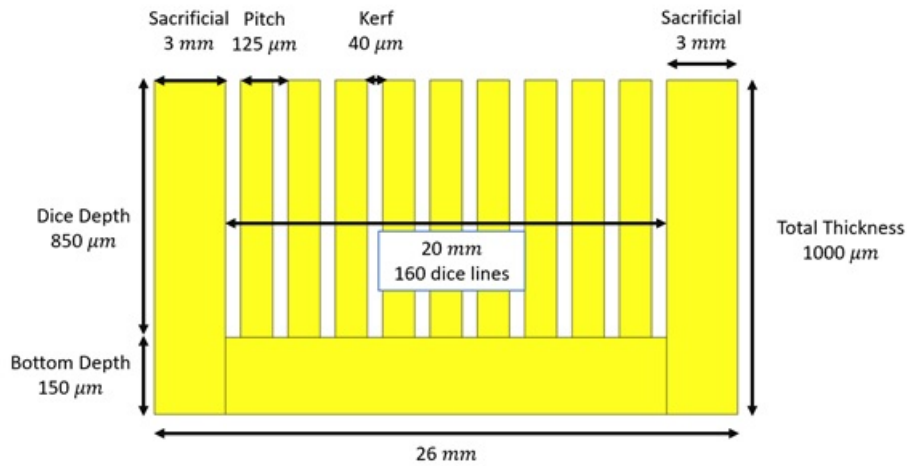


Figure A.2: Side view of the dicing regime showing the total width, thickness, depth of cuts and the sacrificial layer.

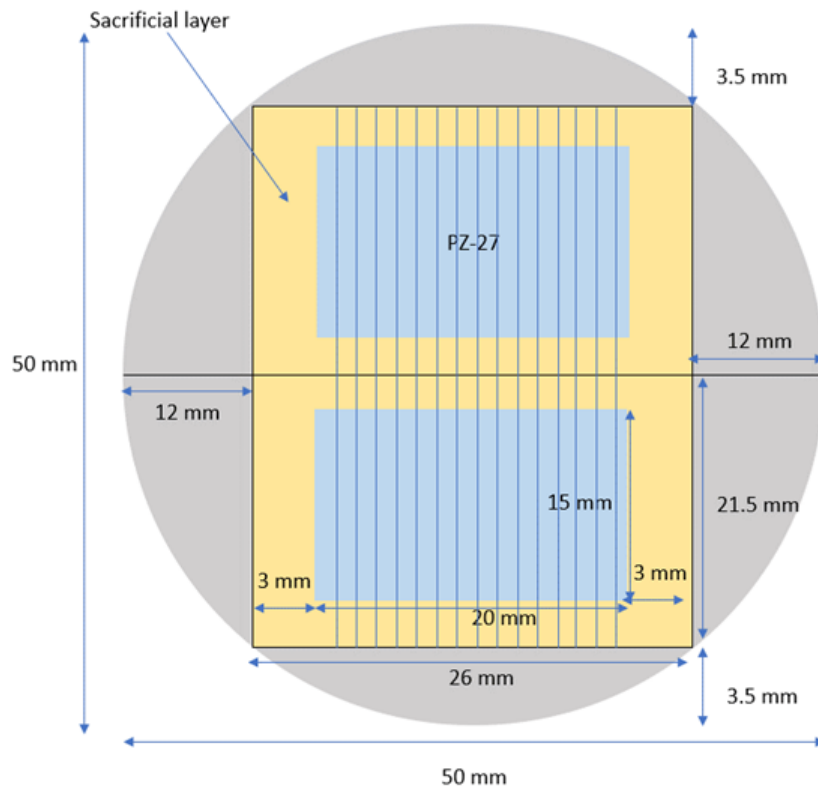


Figure A.3: Top view of the dicing schemes to separate two piezoceramic samples on the bulk PZ-27 disk

A PZ-27 disk with radius of 5 mm and thickness of 1 mm. As the final thickness is 0.724 mm, there was approximately 0.25 mm to be used as sacrificial layers and to be lapped away. Thus, the first dicing cut a shallow depth of 0.85 mm into the ceramic leaving a bottom layer of 0.15 mm. The dicing saw were moved laterally into the piezoceramic to create a sacrificial layer with a width of 10 indexes (i.e. $10 \times \text{pitch}$). This layer can provide rigidity during the sample handling so that the fragile cuts would not be touched or damaged during processing. The characterization at this stage was done by probing the back side of the sample and on top of the individual diced elements. Fig. A.3 shows the dicing scheme along the width and length direction from a top view. A dicing recipe was entered into the dicing saw and the process is automated. The main parameters affecting the dicing quality were the blade condition, feed speed and shower rate. It is important to keep the dicing speed low and the shower rate adequately medium and the dicing was performed with feedspeed of 1 mm/s and shower rate of 0.75 L/mm.. A comparison of dicing quality and feedspeed was discussed in Chapter 6. Fig. A.4 shows a diced sample.



Figure A.4: Diced PZ-27 with air kerf and Kapton tape on the bottom. Feedspeed = 1 mm/s. Shower rate = 0.75 L/mm.

The samples were removed from the dicing tape by exposure to the UV lamp on the back of the tape for 1 to 2 minutes. The adhesion weakened, and the samples were removed. The samples were

then characterized. Diced element breakage and shorting were observed under an optical microscope and is shown in Fig. A.5. In the current laboratory and equipment setup, breakage was often observed to stem from sample edge and around 0.5 to 1 cm into the sample. The non-parallel region of the cuts was diced away.

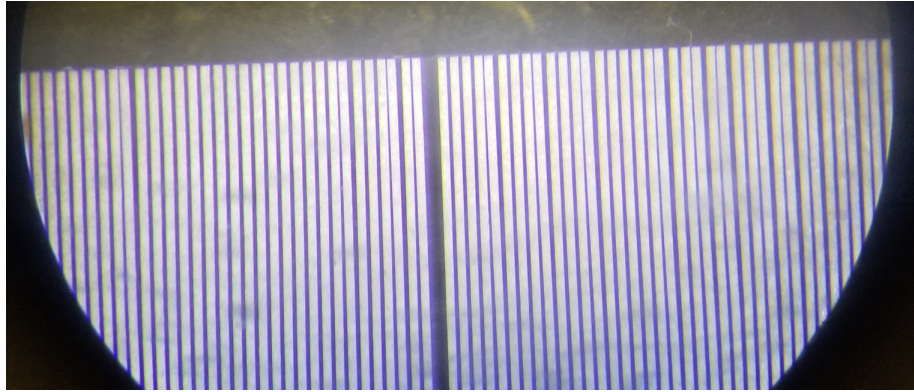


Figure A.5: Breaking and shorting of elements near the edge of the diced sample after dicing.

A.3 Step 3 - Kerf Filling, Degassing and Curing

The unfilled samples were then filled with EpoTek 301-2. Epotek 301-2 consists of two parts. Epotek 301-2 Part A and Part B. According to the technical sheet data in [21], the mix ratio of part A and part B is 100:35. The main component of the epoxy consisted of 5g of part A and 1.75g of part B. One drop of BYK was added to reduce surface tension and formation of air bubbles of the liquid mixture. Table A.1 shows the recipes to make the epoxy. The epoxy was then placed into a mixer (Speed Mixer DAC 150 FVZ-K, Synergy Devices Ltd, UK) at 2500 rpm for 5 minutes as shown in A.6.

Table A.1: Pure EpoTek 301-2 filler epoxy mixing recipes

EpoTek 301-2 A	5 g
EpoTek 301-2 B	1.75 g
BYK	1 Drop
Mixing	2500 RPM for 5 Minutes
Degas	100 mTorr
Cure	80°C for 3 hours



Figure A.6: Mixing of epoxy with Speed Mixer DAC 150 FVZ-K

After mixing, the epoxy is degassed to 100 mTorr with the degassing setup shown in Fig. A.7. The degassed liquid mixture is applied on the unfilled samples by pouring the epoxy slowly on top



Figure A.7: Degassing setup for epoxy.

of the unfilled sample. A 3D printed dam for the correct size was made to facilitate better epoxy application and coverage. The action of application introduced air bubbles again into the epoxy, thus repeated degassing was required. Fig. A.8 showed the epoxy filled diced sample ready for curing.

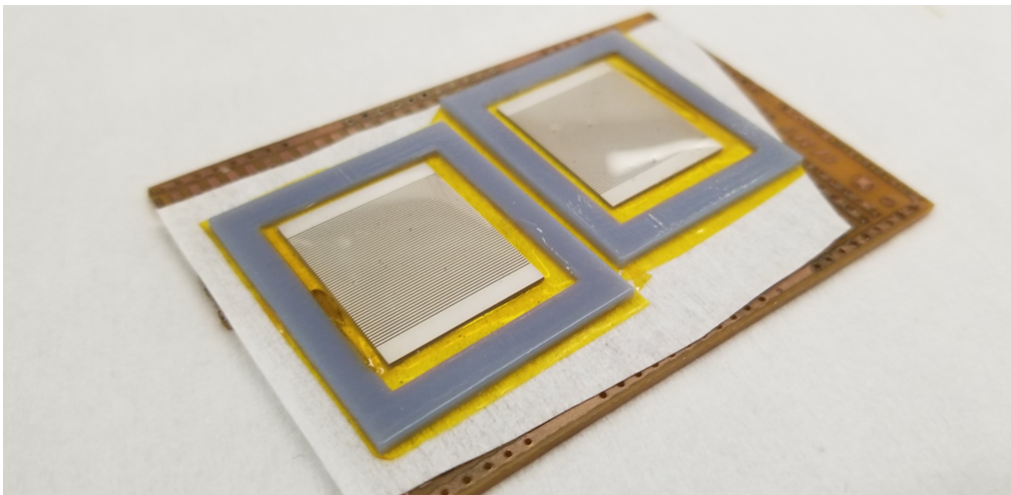


Figure A.8: Filling Epoxy on the diced PZT sample and repeatedly degassed before curing in oven.

When the diced samples were covered by the epoxy sufficiently, the filled samples were sandwiched by Mylar tapes in between the metal brick. The Mylar tapes isolated the liquid epoxy and the metal

chuck. The metal brick served to provide external pressure to promote rigidity and avoid bending of the whole setup during the process of curing as shown in Fig. A.9. The metal brick was then pressed down by a lever with a weight of 5 kg.



Figure A.9: Filled samples sandwiched by insulating tapes and metal brick to avoid bending of the sample.

The whole structure was then placed in an oven to cure at 80°C for 3 hours. The cured samples are shown in Fig. A.10. The excess epoxy and the dam frame are removed.

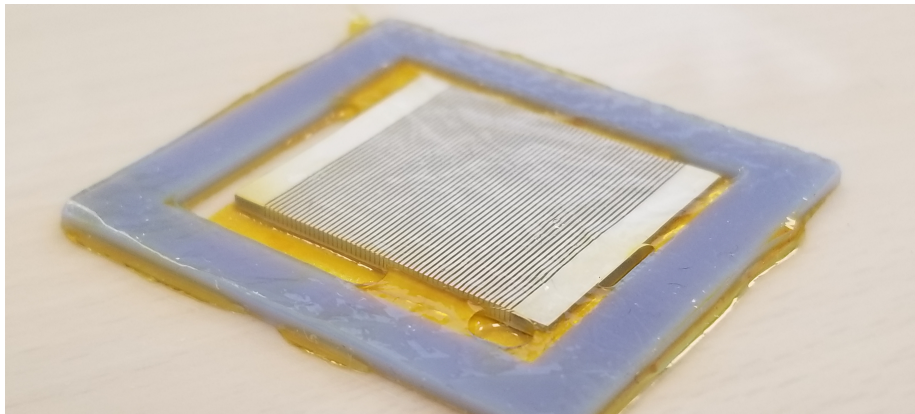


Figure A.10: Filled sampled after curing within the epoxy dam.

For the RTV 3140, the process of degassing was done by Epovac (Sturers, Denmark) as shown in A.11.

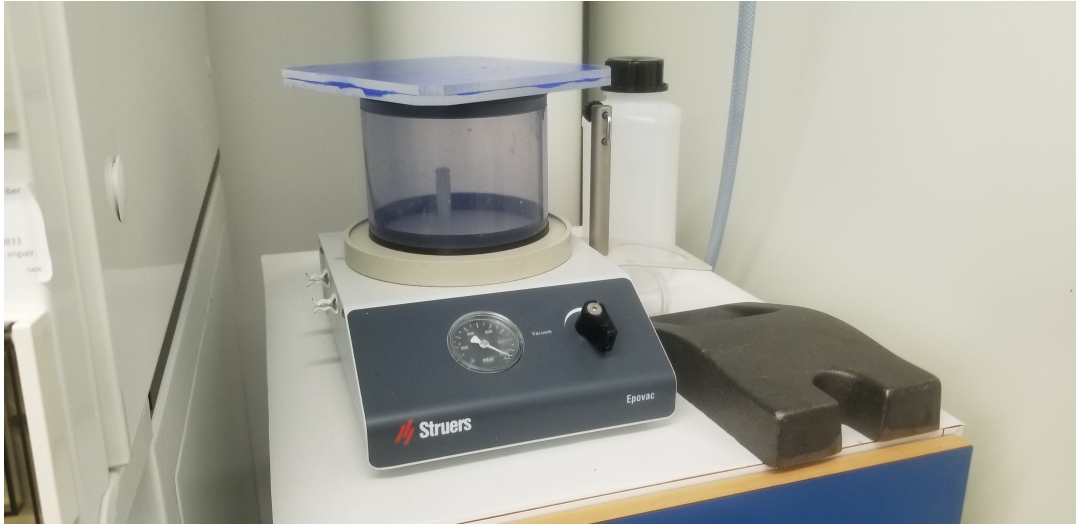


Figure A.11: Degassing equipment for RTV 3140

The chamber was degassed down to 10000 Pa for three hours. The degassing result is presented in Fig. A.12, and it demonstrates that several microscopic air bubbles remain within the material. This indicates insufficient degassing, which is difficult to achieve with the laboratory equipment currently in use. To minimize cross contamination of silicon with the vacuum chamber described above, the process of degassing silicone necessitates additional development of appropriate degassing equipment.

As a result, the material parameters of RTV Silicone was obtained from literature in [6]. The material parameters of RTV 3140 were summarized in Table 3.3.

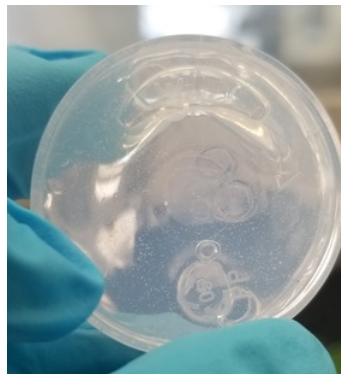


Figure A.12: RTV 3140 after degassing with multiple pockets of voids, indicating a poor degassing quality.

A.4 Step 4 - Sample Inspection

A cross section inspection was done using optical microscope to look for the filling uniformity, kerf shapes and the overall dicing and filling quality. Fig. A.13 shows the cross section of the filled composite prior to lapping with Kapton tape under the composite bottom face. In Fig. A.14, a zoomed picture of the cross-sectional image showed non-vertical dicing. The kerf width at the top was wider than the width at the bottom. The width difference between the top and the bottom is around $20\ \mu\text{m}$. At the top, the sample appears to be uniform around $30\ \mu\text{m}$ into the sample. At the bottom, the sample becomes approximately uniform around $130\ \mu\text{m}$ into the sample. Therefore, in order to obtain the best uniformity, the sample was lapped into $30\ \mu\text{m}$ from the top and $130\ \mu\text{m}$ from the bottom before further lapping to the final thickness.

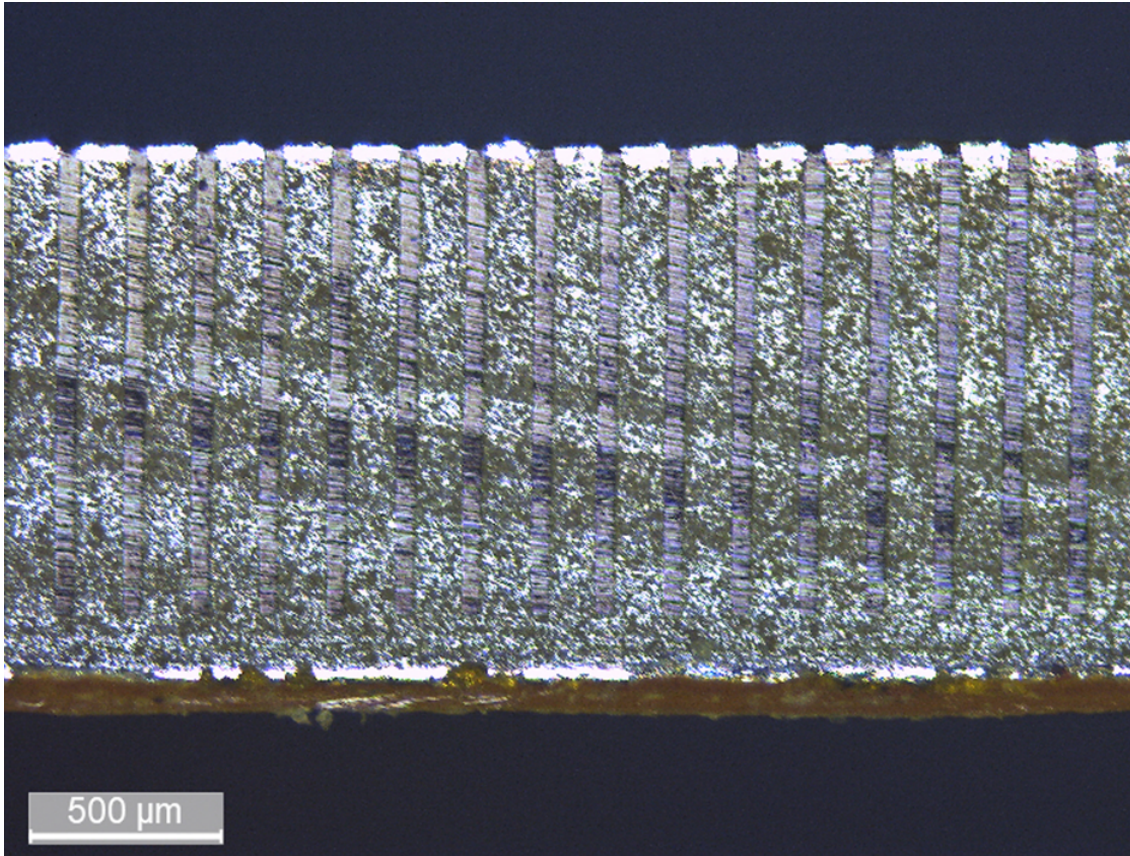
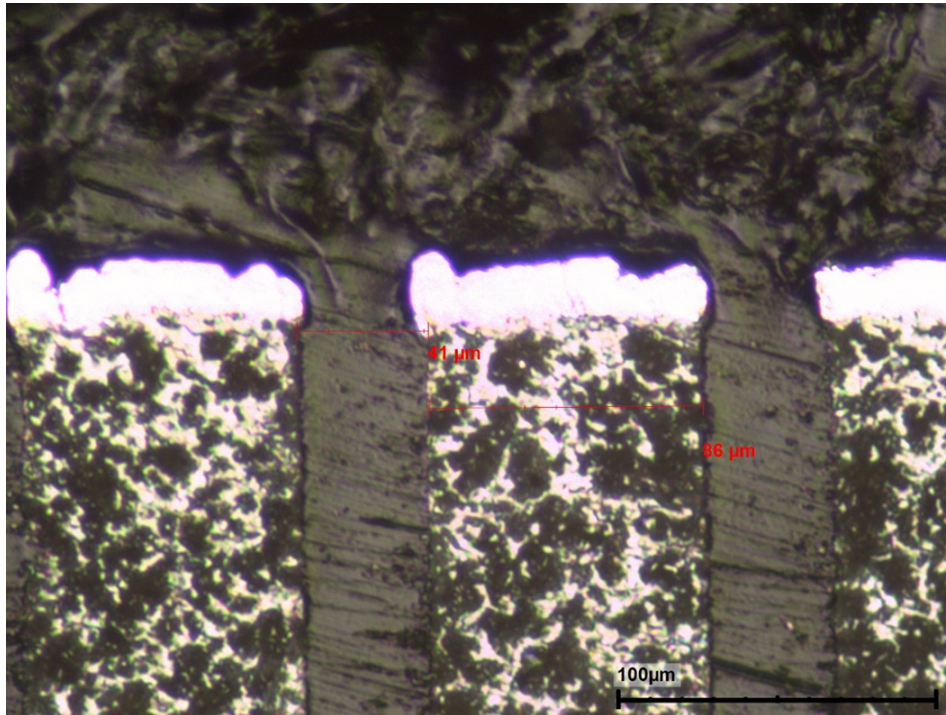
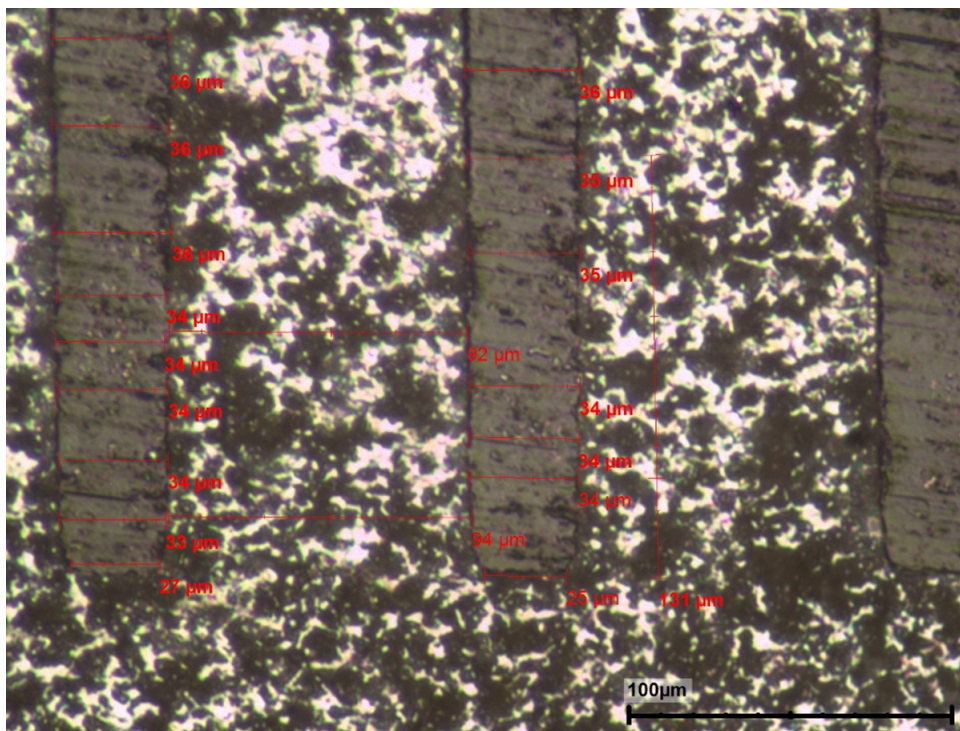


Figure A.13: Filled composite prior to lapping. The diced and filled composite was taped with the yellow Kapton tape at the bottom.



(a) Top section of the filled composite.



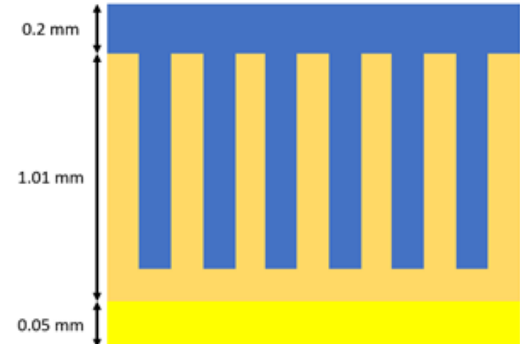
(b) Bottom section of the filled composite. Widths and thicknesses are measured in small spacing to identify variations


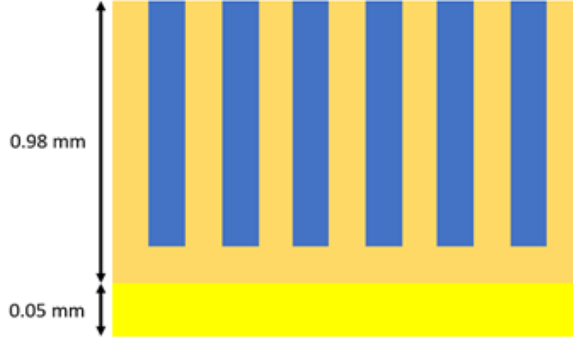
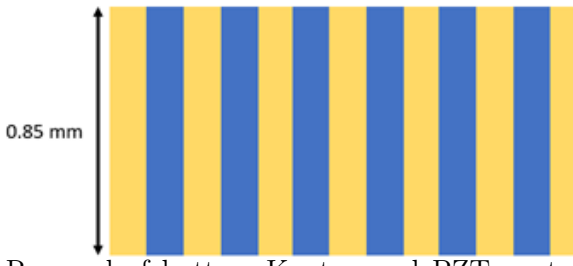

Figure A.14: Piezoceramic and kerf width on the top and the bottom of the diced showing a non-vertical dicing. The brighter portion of the image are the piezoceramics whereas the darker portions are polymer filler. At the thickness with uniform widths, the top width of the kerf is $41 \mu\text{m}$ and the bottom width of the kerf is $36 \mu\text{m}$. The oblique angle here is approximately less than 0.1° .

A.5 Step 5 - Lapping

Reaching the final thickness with high thickness uniformity is crucial in the fabrication procedures. The lapping was performed with MultiPrep™ Polishing System – 8” (ALLIED HIGH TECH PRODUCTS, INC.) and by hand. In general, the sample was wax bonded to a metal chuck, held down by another metal chuck until the wax cools down and keeping the sample flat. Then the wax-bonded composite was placed in the holder arm, and the sample was lapped by abrasive grinding. Final thickness was achieved by adjusting the height of the Z-indexing spindle while the sample was abrasive grinded. The following details and suggestions apply only to the equipment mentioned. To obtain thickness uniformity, the calibration of the polishing machine, sanding paper grit, and wax temperature are important. The machine was calibrated to an error around $20 \mu m$. However, after multiple testing with the machine, the calibration error produced an oblique surface and it was difficult to maintain a consistent thickness variation. The thickness of the sample was measured by a thickness gauge. Table 4-6 shows the detailed lapping steps to reach the final thickness. At step 0, the sample surface was cleaned with isopropyl and lint free paper and was wax bonded for lapping. At step 1, the epoxy was a hard material thus a 600 grit paper was used to lap away the excess epoxy on the top surface up to the composite face in a short time. At step 2, the composite was lapped $30 \mu m$ into the composite from the top surface and the silver electrodes were also removed. At step 3, the Kapton and part of the composite was lapped away at the bottom. At step 4, the composite was lapped from the bottom to reach the thickness at which the width became uniform and was finally lapped to the final thickness.

Table A.2: Procedures for fabricating a 2-2 piezocomposite plate. Dark Yellow is the PZ-27. Bright Yellow is Kapton. Blue is kerf filler EpoTek 3012.

Steps	Illustration	Lapping Thickness	Grit paper
Step 1	 <p>Filled sample for lapping.</p>	-	-

Step 2	 <p>Removal of excess top epoxy.</p>	200 μm	600
Step 3	 <p>Removal of top surface electrode.</p>	30 μm	800
Step 4	 <p>Removal of bottom Kapton and PZT up to kerf bottom exposure.</p>	200 μm	800
Step 5	 <p>Lapping to the final thickness from bottom and to a matte finish.</p>	150 μm	1200

Note that, during wax bonding, the wax on the metal chuck was heated up to 80 °C on a hotplate and then the composite was placed on top with a metal block holding down the composite. It was observed that the heat from the wax can heat up the composite and this heating produced observable bending of the composite due to thermal expansion and the mechanical change of the epoxy as its glass transition temperature is 65 °C. This bending prevented parallel lapping and lead to thickness non-uniformity. If the composite sample is placed on the melted wax while the metal chuck is on the hotplate, the sample will be heated directly and lead to bending. To minimise heating, remove

the metal chuck from the hotplate first, place it on the metal holder, then place the composite on top and held down by another metal chuck so that the wax will not directly heat up the composite as it transfers more heat to the surroundings than to the sample.

The lapped sample is shown in Fig. A.15. The thickness variation should be less than $20\ \mu\text{m}$ and for this sample, the variation along width and length direction were around $6\ \mu\text{m}$ and $8\ \mu\text{m}$ respectively. The final thickness for this sample is approximately $745\ \mu\text{m}$.

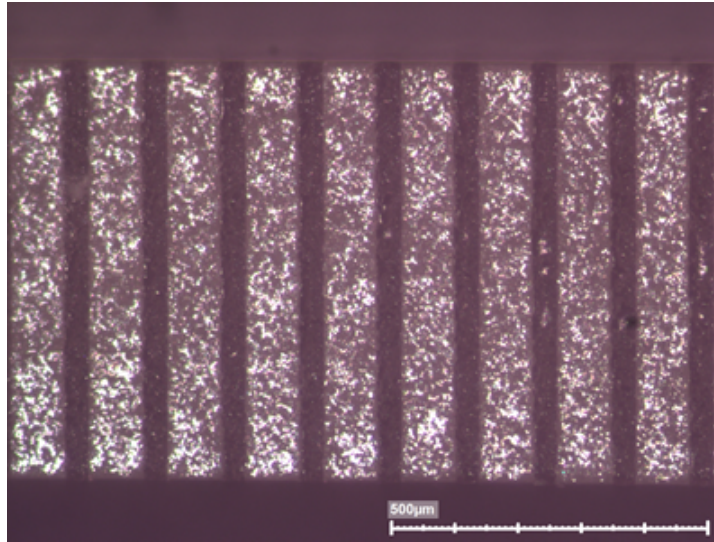


Figure A.15: Cross section of the lapped composite

The surface condition of the is shown in Fig. A.16 and it shows scratches and potential voids within the epoxy after the epoxy was exposed by lapping. The surfaces are polished with 1200 grit sanding paper to matte finish.

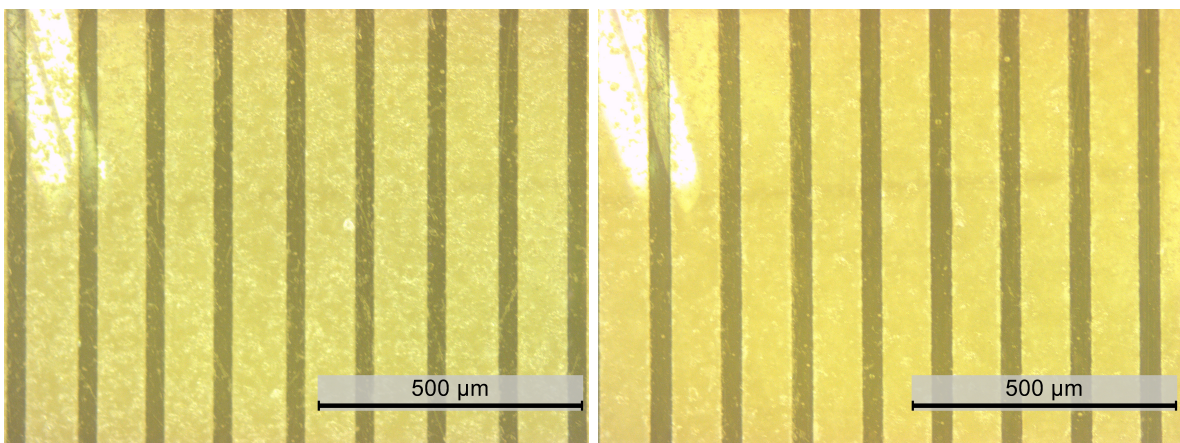


Figure A.16: Surface condition of the lapped composite on the top(left image) and bottom(right image) surface under optical microscope. The brighter portion of the image are the piezoceramics PZ-27 whereas the darker portions are polymer filler EpoTek 3012. The bright spot on the top left corner is the microscope lamp.

A.6 Step 6 - Sputtering

The sputtering of electrode was performed with Sputter AJA (AJA International Inc., MA, United States). The diced and filled sample was cleaned with isopropyl and deionized water in ultrasound cleaner at 60 °C for 5 minutes each to clean away dust and residue wax from the previous lapping procedures. Since the wax melts at approximately 50 °C and the glass transition temperature of EpoTek 301-2 is approximately 65 °C, the temperature of 60 °C is therefore chosen to completely remove the wax while preventing the epoxy to become rubbery and leads to severe bending. Next, the sample was cleaned with a plasma cleaner PX-250 (Nordson MARCH, Concord, CA) with pure Oxygen for 30 seconds on each side. Then, Chromium and Gold were sputtered on both side and a wraparound structure is made to separate electrodes. A tape test was conducted with Kapton tape on both surfaces to ensure the electrode adhesion. Minimal lamination is observed.

Table A.3: Parameters for electrode sputtering.

Material	Deposition Rate [$\text{\AA}/\text{s}$]	Thickness [\AA]
Cr	0.15	200
Au	0.49	2000

A.7 Step 7 - Composite Array Fabrication

In a linear array transducer, array elements are excited individually by the driving voltage along the thickness direction to produce acoustic wave in the thickness mode. An illustration of array element on the composite is shown in Fig. A.17. One piezocomposite element consists of two PZ-27 piezoceramic and sandwiched by kerf filler EpoTek 3012. The element width of the composite element was $250\ \mu\text{m}$. The electrode separation between each element was $125\ \mu\text{m}$. Thus, the element pitch was $375\ \mu\text{m}$ (0.52λ in water at center frequency of 2.13 MHz).

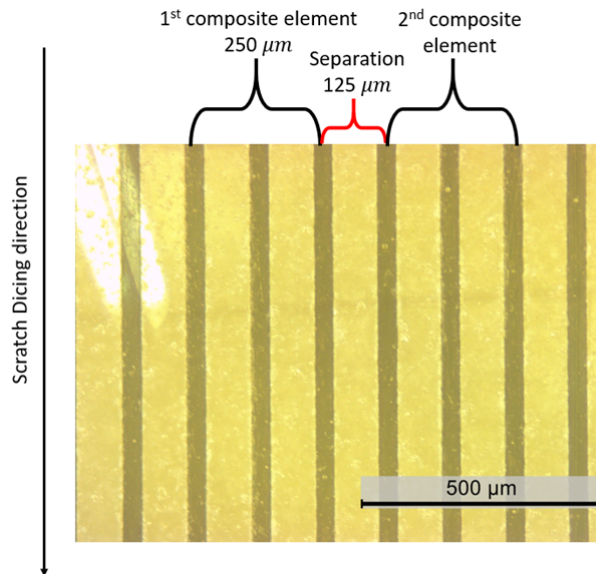


Figure A.17: Top surface of the composite to be scratch diced with the element width and pitch. For ease of understanding of the composite structure, the image before sputtering of electrodes on the composite surface is shown here. Bright spot at the top left is light from microscope lamp.

Prior to electrode separation, all composite elements of the sputtered composite shared common electrode. Then, the sample was scratch diced by the DAD 3220 dicing saw (Disco Corp., Tokyo, Japan) with a $120\ \mu\text{m}$ Diamond blade (P1A851 SD600R10MB01 55X0.12X40) to remove a thin layer of the electrode with a width of approximately $125\ \mu\text{m}$. The thickness to be scratch diced were determined by the largest thickness difference of the sample to ensure complete removal of electrodes. The dicing saw diced approximately $10\ \mu\text{m}$ deep into the sample from the top surface. The completed composite array with PZ-27 and EpoTek 3012 as the polymer filler is shown in Fig. 4.7. The average separation width produced by the dicing saw is $120\ \mu\text{m}$. Same procedure is done with the composite of PZ-27 with RTV 3040 as polymer filler and it is shown in 4.8.